# COMPRESSED SENSING FRAMEWORK FOR MULTI-CHANNEL ECG SIGNALS

*A*

*Thesis submitted*

*for the award of the degree of*

**DOCTOR OF PHILOSOPHY**

By

**ANURAG SINGH**

DEPARTMENT OF ELECTRONICS AND ELECTRICAL ENGINEERING

INDIAN INSTITUTE OF TECHNOLOGY GUWAHATI

GUWAHATI - 781 039, INDIA

APRIL 2017

To my **Parents**

for their love and support

and

To dear **Bhaiya-Bhabhi** (DhirAish) and **Didi-Jijaji** (DevRaj)

for their constant encouragement

# Certificate

This is to certify that the thesis entitled "**Compressed Sensing Framework for Multi-channel ECG Signals**", submitted by **Anurag Singh** (11610230), a research scholar in the *Department of Electronics and Electrical Engineering, Indian Institute of Technology Guwahati*, for the award of the degree of **Doctor of Philosophy**, is a record of an original research work carried out by him under our supervision and guidance. The thesis has fulfilled all requirements as per the regulations of the Institute and in our opinion has reached the standard needed for submission. The results embodied in this thesis have not been submitted to any other University or Institute for the award of any degree or diploma.

Dated:

Guwahati.

Dr. Samarendra Dandapat
Professor
Dept. of Electronics and Electrical Engg.
Indian Institute of Technology
Guwahati - 781 039
India.

# Acknowledgments

At the outset, I would like to express my whole hearted and deep sense of gratitude to my guide Prof. Samarendra Dandapat for his guidance, help and encouragement throughout my research work. I greatly admire his attitude towards research, creative thinking, hard work and dedication in work. I am highly grateful to him for patiently checking all my manuscripts and thesis. This thesis would not have been possible without his bounteous efforts. More than guide, he is my mentor for shaping my personal and professional life, without whom I would not have been where I am today. I owe my profound gratitude to Prof. Samarendra Dandapat for his supports in all respects.

My sincere thanks to my doctoral committee members Prof. S. R. M. Prasanna, Prof. Rohit Sinha, and Prof. H. B. Nemade for their support, encouragement and suggestions rendered during my research work. Many faculty members of the department gave me suggestions and encouragement time to time. The kind support and valuable suggestions from faculty members of the department helped me a lot to improve myself academically and personally. I sincerely acknowledge and thanks the faculties, Dr. Amit Sethi, Dr. B. K. Rai, Prof. P. K. Bora, Dr. Tony Jacob and Dr. A. Rajesh in this regard. I would like to thank other faculties of the department who helped me directly or indirectly during my research work. My special thanks to Dr. S. K. Nayak who helped me a lot during my Ph.D. admission and encouraged me now and then during my PhD.

I would like to express my sincere gratitude to Mr. Sanjib Das and Dr. L. N. Sharma, Senior technical officers, for their enormous help whenever required. I sincerely acknowledge the technical and moral supports provided by Dr. L. N. Sharma during tough phases of my Ph.D. work. I am also grateful to all other technical and office staff members of the department and the computer center for their help. I am very much thankful to my seniors in the EMST Lab, Dr. Syed Shahnawazuddin, Dr. Haris B. C., Dr. Deepak K. T., Dr. Sunil Y., Dr. Samar Shailendra, Dr. Govind D., Dr. Sumitra Shukla, Dr. Debadatta Pati, Dr. S. R. Nirmala, Mr. O. P. Singh, Mr. Malaya Kumar Nath and Mr. Jyoti Medhi for their help and support.

I take this opportunity to extend my gratitude towards Dr. Samdarshi and Mr. Gaurav Kumar Yadav, my bachelor time class mates and close friends, for their constant help and support during good and bad time of my PhD journey. We shared quite memorable time during post-dinner walks at

IITG. After my graduation, it was Samdarshi, who motivated me to join PhD in IITG. His technical and off the research suggestions have really helped me to shape-up my PhD. I also acknowledge the help and support shown by our biomedical signal processing group members, Sibasankar Padhy, Jiss J. Nullikuzhy, Bhanupriya, and Rajesh Tripathy, with whom, I had valuable discussions time to time. I also extend my sincere thanks to Santosh Kumar Yadav in this regard. I am thankful to my friends Sunil Kumar, Nagaraj Adiga, Biswajit Dev Sarma, Sikandar Kumar, Rohan Kumar Das, Tousif Khan Nizami, Neeraj Kumar, Abhishek Vahadane, Suman Deb, Biplab Ketan Chakraborty, Banriskhem K Khonglah, Swati Banerjee, Himakshi Choudhury, Bidisha Sharma, Ganji Sreeram, Tilendra Chaudhary, Subir Dey, Anmol Shrivastava and all other members in the EMST Laboratory. I also wish to thank my friends outside IITG, especially Dr. Rajlaxmi Chauhan, Mr. Anant Singh, and Dr. Ashish Bhandari, who have helped me time to time in proofreading my manuscripts.

Above all, I am deeply grateful to my parents and my siblings. It would not have been possible for me to complete my PhD without their love, support and sacrifice.

***Anurag Singh***

# Abstract

Electrocardiogram (ECG) signals are the manifestation of underlying electrical phenomena of heart, which are responsible for its various functionalities. ECG is used as an important non-invasive tool by the cardiologists to diagnose and assess a wide range of cardiac ailments. With advancements in wireless body area network (WBAN) technologies, significant research has been done in recent decades to develop low-cost personalized remote health monitoring systems for next-generation of e-healthcare solutions. With ever increasing number of cardiovascular patients, WBAN-enabled ECG telemonitoring has generated significant interest among the biomedical community. Ambulatory ECG enables remote monitoring of vital heart parameters and allows early medical interventions in case of life-threatening heart diseases. However, existing ECG monitoring systems still suffer from various challenges, such as limited autonomy, bulkiness, limited functionalities, etc. In recent years, compressed sensing (CS) has emerged as a promising framework to address these challenges. Low-complex and highly energy-efficient data reduction procedure of CS makes it an attractive choice over traditional wavelet-based techniques for embedded on-node ECG data compression in resource-constrained telemonitoring applications.

The main objective of the present dissertation is to explore the CS framework for multi-channel ECG (MECG) signals. CS-based signal processing involves two operations: 1) CS encoding, where the data is linearly projected over a lower dimensional subspace using a sensing matrix to get the compressed *measurements* of the signal, 2) Signal reconstruction (decoding), where the original signal is reconstructed in a sparse domain using incomplete signal measurements. In the present thesis, there are three major contributions. First work focuses on efficient MECG signal encoding using an eigenspace CS approach. Second and third works contribute towards faithful signal reconstruction when low signal measurements are available at low data rates (or at high compression ratio).

There is inherent spatio-temporal correlation present across different channels of MECG signals due to their common origin at sinus node. It is important to exploit this correlation information for an effective CS implementation. We proposed a CS framework of data reduction in eigenspace for MECG signals. Principal component analysis (PCA) is used to decorrelate different channels and the resulting principle eigenspace signals are gone through further dimensionality reduction using CS approach by exploiting their sparsity either in eigenspace itself or in any other sparsifying domain. This joint PCA-CS approach gives significant boost to the compression efficiency compared to the existing CS-based ECG compression methods. The average value of $PRD$ across the PTB database is found to be 5.24% in lead V3 at a compression ratio of 17.76. The visual quality of the reconstructed MECG signals is validated through mean opinion score (MOS) and it is found to be 6.66%, which implies a very good signal reconstruction quality.

The encoders in WBAN-enabled ECG telemonitoring are resource-constrained due to their small size and battery operation. Therefore, to minimize the computational resources at the encoder, a low complex joint CS-based compression/reconstruction algorithm is proposed in the next work. Here, directly time domain MECG signals are jointly compressed and reconstructed using a weighted mixed norm minimization (WMNM)-based CS recovery algorithm by exploiting the wavelet domain joint sparsity of different ECG channels. WMNM algorithm emphasizes important high amplitude sparse wavelet coefficients through a weighting strategy while exploiting spatial or inter-channel correlation at the decoder. It is found that coefficient-level weighting-based WMNM algorithm associated with low-complexity encoder leads to substantial improvement in the signal recovery performance (up to 77% drop in $PRD$ value) and measurements requirement (41.18% saving) compared to the non-weighted CS approaches.

In the weighting-based CS recovery algorithms, there is flexibility to adopt different weighting rules depending on the understanding of the problem and that in return, improves the estimation of latent data. This has motivated to explore more effective and diagnostically relevant weighting schemes in our next work through which clinically important MECG features can be preserved more precisely during joint CS recovery. We studied

the multi-scale wavelet structure of MECG signals and exploited the subband level ECG features/information in the joint CS recovery problem through a subband-based weighting scheme. Such a weighting approach emphasizes ECG features present in wavelet subbands having high diagnostic importance. Coefficients in clinically less relevant high frequency subbands are deemphasized simultaneously, resulting in a sparser (and hence, more accurate) solution. Accuracy of reconstruction is validated through a post-reconstruction classification task, which gives classification accuracy of 73.2% even when MECG signals are jointly reconstructed using only about 10% of compressed measurements. Additionally, a block-sparsity-based joint CS recovery is also explored for MECG signals.

**Keywords:** Multi-channel electrocardiogram, Compressed sensing, PCA, OMP, Data reduction, Joint sparse recovery, Weighted mixed-norm minimization, DWT, PRD, CR.

# Contents

# List of Figures

भारतीय प्रौद्योगिकी संस्थान गुवाहाटी
Indian Institute of Technology Guwahati

# List of Tables

# List of Acronyms

| | |
|---|---|
| ADC | Analog to Digital Conversion |
| AIC | Analog to Information Conversion |
| AMI | Anterior Myocardial Infarction |
| APRD | Average Percentage Root-Mean-Square Difference |
| AV | Atrioventricular |
| AWEDD | Average Wavelet Energy-based Diagnostic Distortion |
| AWGN | Additive White Gaussian Noise |
| AWWPRD | Average Wavelet Weighted PRD |
| BBB | Bundle Branch Block |
| BBB | Bundle Branch Block |
| BP | Basis Pursuit |
| BPDN | Basis Pursuit Denoising |
| BSBL | Block Sparse Bayesian Learning |
| BWMNM | Binary Weighted Mixed-Norm Minimization |
| CR | Compression Ratio |
| CS | Compressed Sensing |
| CSE | Common Standards for Electrocardiography |
| DCS | Distributed Compressed Sensing |
| DCT | Discrete Cosine Transform |
| DFT | Discrete Fourier Transform |
| DWT | Discrete Wavelet Transform |
| DSP | Digital Signal processing |

| | |
|---|---|
| ECG | Electrocardiogram |
| EMG | Electromyogram |
| EEG | Electroencephalogram |
| FPGA | Field-Programmable Gate Array |
| GPRS | General Packet Radio Service |
| HC | Healthy Control |
| HRV | Heart Rate Variability |
| IHT | Iterative Hard Thresholding |
| INCART | Institute of Cardiological Technics |
| JCS | Joint Compressed Sensing |
| LA | Left Arm |
| LAE | Left Atrial Enlargement |
| LASSO | Least Absolute Shrinkage and Selection Operator |
| LBBB | Left Bundle Branch Block |
| LL | Left Leg |
| MAE | Maximum Absolute Error |
| MAP | Maximum Aposterior |
| MAX | Maximum Amplitude Error |
| MBSBL | Modified Block Sparse Bayesian Learning |
| MCS | Multi-scale Compressed Sensing |
| MECG | Multi-channel Electrocardiogram |
| MI | Myocardial Infarction |
| MIT-BIH | Massachusetts Institute of Technology-Boston's Beth Israel Hospital |
| MMV | Multiple Measurement Vector |
| MNM | Mixed-Norm Minimization |
| MOS | Mean Opinion Score |
| MSBL | Modified Sparse Bayesian Learning |
| MSE | Mean Squired Error |
| MSPCA | Multi-scale Principal Component Analysis |

| | |
|---|---|
| NCC | Normalized Cross-Correlation |
| NMAX | Normalized Maximum Amplitude Error |
| NMSE | Normalized MSE |
| NRMSE | Normalized Root Mean Squared Error |
| NRWSE | Normalized Relative Wavelet Subband Energy |
| NSTDB | Noise Stress Test Database |
| OMP | Orthogonal Matching Pursuit |
| PC | Principal Component |
| PCA | Principal Component Analysis |
| PCR | Power to Compression Ratio |
| PDF | Probability Density Function |
| PE | Peak Error |
| PKS | Partial Known Support |
| PRD | Percentage Root Mean Square Difference |
| PTB | Physikalisch-Technische Bundesanstalt |
| PWMNM | Prior Weighted Mixed-Norm Minimization |
| QS | Quality Score |
| RA | Right Arm |
| RAM | Random Access Memory |
| RBBB | Right Bundle Branch Block |
| RIP | Restricted Isometric Property |
| RAE | Right Atrial Enlargement |
| RL | Right Leg |
| RMSE | Root Mean Square Error |
| RNG | Random Number Generator |
| ROM | Read Only Memory |
| SAR | Synthetic Aperture Radar |
| SGAP | Simultaneous Greedy Analysis Pursuit |
| SMV | Single Measurement Vector |

| | |
|---|---|
| SNR | Signal-to-Noise Ratio |
| SOMP | Simultaneous Orthogonal Matching Pursuit |
| SPIHT | Set Partitioning in Hierarchical Trees |
| SVD | Singular Value Decomposition |
| SVM | Support Vector Machines |
| SWMNM | Subband Weighted Mixed-Norm Minimization |
| WBAN | Wireless Body Area Network |
| WDD | Weighted Diagnostic Distortion |
| WEDD | Wavelet Energy-based Diagnostic Distortion |
| WLAN | Wireless Local Area Network |
| WLM | Weighted $\ell_1$-Minimization |
| WMNM | Weighted Mixed-Norm Minimization |
| WPRD | Weighted Percentage Root Mean Square Difference |
| WWPRD | Wavelet Weighted Percentage Root Mean Square Difference |

# 1

# Introduction

Contents

This thesis investigates multi-channel electrocardiogram (MECG) signals in a compressed sensing (CS) framework. CS is an important signal processing technique that has emerged in recent years as an effective alternative to traditional wavelet-based methods for energy-efficient embedded data compression applications in wireless body area networks (WBANs) [1]. The WBAN-enabled telemonitoring systems have found important applications in continuous remote monitoring of vital health parameters in order to maintain an optimal health status, especially for elderly people and pregnant women who require frequent medical attention. Energy-efficient systems are required for long-term and clinically relevant telemonitoring. CS framework offers potential solution to minimize the complexity and power consumption of the existing WBAN systems. However, most of the existing CS-based WBAN-enabled telemonitoring systems are limited to single channel ECG signals. This motivated us for the study of MECG signals in the CS framework for remote healthcare applications. MECG signals recorded in 12-channel format, capture three dimensional view of heart and hence consist of detailed cardiac information. Cardiologists prefer MECG signals as they carry significant pathological clues in different leads, which are helpful in diagnosis of various heart's ailments. Since each channel views the heart from different narrow angles, there exists significant spatio-temporal information which is common across the channels. This inherent correlated structure must be exploited for effective implementation of CS for MECG signals.

The work carried out in this thesis has three major contributions. First, a joint principal component analysis (PCA)-CS approach is investigated for effective exploitation of correlation information in MECG system. The MECG signals are spatially decorrelated using PCA and then the sparsity of dimension-reduced eigenspace MECG signals is exploited to apply CS. The resulting compressed measurements are quantized using a uniform quantizer and encoded by a lossless Huffman encoder.

The second work proposes a low-complexity joint CS encoder and a weighted mixed-norm minimization (WMNM)-based joint CS recovery algorithm, which utilizes wavelet domain joint sparsity of MECG signals. WMNM algorithm exploits inter-channel or spatial correlation while emphasizing high amplitude sparse wavelet coefficients through a coefficient-level weighting approach. The proposed approach helps to successfully recover all the ECG channels together using a low number of measurements.

In the third work, we studied the multi-scale wavelet structure of MECG signals and explored the

WMNM-based joint CS approach further with a new diagnostically relevant weighting criterion, which helps preserve clinically important MECG features more precisely. Observing the gross segmentation of clinical ECG features (P wave, P-R interval, QRS interval, ST segment, T wave) in different wavelet scales, a subband weighting-based WMNM algorithm is proposed. The proposed algorithm exploits multi-scale signal information through a multi-scale weighting approach. Under this strategy, weights are designed based on the diagnostic information contents of each wavelet subband/scale, which emphasizes ECG features present in wavelet subbands having high clinical importance during joint CS recovery. Additionally, a block-sparsity-based joint CS recovery is also explored in this work for MECG signals.

The performance evaluation of the works carried out in this thesis is done using various publicly available MECG databases [2,3] such as Physikalisch-Technische Bundesanstalt (PTB), Massachusetts Institute of Technology-Boston's Beth Israel Hospital (MIT-BIH), St.-Petersburg Institute of Cardiological Technics 12-lead Arrhythmia Database (INCART), and Noise Stress Test Database (NSTDB). Commercially available Common Standards for Electrocardiography (CSE) database [4] is also used for the evaluation purpose.

## 1.1 Electrocardiogram and its Clinical Components

There are many physiological signals which can be recorded easily in a non-invasive manner and have high clinical relevance. These signals depict underlying physiological activities of a specific organ in the human body. Electrocardiogram (ECG) is one such signal which records cardiac phenomenon and reflects the nature and the activities of human heart. In a clinical practice, it is used to diagnose and assess chronic cardiovascular diseases. In standard clinical practices, ECG is recorded with single channel/lead or multiple channel/lead configuration from the surface of human body. ECG signals are recorded at different locations of the body surface in order to capture the three-dimensional view of the human heart. In general, 12-lead format is used for various diagnostic purposes and it is termed as multi-channel or multi-lead ECG (MECG). Because of the presence of pathological clues in multiple leads, cardiologists prefer MECG for detailed and reliable diagnosis [5].

Figure 1.1 depicts a single channel ECG. Different ECG features having clinical relevance have been marked. Important ECG features include mainly amplitude and duration features whose description

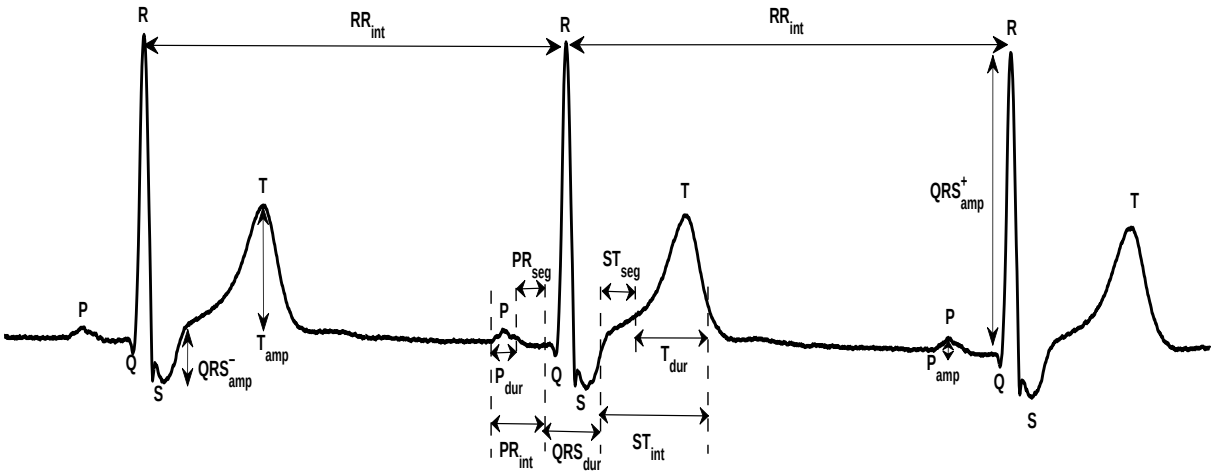


**Figure 1.1:** Clinical components of an ECG signal with their duration and amplitude

is given below:

***P wave***: The electrical impulses generated at the sinoatrial node travel from atria towards ventricles. This causes depolarization in atria, which generates P wave in the ECG signal. Both right and left atria get electrically activated simultaneously and this composite activation is represented by P wave. For a healthy person, P wave duration varies from 80 to 100 ms with a maximum amplitude of 0.25 mV. Any deviation from above specified values indicates heart abnormalities. For example, a P wave amplitude $>$ 0.25 mV indicates right atrial enlargement (RAE) and a widened P wave signifies left atrial enlargement (LAE). If P wave amplitude is decreased, it may be a case of hyperkalemia.

***PR interval***: After activating the atria, the electrical impulses reach to the ventricles and cause ventricular depolarization. The duration between atrial depolarization and beginning of ventricular depolarization is called PR interval. It is measured as the time interval between P wave and Q wave. In some heart diseases, Q wave is absent. In those cases, R wave is taken in place of Q wave. In normal conditions, PR interval is of 120-200 ms. Heart diseases such as pheochromocytoma and Wolfe-Parkinson-White syndrome are generally found in patients with a short PR interval in the ECG signal. On the other hand, a long PR interval indicates $1^{st}$ degree atrioventricular (AV) block, $2^{nd}$ degree AV block and rheumatic heart diseases.

***QRS complex***: It is generated during ventricular depolarization, when the myocardial cells of the ventricles get depolarized. It is made of three waves, i.e., Q wave, R wave, and S wave, and hence

called a complex. As the ventricles have larger muscle mass, it generates large electric potential during depolarization process. This is the reason, QRS complex has the highest amplitudes in the ECG waveform. The normal QRS complex duration is between 60-100 ms. Disruption in heart's conduction system is observed in patients with wider QRS complexes. This includes diseases like left bundle branch block (LBBB), right bundle branch block (RBBB), ventricular tachycardia, etc. An exceptional increase in the hight of QRS complex indicates left ventricular hypertrophy, while a very low-amplitude QRS complex may represent pericardial effusion or infiltrative myocardial diseases.

***Q wave***: The first wave of QRS complex is the Q wave. It is the point where QRS complex takes its first downward deflection. Q wave represents the depolarization of intra-ventricular septum. A normal Q wave has a duration of 40 ms and an amplitude of 25% of the amplitude of R wave. Abnormal Q wave (wider or deeper) indicates myocardial infarction.

***R wave***: The peak or upward deflection of QRS complex is termed as R wave. During ventricular depolarization, R wave represents a part of the depolarization cycle. A distorted R wave either in terms of polarity or amplitude, indicates bundle branch block (BBB).

***S wave***: The last part of the QRS complex, where it takes downward deflection, is termed as S wave. The remaining part of the ventricular depolarization is represented by S wave. Similar to R wave, the irregular shapes of S wave in the ECG signal may be the indication of BBB.

***T wave***: After the depolarization of ventricles is completed, the myocardial cells of ventricles start repolarization and make T wave in the ECG waveform. Its normal duration varies from 100 ms to 250 ms. Normal amplitude of T wave is $< 0.5$ mV. Inverted T wave may be indicative of myocardial infarction, high intracranial pressure, or metabolic abnormalities.

***ST segment***: The segment between the end of QRS complex and beginning of T wave in the ECG waveform is called ST segment. Its normal duration is 80-120 ms. In normal conditions, it is an isoelectric line. However, in abnormal condition it may get up or down slope. The shape of ST segment plays an important role during heart diagnosis. A depressed or elevated ST segment represents a case of myocardial infarction or ischemia.

***QT interval***: It represents the duration in ECG signal between start of QRS complex and end of T wave. Normally, QT interval lies between 350 to 450 ms. A reduced QT interval may be a sign of tachycardia, whereas a prolonged QT interval indicates ventricular tachyarrhythmias.

***U wave***: It is generally not found in most of the ECG waveforms. U wave is a small deflection after T wave. In abnormal conditions, U wave amplitude may get inverted or becomes tall with amplitude of 0.2 mV or more.

***RR interval***: The duration between one R wave in one heart beat to the neighboring R wave is termed as RR interval. It is the heart rate, which represents the duration of cardiac cycle.

The bandwidth of ECG signal is 0.05 to 100 Hz. In some pathological cases, it may also go up to 120 Hz.

## 1.2 Multi-channel/Multi-lead ECG

In standard practice, ECG signals are recorded in a 12-lead format [5]: Lead I, Lead II, Lead III, aVR, aVL, aVF, V1, V2, V3, V4, V5, V6. This simultaneous recording of twelve channels is called multichannel/multi-lead ECG (MECG). In this lead format, Lead I, Lead II, Lead III are called limb leads as they are captured from the surface of body limbs. Lead aVR, aVL, aVF are called augmented limb leads. Remaining six leads, i.e., V1 to V6 are captured from the standardized positions on the chest and called precardial or chest leads. From these twelve leads, eight leads, i.e., Lead I, Lead II, V1, V2, V3, V4, V5, V6 are also called independent leads, and the remaining four, i.e., Lead III, aVR, aVL, aVF are called derived leads. There are 10 electrodes that are used to record 12-channel ECG. Four electrodes are placed at the limbs and six at the chest. Right leg (RL) electrode is taken as the reference electrode. Leads I, II, and III are also termed as bipolar leads as they are recorded as the difference of potentials of two electrodes. Augmented limb leads are also derived from the same three electrodes from where limb leads are derived. Chest leads are called unipolar leads as they are recorded as the direct potential at chest electrodes. Figure 1.2 shows the lead configuration during MECG recording using right arm (RA), left arm (RA), and left leg (LL). The three limb leads, i.e., Lead I, Lead II, and Lead III forms a hypothetical triangle around the heart, which is called as Einthoven's triangle. Among the limb leads, only lead I and lead II are independent and other dependent leads can be derived using these two leads.

For augmented leads aVR, aVL, aVF, Wilson's central terminal plays the role of negative electrode, i.e., reference. Along with Einthoven's triangle, Figure 1.2 also shows the Wilson's central terminal. This terminal is formed when all the three limb leads are combined. The augmented leads can be

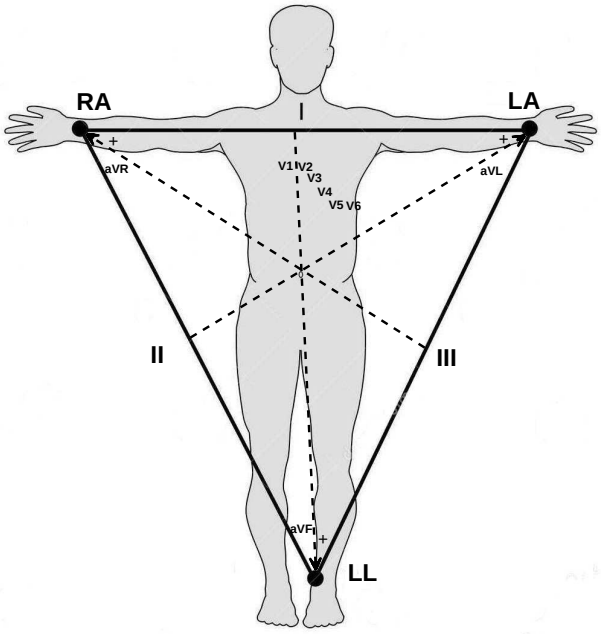


**Figure 1.2:** Lead configuration for 12-channel MECG recording. Einthoven's triangle and Wilson's central terminal are also shown.

synthesized with the help of limb leads using the following linear relations:

$$aVR = (Lead\ I + Lead\ II)/2$$

$$aVL = Lead\ I - (Lead\ II)/2$$

$$aVF = Lead\ II - (Lead\ I)/2$$

.

Wilson's central terminal is also taken as reference for the chest leads. For recording of chest leads, there are standardized positions on the chest. For example: electrodes are placed at the fourth intercostal space just to the right and left of the sternum, respectively, to record signals from lead V1 and V2. ECG signal at lead V4 is recorded by placing the electrode at the fifth intercostal space at the midclavicular line. Lead V3 is placed between lead V2 and lead V4. For V5 and V6, electrode positions remain at the same level as in the case of lead V4 but positions are at anterior axillary line and midaxillary line.

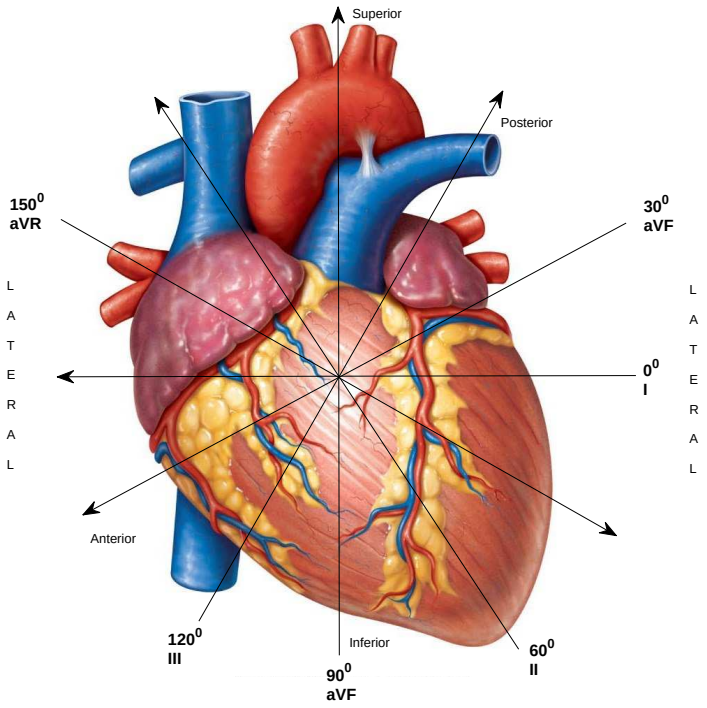


(a)

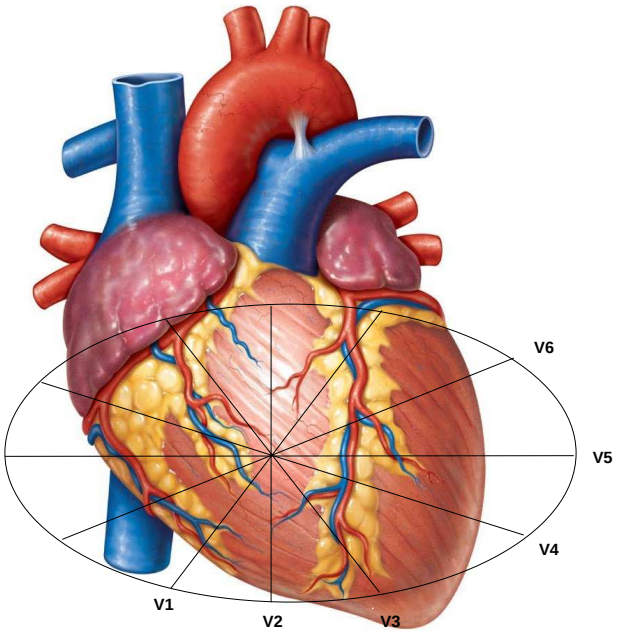


(b)

**Figure 1.3:** (a) Electrical axes for vertical directional views of the heart for bipolar limb leads and augmented limb leads. (b) Viewing the heart in horizontal plane with chest leads.

**Table 1.1:** Orientations of important ECG waveforms in different leads of 12-lead MECG with different views of heart

| Leads | P Wave | QRS-complex | T wave | Views |
|---|---|---|---|---|
| I | upright | upright | upright | lateral |
| II | upright | upright | upright | inferior |
| III | upright | upright | upright | inferior |
| aVR | negative | negative | negative/upright | right atrium/left ventricle |
| aVL | upright | upright | upright | lateral |
| aVF | upright | upright | upright | inferior |
| V1 | upright/biphasic | small R wave/QS | upright | septum |
| V2 | upright/biphasic | small R wave/QS | upright | septum |
| V3 | upright | equiphasic/QRS upright | upright | anterior |
| V4 | upright | upright | upright | anterior |
| V5 | upright | upright | upright | lateral |
| V6 | upright | upright | upright | lateral |

### 1.2.1 Clinical significance of MECG

The human heart is a three-dimensional organ. Therefore, viewing it from all the directions is important from diagnostic point of view. The clinical 12-lead ECG system captures electrical activities of heart from different narrow angles in the three-dimensional space. A three-dimensional view of heart with the direction of different leads is shown in Figures 1.3(a) and 1.3(b). Original heart image is taken from the web source (https://www.thinglink.com/scene/715516620675481600). It can be seen that the six limb leads (three bipolar and three augmented) and six chest leads view the heart in vertical (frontal) and transverse (horizontal) planes, respectively. The twelve leads align with different anatomical areas of the heart and are categorized in four groups: inferior, lateral, septal, and anterior. The inferior leads include lead II, III, and aVF and look at the heart from inferior or diaphragmatic surface. Lateral leads include lead I, aVL, V5, and V6 and view the heart from lateral wall of left ventricle. Lead V1 and V2 are called septal leads and depict electrical activities of the heart from septal surface (inter-ventricular septum). Anterior anatomy (sternocostal surface) of the heart is captured by lead V3 and V4. Thus, it can be concluded that the MECG signals provide spatio-temporal variations of various electrical activities of the heart and help in better understanding of its functionalities. Any deviations in these signals from their normal characteristics may provide pathological clues, important for detection of cardiac abnormalities.

### 1.2.2 Characteristics of ECG signals in different leads

ECG signal characteristics in different channels vary in normal and pathological cases. Different waveforms in the ECG also vary with different views of the heart (from different angles) in all leads. A summary of the orientations of different ECG waveforms in normal cases is given in Table 1.1. In normal conditions, P wave is upright in leads I and II and always inverted in lead aVR. In abnormal atrial rhythm conditions like in dextrocardia, P wave may get inverted in lead I. The duration of P wave changes in left atrial enlargement, which is prominently visible in leads I, II, and aVF. Most important ECG waveform, i.e., QRS-complex, is positive in lead I and lead V6 and its polarity reverses in lead aVR and lead V1. The height and width of QRS-complex signifies important pathological characteristics in conduction diseases such as bundle branch block. Changes appear in the form of wide, slurred S wave in leads V5, V6, I and a secondary R wave (R') in V1 or V2 (i.e., M-shaped rSR', rsR', or rsr' complex). The T wave usually follows the orientation of QRS-complex and hence is inverted in aVR and may get inverted in lead III. It is always upright in leads I, II, and V4 through V6. Commonly, T wave is inverted in lead V1 and occasionally it is accompanied by similar inversion in lead V2. However, isolated T wave inversion is a pathological condition. An inverted T wave in leads I, II, and V3 through V6 accompanied by ST segment depression is highly suggestive of myocardial ischaemia. A tall T wave is observed in the case of severe myocardial ischemia.

## 1.3 Telemonitoring Systems for Physiological Signals

The ever increasing population of elderly people and skyrocketing healthcare costs have posed many challenges for current healthcare systems worldwide [1, 6]. More importantly, traditional healthcare infrastructures seem unsustainable under future healthcare demands and require a major technological up-gradation. In recent years, there has been significant academic and industrial interests towards development of more scalable and cost-effective healthcare solutions. Wireless body area networks (WBANs) promise affordable remote healthcare solutions for next-generation of e-healthcare systems [6–9]. It focuses more on managing of wellness rather than illness by allowing early medical intervention. WBAN-enabled telemonitoring systems allows personalized real-time and long-term ambulatory monitoring of vital health parameters of a patient and provide medical feedback to maintain optimal health status. Integrated with smart telemedicine system, it can even alert to a medical

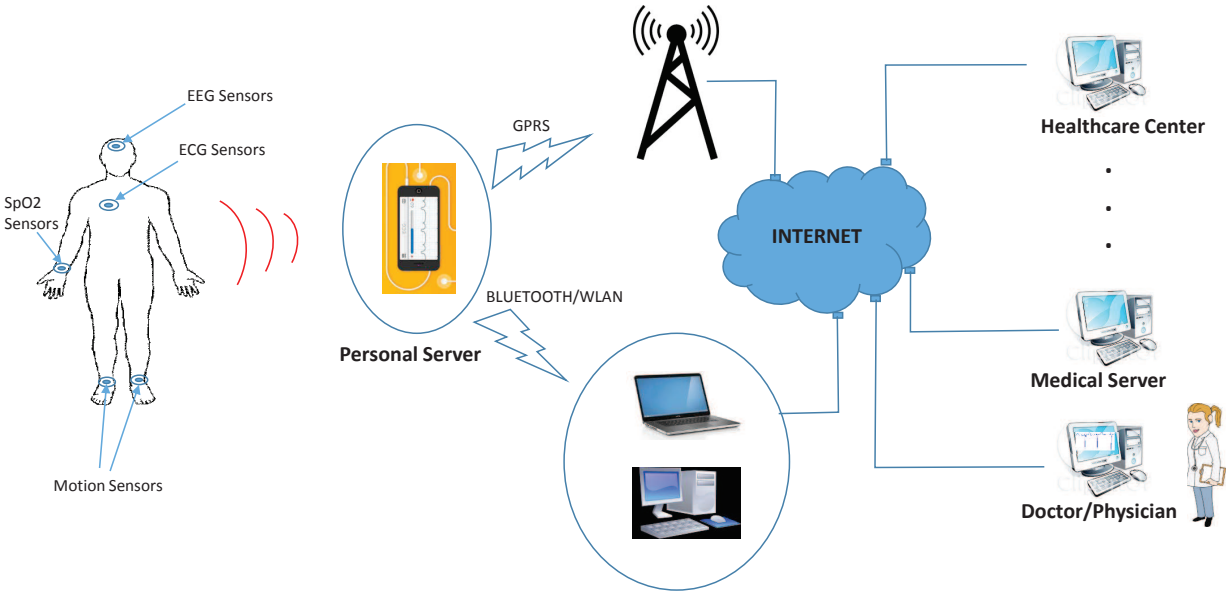


**Figure 1.4:** Illustration of a typical wireless body area network (WBAN)-enabled health monitoring system for acquisition and transmission of physiological signals

expert/physician during medical emergency conditions.

A typical WBAN-enabled physiological signal monitoring system is shown in Figure 1.4. It consists of various battery powered wireless sensors that operate within, on, or at close proximity to the human body [6]. They capture physiological signals such as ECG, electroencephalogram (EEG), blood pressure signals, etc. from different parts of the body. These signals are then wirelessly transmitted to a personal server that may run on a cell phone or personal computer. The acquired physiological signals are finally sent to the physician/medical server/healthcare centers through Internet/GPRS services. There may be another communication scenario possible, where the personal server running on a Bluetooth or WLAN can communicate to the remote terminals through a home computer. The personal server acts as an interface between senor nodes and medical server. There can be temporary medical data storage on the personal servers which upload the data to medical servers when network connection is available. Finally, the medical servers recover the original data via Internet, which is then analyzed by the medical experts and medical feedback is provided to the patient accordingly.

Recent decade has witnessed significant development in WBAN-enabled monitoring applications ranging from healthcare [10–13] to physical activities monitoring [14, 15]. Healthcare monitoring

applications include monitoring of vital health parameters, such as blood pressure [12], pulse rate [16, 17], neural activity, etc. For neural activity monitoring, EEG signal is monitored [18]. Wireless sensor devices have also been developed for gait parameters monitoring [19, 20]. WBAN systems with EMG sensors are proposed for human balance and fall detection [21, 22]. The issue of security of medical data in telemonitoring applications is studied by Zhang et al. [23], who proposed a ECG-based cryptography and authentication method.

## 1.4 ECG Telemonitoring Systems

Continuous heart monitoring is required to diagnose any life-threatening changes that may occur for a heart patient. For example, a probable myocardial infarction case can be diagnosed through continuous ECG monitoring for a couple of days. Also, while tracking the recovery status of a cardiac patient after myocardial infarction, long-term ECG monitoring proves to be quite helpful in capturing the diurnal and circadian variations, which are very good recovery indicator of myocardial infarction [6]. This is the reason, ECG signal telemonitoring plays a vital role in WBAN-based remote healthcare applications [24–26]. Important heart parameters, such as heart rate and heart rate variability (HRV) can be easily analyzed using ECG signals. Wired ECG acquisition in hospitals allows limited autonomy and maximum discomfort to the patients, whereas WBAN-enabled ambulatory ECG provides greater patient mobility and may even allow heart monitoring in practical real world conditions, such as exercising, running, etc., thus making heart monitoring clinically more relevant.

Existing telemonitoring systems are mostly for single channel ECG [27–30]. However, researches have been underway to develop efficient and inexpensive multi-channel ECG monitoring systems [24, 31–34]. Alesanco et al. [27] have presented a real-time cardiac telemonitoring system where the authors have taken into account both the technical and clinical aspects. ECG transmission and reception is studied under a new protocol, which manages to introduce a monitoring buffer and allows retransmissions of erroneous packets and also evaluates it from a clinical point of view. In another work, a multipoint video conference-based ECG monitoring system is proposed by Matsunaga et al. [28]. An approach for source compression is presented by Agarwal et al. [29], where the authors have proposed an architecture for analog-to-information converter for ultra-low-power ECG monitoring applications. An ECG acquisition system with ZigBee protocol is proposed, which is specialized for wireless ECG

monitoring [35]. A joint compression and QRS detection algorithm in wireless wearable sensor is proposed recently by Deepu et al. [30].

WBAN-enabled ambulatory ECG systems capable of operating for longer duration is the primary requirement for their large-scale and cost-effective deployment. However, higher energy cost of the state-of-the-art systems does not allow them for long time operation resulting into limited autonomy and low clinical relevance [24–26]. This is one of the potential challenge before existing systems and needs major breakthroughs.

Power consumption profile of WBANs suggests that there are three major energy consuming processes: signal processing, sensing, data transmission [36, 37]. The signal processing and sensing involve energy consumption during signal sampling and acquisition operations. Transmission power is the power required in transmitting the medical data through wireless links and can be minimized by compressing the ECG signals at the sensor nodes before their transmission. Mamaghanian et al. [1] have experimentally proved through a hardware demonstration that signal sensing/sampling operation consumes a significant chunk of power in WBAN operation. This study highlighted the importance of energy-efficiency of the embedded data compression algorithms apart from their data compression capabilities for power-limited telemonitoring applications. The traditional wavelet-based ECG compression techniques have high data compression capabilities, but their data encoding cost is too high [1]. Different process such as filtering, thresholding, peak detection, etc. involved with wavelet-based techniques increase the circuitry complexity and hence power consumption [38, 39]. Therefore, they are not preferred in resource constrained data compression applications [1, 39]. In recent years, compressed sensing (CS)-based data compression techniques have emerged as a potential alternative to wavelet-based methods in wearable ECG applications. CS allows merger of sensing/sampling and compression operations in a single process, hence also called compressive sampling [40], and substantially reduces the energy cost of the existing WBAN systems. Most of the recent works [1, 41–46] in ambulatory ECG are based on this new signal processing paradigm.

## 1.5 Compressed Sensing-based Telemonitoring Systems

CS-based data compression techniques are more preferable in WBAN applications because of their capability to boost the energy efficiency of the system through substantial reductions in the signal

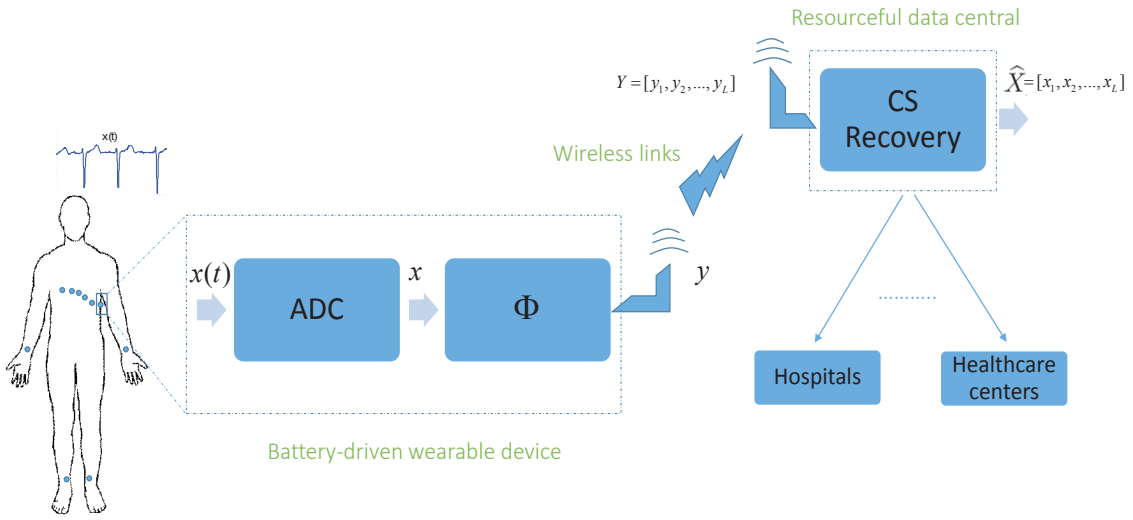


**Figure 1.5:** A typical compressed sensing-based wireless telemonitoring system

processing resources (computations and memory) and architecture [1,47]. During recent years, CS has emerged as a promising framework to address the energy consumption and complexity issues in long-term telemonitoring of physiological signals. CS is a signal processing technique that enables signal reconstruction from a small set of linear projections, called *measurements*, provided the signal is sparse in some domain [40]. CS exploits the signal structure and enables data acquisition at sub-Nyquist rate, outputting directly the compressed form of the signal. Consequently, the signal encoding becomes quite simple and energy-efficient in the CS framework. This feature of CS motivated its use in many resource-constrained applications [48–52]. A typical block diagram of a CS-based telemonitoring system is shown in Figure 1.5. The figure illustrates a digital paradigm of CS, called 'digital CS' [1], where a simple matrix-vector multiplication after analog to digital conversion (ADC) gives the compressed form of the physiological signal $\boldsymbol{x}$. The reduced dimension vector $\boldsymbol{y}$, also called the compressed measurement vector, is sent to the remote terminals (Hospitals/Health care centers) through the wireless links, where the original signal is reconstructed using CS-based recovery techniques and can be used further for clinical purposes.

In WBAN-enabled health monitoring applications, CS has been extensively used in a energy-efficient data compression framework. In one of the earliest work, Aviyente et al. [53] have investigated the CS framework of data compression for single and multi-channel EEG signals. Further, a similar framework is proposed by Kamal et al. [54] for multi-channel cortical signals. Implementations and

practical details of CS application to EEG signals is presented by Abdulghani et al. [55]. More details about CS application to WBAN system can be found in a survey presented by Balouchestani et al. [56].

Mazumdar et al. [36,57] have done extensive study on the CS-based applications and contributed significantly in the area of WBAN-based EEG signal monitoring. They have mainly proposed multiple measurement vector-based analysis prior formulation for EEG signals in CS-based applications. Shukla and Mazumdar have studied multi-channel EEG signals in WBAN applications [37] and proposed a blind CS approach for their reconstruction [58,59]. A co-sparsity and low-rank optimization-based CS for EEG signal is proposed by Liu et al. [60]. Here, the authors have introduced a co-sparsity-based CS recovery approach in place of widely used sparsity-based recovery for simultaneous reconstruction of multi-channel EEG signals.

In recent years, Zhang and his co-workers have given a new thrust to the CS and sparse representation-based biomedical applications using Bayesian learning framework. They reported several works that include EEG signal monitoring [18, 39, 61], fetal-ECG extraction and its remote monitoring [42, 62], heart monitoring through photoplethysmographic signals [63–67], and Alzheimer's disease analysis [68].

Analog CS framework has been studied by Balouchestani et al. [69–71] for surface EMG monitoring applications . They have also employed the analog CS approach to design biomedical sensors [72]. A new channel model for WBAN is proposed by the same authors using the CS theory [73].

In WBAN-enabled ECG telemonitoring applications, CS has been successfully used to lower the on-chip computations, energy consumption, and complexity of the system [1]. Sparse nature of ECG signals enables application of CS for ECG data compression/reconstruction. CS-based data reduction approaches have exploited the sparsity of ECG signals either in time domain [41–43], or in wavelet domain [1,44–46]. A signal is said to be sparse or compressible in a transform domain if it is representable in terms of a few basis functions of that domain. The amplitude plot of transform domain signal coefficients should have a exponential decay characteristic. Faithful CS recovery of a signal depends on its sparse nature, which makes possible the recovery of a higher dimensional signal from low dimensional signal measurements. Sparser the signal, better is the recovery. For ECG signals, Mamaghanian et al. [1] have established and quantified the potential of CS for the first time for low-complexity and energy-efficient data reduction in the WBAN-enabled ECG monitors. Various design considerations are further studied by Dixon et al. [41] for the CS-based data acquisition and reconstruction systems.

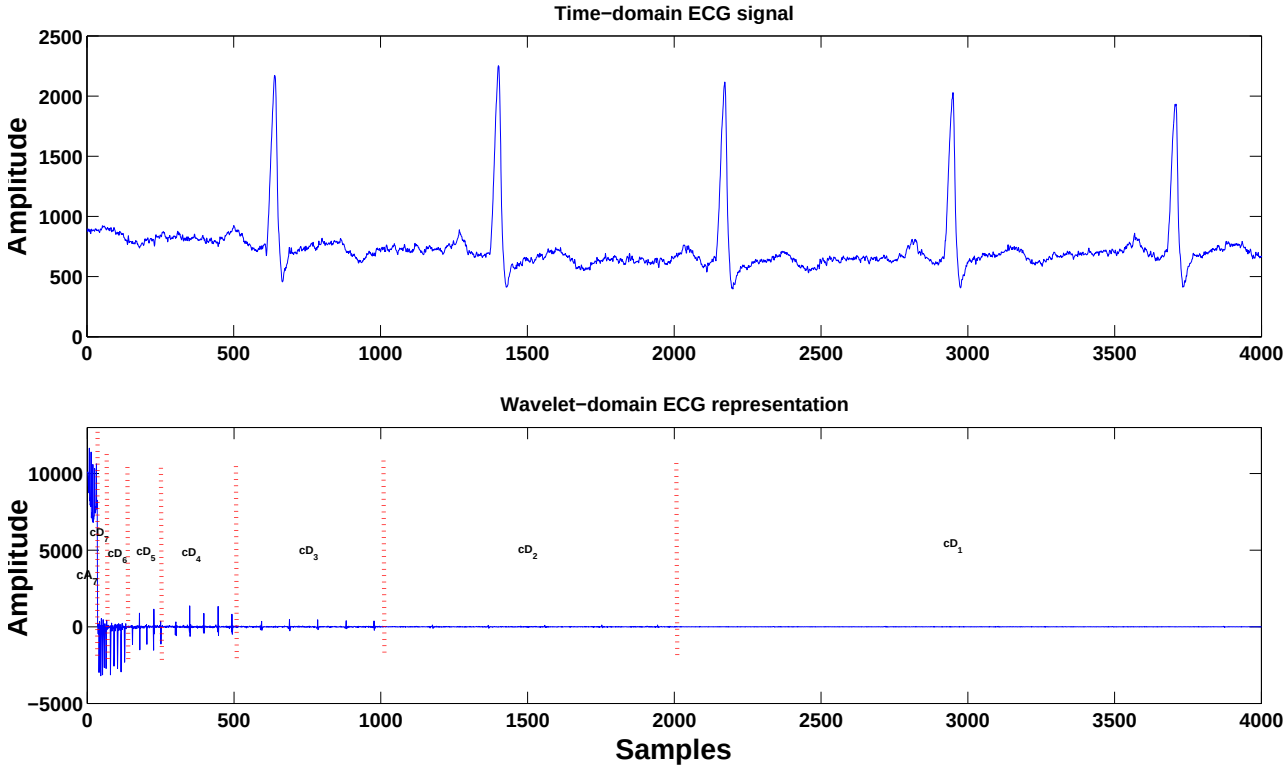


**Figure 1.6:** Time-domain and wavelet-domain ECG representation to illustrate the sparse nature of ECG signals in wavelet transform. Different wavelet subbands ($cA_7$ and $cD_1$-$cD_7$) at 7-level decomposition are also shown with demarcation lines.

In a similar framework, block sparse Bayesian learning-based approach is employed by Zhang et al. [42] for the fetal-ECG telemonitoring applications. Recently, some techniques utilizing prior knowledge about ECG signals in the traditional CS reconstruction algorithms have been reported with improved results [45,46]. Balouchestani et al. [74] proposed recently an advanced $K$-means clustering algorithm for large scale ECG data based on CS theory in combination with the $K$-singular value decomposition.

### 1.5.1 Sparsity analysis of ECG signals

The sparsity of ECG signals is a important characteristic, which enables application of CS to these signals. CS exploits this sparsity feature to retrieve back the time domain ECG signals using only a small set of signal measurements, $\boldsymbol{y}$. For ECG signals, there exist high activity region and low activity region in the signal waveform. Intense electrical activity is seen around QRS- complex whereas

minimum or no activity is noticed in isoelectric line in an ECG signal (Figure 1.6). So a fair amount of sparseness exist in time-domain [41]. This time-domain sparseness can be enhanced many folds by representing ECG signals in a transform domain. Sophisticated orthonormal transforms such as discrete wavelet transform (DWT), discrete cosine transform (DCT), and discrete Fourier transform (DFT), etc. are used generally for sparse representation. For ECG signals, DWT is mostly preferred as the sparsifying basis. The better time-frequency localization and high energy compaction property of DWT make it suitable for this purpose [1, 41, 42].

If $\boldsymbol{x} \in \mathbb{R}^N$ be the $N$-dimensional signal vector (say, a single channel ECG signal), then its sparse representation in terms of wavelet basis $\boldsymbol{\Psi} = [\boldsymbol{\psi}_1, \boldsymbol{\psi}_2, \boldsymbol{\psi}_3, \ldots, \boldsymbol{\psi}_N]$ can be written as follows: $\boldsymbol{x} = \sum_{i=1}^{N} \alpha_i \psi_i \quad or \quad \boldsymbol{x} = \boldsymbol{\Psi}\boldsymbol{\alpha}_k$, where $\boldsymbol{\alpha}_k$ is a $N$-dimensional transform coefficient vector with only $k$ significant (non-zero) coefficients ($k << N$). So, a sparse signal is representable in terms of linear combinations of $k$ terms of an orthogonal basis only, i.e., $\ell_2$-norm error $\|x - x_k\|_2$ (or $\|\alpha - \alpha_k\|_2$) is very small. Here, $x_k$ is the reconstructed version of $x$ using only $\alpha_k$ wavelet coefficients. An amplitude plot of wavelet coefficients of one lead ECG signal is shown in Figure 1.6. Sparse nature of ECG can be clearly seen in its wavelet-domain representation where only few coefficients carry most of the information. It is worth noting that significant number of coefficients are of very small amplitude and they belong to the clinically less important high frequency wavelet subbands ($cD_1$, $cD_2$ and $cD_3$). These wavelet coefficients can be considered zero without affecting the diagnostic contents of ECG signal, giving ECG a sparser behavior. The resultant representation is called best $k$-term sparse approximation or $k$-sparse ECG. To measure the sparsity following relation is used [41].

$$Sparsity\ (\%) = (1 - k/N) \times 100 \tag{1.1}$$

## 1.6 Distortion Measures

Any processing with ECG signals involves certain loss of information. Therefore, it becomes important to quantify the loss of information from the clinical perspective in order to make correct diagnostic decision. In an ECG signal, the clinical information lies in PQRST morphologies. The amplitude and duration of different waves and segments within PQRST gives significant clues to cardiologists to detect/locate the pathological condition of a patient. To determine the same, delineation algorithms are required which give start and end points of ECG waves. Once the time instants are located, other

wave characteristics can be computed for automated beat classification. The classification results can be used to establish the accuracy of the processed ECG signals.

QRS-complex is a very important wave in the ECG signals and carry vital clinical information. Its preservation in the processed/reconstructed ECG is very important from diagnostic perspective. In arrhythmia monitoring, accurate QRS detection is important, which is used to compute the heart rate of the patient. There are numerous algorithms reported in the literature for QRS detection which are mainly based on derivatives, filter-banks, wavelets, mathematical morphology and correlation [75, 76]. The detected R-wave can also be used further to compute other important ECG parameters, such as ST segment which is used for the reliable classification of normal and ischemic beats. Pan-Tompkins [77] and its successor Hamilton-Tompkins [78] are two well known algorithms for R wave detection with highest detection accuracy of 99.68% with sensitivity 99.63%.

There are some specific signal distortion measures which are used to compute the distortions in ECG data compression applications. These fidelity assessment parameters include normalized mean square error (NMSE), root mean square error (RMSE), normalized RMSE, percentage-root mean square difference (PRD), and signal to noise ratio (SNR). These are the global error analysis parameters and measure the difference between the original and final reconstructed ECG signal. For local error analysis maximum absolute error (MAE/MAX) or peak-error (PE), standard error (StdErr), and normalized NMAE are used. Signal similarity can also be calculated using normalized cross correlation. Though above distortion measures give an idea about the distortion being incurred during various ECG processing, ECG signal should also be evaluated from clinical point of view to assess diagnostic distortion. There are few diagnostic distortion measures reported in the literature, such as weighted diagnostic distortion (WDD) [79], wavelet weighted PRD (WWPRD) [80], and wavelet energy-based diagnostic distortion (WEDD) [81]. Sometimes, classification accuracies are also used to establish the clinical information preservation in the reconstructed ECG signals.

## 1.7 Scope for the Present Work

During diagnosis of a heart abnormality, patients are kept under continuous supervision and ECG signal is monitored for several hours/days to reach a diagnostic conclusion. The ever increasing number of cardiac patients and the escalating levels of medical supervision are attributing towards increasing

healthcare costs [1]. Also, it is not always possible for the patient to be physically present in the hospital/healthcare center, especially for elderly patients and pregnant women who require frequent medical attention. So, there is scope for major technological up-gradation of existing traditional healthcare systems. WBAN promises next-generation affordable healthcare solutions for remote health monitoring. However, the practical requirements for WBANs to perform long-term clinically relevant telemonitoring in free living conditions impose various limitations on it, such as energy efficiency, computational complexity, memory usage, etc. Therefore, there is a need to develop ultra-low power signal processors embedded with low complex and energy-efficient data compression algorithms to reduce the overall power consumption. CS-based data compression approaches have shown encouraging results in this area and emerged as a potential alternative to traditional wavelet-based methods. The wavelet-based ECG encoders have more number of signal processing modules, which attributes towards bulky and power-inefficient system. This is the reason, wavelet-based encoders are not preferred in energy-constrained telemonitoring applications. On the other hand, CS allows to save significant amount of energy during data encoding [1], minimizes on-chip computational resources [61] and is robust to packet loss during wireless data transmission [39, 82].

MECG signals are preferred by cardiologists over single channel ECG since they represent complete conduction sequence of heart and carry significant clinical clues in multiple leads required for reliable diagnosis [5]. However, MECG signals have not been explored much in the CS framework and the existing CS-based ECG telemonitoring systems [1, 41, 42, 45, 46] are mostly limited to single channel only. Therefore, to make remote heart monitoring diagnostically more relevant and reliable, there is a need to develop an effective CS framework for MECG signals. Also, the inherent inter-channel (spatial) correlation across different channels in MECG is expected to boost significantly the CS recovery performance at low measurements (high compression ratios). Low measurement requirement directly corresponds to lower on-chip computations at node sensors and reduced volume of data to be sent over the power hungry wireless links. This may result in significant saving in energy cost of existing ECG telemonitoring systems, making them more autonomous with enhanced functionalities.

## 1.8 Organization of the Thesis

The contents of the thesis are organized as follows: In **Chapter 1**, introduction to ECG signals and CS-based WBAN system for ECG telemonitoring are discussed. In **Chapter 2**, a related review of different CS-based works for ECG signals is given. CS framework for multi-channel ECG signals and the motivation for the present work is discussed. An eigenspace CS approach is discussed for multi-channel ECG data compression in **Chapter 3**. In **Chapter 4**, a low-complex joint CS encoding scheme along with a weighted mixed-norm minimization (WMNM)-based joint sparse recovery algorithm is proposed for joint CS of MECG signals. Emphasizing important ECG features during CS recovery through weighting approach is investigated. In **Chapter 5**, a new subband weighting-based WMNM algorithm is explored, which exploits multi-scale ECG signal information to emphasize clinically important ECG features lying in different wavelet subbands. Additionally, a block-sparsity-based joint CS recovery is also explored in this chapter. The thesis is concluded in **Chapter 6** with major contributions from this thesis and scope for further research.

# 2

# Compressed Sensing for ECG Signals- A Review

Contents

Telemonitoring is an e-healthcare application where vital health parameters of a patient are monitored remotely and medical feedback is provided accordingly. It generated significant interest in research community in recent years due to the advancements in the area of wireless body area network (WBAN). ECG telemonitoring is important for early medical intervention for cardiac patients, whose numbers have been on the rise in recent decades [1]. So far, ECG remote monitoring being a costly affair is limited to mostly single channel ECG signals. The 12-lead multi-channel ECG (MECG) system shows a spatiotemporal sequence of cardiac events and hence cater the need of a diagnostic and prognostic tool for the cardiologists. Hence, it is required to study MECG telemonitoring systems for quick and reliable detection of cardiovascular diseases. WBAN technology promises affordable and continuous personalized health monitoring for next-generation of tele-cardiology systems. However, state-of-the-art WBAN-enabled ECG telemonitoring systems still face challenges in terms of energy efficiency, computational complexity, memory usage [1], etc. To address these challenges, ultra-low power digital processors associated with low-complex and energy-efficient data compression algorithms are required. Traditional wavelet-based data encoders do not cater to these needs due to their high data encoding cost. Compressed sensing (CS) framework may be a viable option for WBAN-enabled telemonitoring applications due to its simple and energy-efficient data reduction procedure.

In this chapter, a brief introduction of CS and its application to ECG/MECG signals are discussed. The organization of this chapter is as follows: Section 2.1 discusses background of CS technique. It also includes discussion of wavelet transform and its employability as a sparsifying basis for CS. In Section 2.2, a thorough review of different CS-based single channel ECG data compression methods have been discussed. Multi-measurement vector framework of CS for multi-channel ECG signals is discussed in Section 2.3. In Section 2.4, various distortion measures which are used to gauze the distortion incurred during different ECG processing are discussed. Details about the databases used for the thesis evaluation are discussed in Section 2.5. Motivation for the present work is presented in Section 2.6.

## 2.1 Basics on Compressed Sensing

Let $\boldsymbol{x} \in \mathbb{R}^N$ be the $N$-dimensional signal vector (say, a single channel ECG signal). Let us also assume that $\boldsymbol{x}$ is having sparse behavior in a transform domain, i.e., signal is representable in terms of linear

combinations of only $k$ terms of an orthogonal basis $\boldsymbol{\Psi} = [\boldsymbol{\psi}_1, \boldsymbol{\psi}_2, \boldsymbol{\psi}_3, \ldots, \boldsymbol{\psi}_N]$ as follows:

$$\boldsymbol{x} = \sum_{i=1}^{N} \alpha_i \psi_i \quad or \quad \boldsymbol{x} = \boldsymbol{\Psi}\boldsymbol{\alpha}_k \tag{2.1}$$

where $\boldsymbol{\alpha}_k$ is a $N$-dimensional transform coefficient vector with only $k$ significant (non-zero) coefficients ($k << N$). For such sparse signals, the compressed sensing (CS) theory states that acquiring $k$ samples through a nonadaptive linear measurement/projection would be suffice to capture the underlying signal information [40,83]. Thus, CS enables a merger of sensing/sampling and compression processes, which take place simultaneously during CS operation, hence also called compressive sampling. In this way, CS allows a significant reduction in the circuitry requirement during signal acquisition, which makes data encoding quite simple and energy efficient. In a linear measurement process, CS collects $M$ samples using measurement vectors $\{\boldsymbol{\phi}_j\}_{j=1}^{M}$ as follows:

$$y_j =< \boldsymbol{x}, \boldsymbol{\phi}_j >, \quad j = 1, 2, ..., M \quad or \quad \boldsymbol{y} = \boldsymbol{\Phi}\boldsymbol{x} \tag{2.2}$$

where $\boldsymbol{\Phi} \in \mathbb{R}^{M \times N}$ is a sensing or measurement matrix comprising of measurement vectors $\boldsymbol{\phi}_1$, $\boldsymbol{\phi}_2$,...,$\boldsymbol{\phi}_M$ in rows on which signal vector $\boldsymbol{x}$ is linearly projected to get measurements $\boldsymbol{y}$. By employing measurement vectors $\{\boldsymbol{\phi}_j\}_{j=1}^{M}$ as continuous sensing waveforms $\{\boldsymbol{\phi}_j(t)\}_{j=1}^{M}$, directly compressed measurements of analog signals can also be obtained prior to analog to digital conversion (ADC). This approach is called 'analog CS' and allows analog to information conversion (AIC) in place of ADC, where signal can be sampled at the information rate that is much below the traditional Nyquist rate sampling [1,84]. However, the present thesis confines to the study of discrete signals in CS framework, which is sometimes also referred to as 'digital CS' [1].

CS recovery involves reconstruction of original sparse signal given its compressed measurements and sensing matrix. In (2.2), it is assumed that signal $\boldsymbol{x}$ is sparse in itself, i.e., $\boldsymbol{\Psi} = \boldsymbol{I}$ in (2.1). So, the same relation (2.2) is used for CS recovery. However, if the signal is not sparse in itself, but sparse in a transform domain $\boldsymbol{\Psi}$ , the signal is replaced by its transform domain representation in (2.2) as:

$$\boldsymbol{y} = \boldsymbol{\Phi}\boldsymbol{\Psi}\boldsymbol{\alpha}_k = \boldsymbol{\Theta}\boldsymbol{\alpha}_k \tag{2.3}$$

where $\boldsymbol{\Phi}\boldsymbol{\Psi} = \boldsymbol{\Theta}$. In this case, CS recovers the transform domain signal, which can be transformed back to time domain using inverse transformation. For instance, ECG signal is sparse in wavelet domain,

therefore, sparsifying basis $\mathbf{\Phi}$ is generally taken as wavelet transform and the recovered sparse vector $\boldsymbol{\alpha}_k$ consists of the wavelet coefficients.

Now, there are three issues to be addressed in a CS problem:

- To find a sparsifying transform where signal $\boldsymbol{x}$ can be represented in sparse form.
- To design an efficient sensing matrix $\mathbf{\Phi}$ so that the salient information in $\boldsymbol{x}$ do not lost while dimensionality reduction from $N$-dimensional signal space to $M$-dimensional measurement space ($M << N$).
- To have a sparse recovery algorithm that can reconstruct back the $N$-dimensional signal $\boldsymbol{x}$ using only $M \approx k$ measurements $\boldsymbol{y}$.

### 2.1.1 Wavelet transform as sparsifying basis in CS-based applications

Discrete Wavelet Transform (DWT) is an alternate way of signal representation. DWT has very good energy compaction and time-frequency localization property which helps grossly segment the clinical information present in ECG signals in different wavelet subbands (Figure 2.1). The gross segmentation of features in specific wavelet subbands gives more control over clinically relevant information and helps retain them in various signal processing tasks. This is the reason DWT has been a very attractive tool among the signal processing community for analyzing biomedical signals like ECG. DWT has been extensively used for ECG data compression applications [85–88]. DWT helps confine the diagnostically important ECG features within a few low frequency subbands. Therefore, a large number of high frequency wavelet subband coefficients (especially from $cD1$, $cD2$, and $cD3$ subbands) can be zeroed without affecting the clinical features of ECG. This helps in data compression and signal denoising as well. However, despite their high data compression abilities, the DWT-based techniques are not found suitable for resource-limited applications, such as WBAN-enabled ambulatory ECG monitoring. This is because of different processes involved in transform-based data encoders such as noise-cancellation, filtering, thresholding, etc., which increase the circuitry complexity and results in a slower, bulkier and power-inefficient data-encoder [1, 39]. WBAN-enabled ECG telemonitoring involves miniaturized sensors driven by power-limited batteries. So, in these applications, transform-domain ECG compressors are not found suitable. CS-based embedded data compression techniques

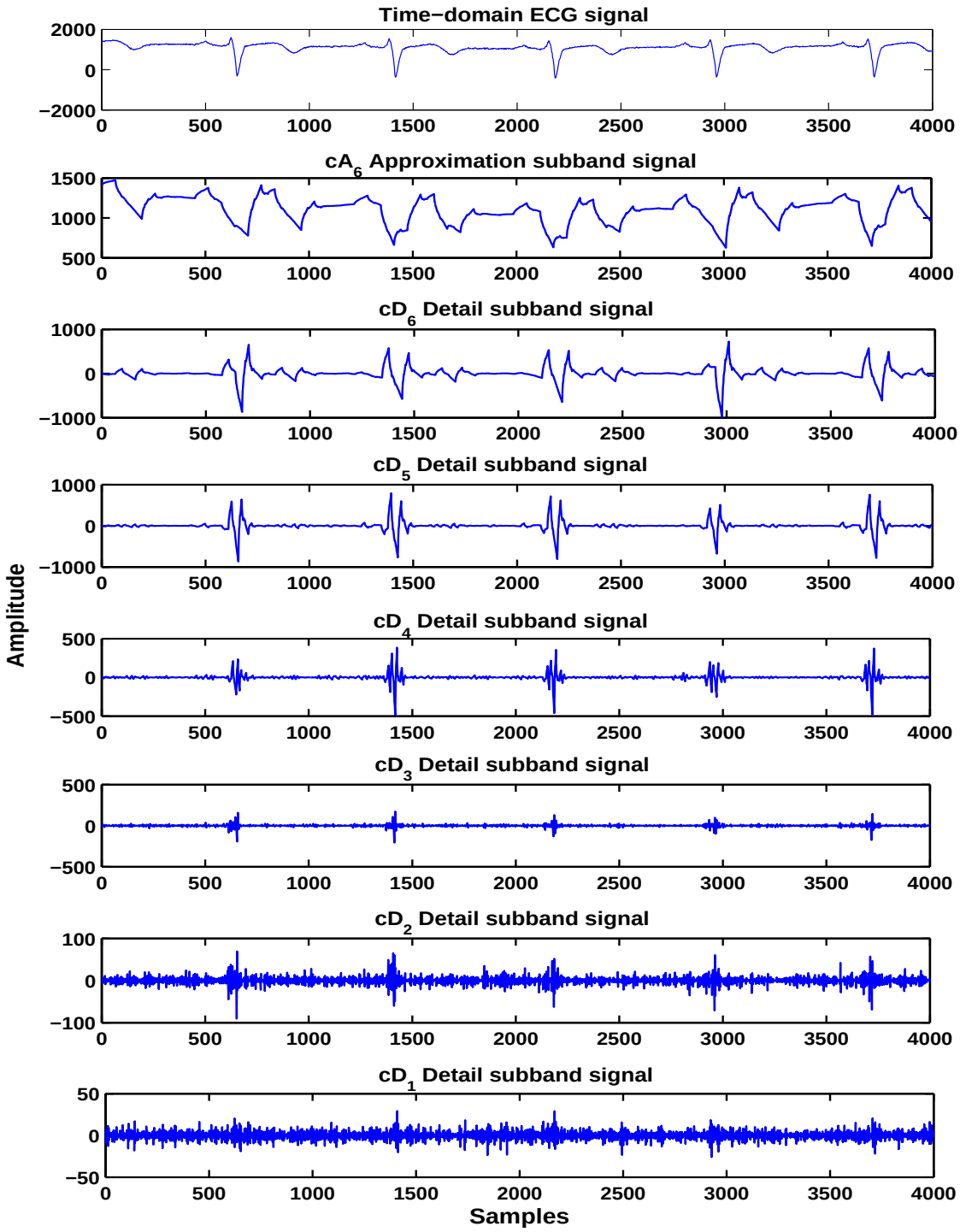


**Figure 2.1:** Distribution of ECG information in various wavelet subbands

involve low-complex and energy-efficient data reduction procedure and emerged as an effective alternative to wavelet-based ECG compression techniques for telemonitoring applications [1]. In CS-based

applications, sparsity feature of DWT is employed for data recovery task. DWT plays a vital role as the sparsifying transform ($\mathbf{\Psi}$) in CS-based ECG data compression applications [1, 41, 45, 46].

In DWT domain, the signal is decomposed and represented in terms of finite-energy waves called wavelets. Here, wavelets are the basis functions in DWT representation. Wavelets can be defined as the families of functions $\psi_{a,b}(t)$ generated by dilation and translation of a single mother wavelet $\psi$ and is given as follows [89, 90]:

$$\psi_{a,b}(t) = \frac{1}{\sqrt{a}}\psi\left(\frac{t-b}{a}\right) \tag{2.4}$$

where $a$, $b$ are the dilation (scaling) and translation parameters. The dilated wavelet function corresponds to the low frequency components, whereas the translated version corresponds to the high frequency components of the signal. Therefore, DWT allows a multi-resolution decomposition of the signal, where the signal is separated into finer parts called "details" and coarser representation called "approximation" [91, 92]. A function $f(t)$ can be represented as the linear combination of shifted and scaled version of the mother wavelet $\Psi(t)$ as:

$$f(t) = \sum_a \sum_b w_{a,b}\psi_{a,b}(t) \tag{2.5}$$

where $\psi_{a,b}(t)$ is the shifted and scaled version of the mother wavelet $\mathbf{\Psi}(t)$ and $w_{a,b}$ are the wavelet coefficients. Hence, from (2.5), the wavelet coefficients $w_{a,b}$ of a signal $f(t)$ are given by [93]:

$$w_{a,b} = \langle f(t), \psi_{a,b}(t) \rangle \tag{2.6}$$

Figure 2.2 shows an amplitude plot of wavelet coefficients in different ECG channels. Seven level wavelet decomposition is performed for each of the eight fundamental channels/leads using same Daubechies wavelets ($db4$). The clinically important ECG information are captured by only few significant wavelet coefficients in low frequency subbands of each lead. This results in a sparse representation of each individual lead signal and a joint sparse representation by all leads.

Multi-resolution analysis of DWT allows detailed study of subband level signals. It is obtained through filter bank implementation of DWT, where signal is passed through low-pass and high-pass filters. Low-pass filtered version of the signal is again filtered through a low-pass and high-pass filter pair in the next level of wavelet decomposition and this continues for further levels. If $\Phi(t)$ is a scaling function and $\Psi$ is a wavelet function, approximation ($cA_n(b)$) and detail ($cD_j(b)$) subbands coefficients

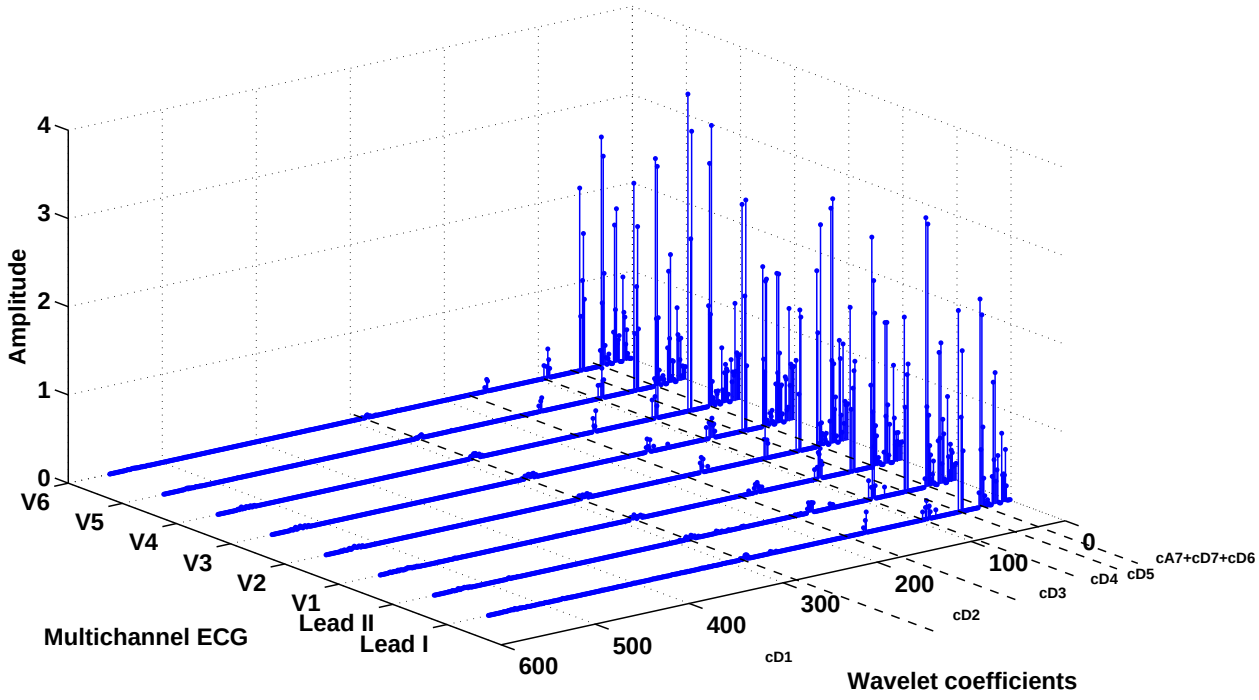


**Figure 2.2:** Amplitude plot of ECG wavelet coefficients in all eight independent channels in various subbands for 7 level wavelet decomposition

after $n$-level decomposition can be defined as: $cA_n(b) = \langle f(t), \phi_{a,b}(t) \rangle$ and $cD_j(b) = \langle f(t), \psi_{a,b}(t) \rangle, j = 1, ..., n$. Taking the example of ECG signal, the $n$ level wavelet decomposition of each lead of MECG gives $n+1$ number of subbands: $cA_n, cD_n, cD_{n-1}, ..., cD_2, cD_1$. Here, the subband $cA_n$ consists of the approximation coefficients and carries most of the low frequency information of the ECG signal. The finer details (or high frequency ECG information) are associated with $n$ number of detail subbands $cD_j, j = 1$ to $n$. This can also be verified from the Figure 2.1, where the distribution of ECG information is shown in various subbands.

In order to decide the number of levels of wavelet decomposition, frequency range of wavelet subbands should be known. The bandwidth $\Delta F_j$ of $j$-th wavelet subband is given by [81]:

$$2^{-j-1}.F_s \leq \Delta F_j \leq 2^{-j}.F_s \tag{2.7}$$

where $F_s$ is the sampling frequency of the signal. There is also a heuristic formula proposed by Fahoum

et al. [80] to decide the number of levels ($n$) and is given as:

$$n = [log_2(F_s) - 2.96] \tag{2.8}$$

### 2.1.2 Sensing matrix selection

The sensing matrix chosen for CS operation must satisfy two conditions, called incoherency and restricted isometry property(RIP), for faithful recovery of $N$-dimensional signal from an incomplete set of measurements $M(M < N)$. According to first condition, sensing matrix ($\mathbf{\Phi}$) should be incoherent to the selected sparsifying basis $\mathbf{\Psi}$, i.e., rows $\{\phi_j\}_{j=1}^{M}$ of $\mathbf{\Phi}$ can not be sparse representable in terms of columns of $\mathbf{\Psi}$ and vice-versa. Second condition, i.e., RIP says that $\mathbf{\Psi}$ must preserve the Euclidean length of $k$-sparse signals, i.e., $k$-sparse signals cannot be in the null space of $\mathbf{\Phi}$ [40, 83].

**Measure of incoherency**

The incoherency between the orthobases pair $(\mathbf{\Phi}, \mathbf{\Psi})$ is measured in terms of amount of coherency between the two orthobases. The coherence between the pair $(\mathbf{\Phi}, \mathbf{\Psi})$ is defined as [40]:

$$\mu(\mathbf{\Phi}, \mathbf{\Psi}) = \sqrt{N} \underbrace{\max}_{1 \leq j,k \leq N} |\langle \phi_j, \psi_k \rangle| \tag{2.9}$$

The coherence is a measure of largest correlation between any two elements of $(\mathbf{\Phi}, \mathbf{\Psi})$. If $(\mathbf{\Phi}, \mathbf{\Psi})$ have correlated elements $\mu$ would be larger and vice-versa. The maximum value of $\mu$ can be $\sqrt{N}$ and minimum is 1, i.e., $\mu(\phi, \psi) \in [1, \sqrt{N}]$.

**Restricted isometry property**

RIP states that for all $k$-sparse signals $\boldsymbol{x}$, following condition should be satisfied [40, 83]

$$(1 - \delta_k) \leq \frac{\|\mathbf{\Theta}\boldsymbol{\alpha}\|_{l_2}^2}{\|\boldsymbol{\alpha}_k\|_{l_2}^2} \leq (1 + \delta_k) \tag{2.10}$$

where $\delta_k > 0$ is a isometry constant. The sensing matrix $\mathbf{\Theta}(= \mathbf{\Phi}\mathbf{\Psi})$ is said to follow RIP of order $k$ if the isometry constant $\delta_k$ is not too close to 1. If RIP holds for the sensing matrix $\mathbf{\Theta}$, this implies that $\mathbf{\Theta}$ preserves approximately the lengths of all $k$-sparse vectors. In other words, the subset of $k$ columns of matrix $\mathbf{\Theta}$ are nearly orthogonal. To see how RIP helps in recovering sparse signals, let us assume that there are two $k$-sparse signals, $\alpha_1$ and $\alpha_2$. If $\mathbf{\Theta}$ follows RIP then according to (2.10)

pair-wise distance between the two $k$ sparse vectors is given by

$$(1-\delta_k) \leq \frac{\|\boldsymbol{\Theta}\boldsymbol{\alpha}_{k1} - \boldsymbol{\Theta}\boldsymbol{\alpha}_{k2}\|_{l_2}^2}{\|\boldsymbol{\alpha}_{k1} - \boldsymbol{\alpha}_{k2}\|_{l_2}^2} \leq (1+\delta_k) \tag{2.11}$$

The relation (2.11) suggests that all pair-wise distance between $k$-sparse signals will be well preserved both in original signal space and in measurement space, provided $\delta_k$ is sufficiently less than 1. This encouraging fact allows the development of efficient sparse recovery algorithms to find discriminating $k$-sparse signals based on their compressive measurements [40].

Random matrices with independent and identically distributed (i.i.d) Gaussian entries obey RIP and are incoherent to any chosen basis with overwhelming probability, provided $M \geq Ck\log(N/k) << N$, where $C$ is a constant [40, 83]. Therefore, for sensing operation during CS, random Gaussian matrices are best suited. If $\boldsymbol{\Phi}$ satisfies RIP then $\boldsymbol{\Theta} = \boldsymbol{\Phi}\boldsymbol{\Psi}$ also obeys RIP for any basis $\boldsymbol{\Psi}$. This makes the random sensing matrices $\boldsymbol{\Phi}$ universal in nature, where sparsifying basis $\boldsymbol{\Psi}$ is not even required to be known during sensing operation [40]. Throughout the thesis, we have used random sparse binary sensing matrix $\boldsymbol{\Phi} \in \mathbb{R}^{M\times N}$ with binary entries, i.e., $0s$ and $1s$. Each column of $\boldsymbol{\Phi}$ contains only $d$ number of nonzero values equal to 1 at random positions [46]. Random sparse binary matrices satisfy a modified RIP, referred to as $RIP_p$ [1]. Sparse matrices are memory efficient and involve lesser computations, thus help in minimizing the computational cost at the encoder [46].

### 2.1.3 Sparse recovery

In sparse recovery problem, also called CS recovery, the aim is to find a sparse vector $\boldsymbol{\alpha}_k$ given the measurements $\boldsymbol{y}$ and sensing matrix $\boldsymbol{\Theta}$ such that $\boldsymbol{y} \approx \boldsymbol{\Theta}\boldsymbol{\alpha}_k$. After getting $\boldsymbol{\alpha}_k$, original $\boldsymbol{x}$ can be recovered using $\boldsymbol{x} = \boldsymbol{\Psi}\boldsymbol{\alpha}_k$. For ECG signals, the sparse vector $\boldsymbol{\alpha}_k$ recovered after CS recovery is the wavelet coefficient vector, which is transformed back into time domain ECG signals using inverse wavelet transform.

CS recovery is an under-determined or ill-conditioned problem as sensing matrix $\boldsymbol{\Theta} \in \mathbb{R}^{M\times N}(M < N)$ is non-invertible, and infinitely many solutions exist for problem (2.3) [40]. A optimization approach is generally followed for sparse recovery. Since, the interest here is to find sparse signals, CS recovery searches for the sparsest signal that can best yield $\boldsymbol{y}$. The $\ell_0$-norm of a vector is defined as the number of nonzero entries, therefore, CS recovery problem is formulated as a optimization problem

with $\ell_0$-norm-minimization [40, 83, 94]:

$$\min\|\boldsymbol{\alpha}\|_0 \text{ subject to } \boldsymbol{y} = \boldsymbol{\Theta}\boldsymbol{\alpha}_k \tag{2.12}$$

Solution (2.12) is however computationally intensive as it involves combinatorial computational complexity. A feasible solution is to mathematically relax the $\ell_0$-norm and replace it with $\ell_1$-norm, defined as $\|\alpha\|_1 = \sum_{i=1}^{N} |x(n)|$. The problem (2.12) is reformulated as:

$$\min\|\boldsymbol{\alpha}_k\|_1 \text{ subject to } \boldsymbol{y} = \boldsymbol{\Theta}\boldsymbol{\alpha}_k \tag{2.13}$$

This approach is termed as basis pursuit (BP). The problem (2.13) can be seen as a convex relaxation of (2.12) and can be solved using linear programming with lesser computational complexity. This method gives a robust signal recovery with lesser error bound, provided the signal is sufficiently sparse in some transform domain $\boldsymbol{\Psi}$. For robust signal recovery in noisy conditions, the equality criterion in (2.13) is relaxed as:

$$\min\|\boldsymbol{\alpha}_k\|_1 \text{ subject to } \|\boldsymbol{y} - \boldsymbol{\Theta}\boldsymbol{\alpha}_k\|_2 \leq \varepsilon \tag{2.14}$$

where $\varepsilon$ is the noise tolerance. This relaxed approach is called basis pursuit denoising (BPDN). Beyond the convex optimization solutions, there are other sparse recovery algorithms also, such as greedy algorithms (orthogonal matching pursuit (OMP), compressive sampling matching pursuit (CoSaMP), etc.) [95, 96], Bayesian learning based algorithms [42], etc.

## 2.2 CS-based ECG Compression Techniques

In recent years, CS has emerged as a potential signal processing tool, which enables ultra-low-power ECG data compression and allows easy hardware implementation in wearable sensor devices for telemonitoring applications [1, 41, 42, 44–46, 52]. CS has been successfully used to reduce the energy consumption and complexity of the WBAN-enabled ambulatory ECG systems [1, 41, 42, 44–46]. For energy-efficient data reduction, CS-based techniques exploit the inherent sparse nature of ECG signals either in the time domain [41, 42], or wavelet domain [1, 44–46]. A brief review of CS-based ECG compression techniques employed for telemonitoring applications is summarized in Table 2.1.

Extensive study of CS application for ECG signals was first carried out by Mamaghanian et

**Table 2.1:** Review of CS-based ECG data compression/reconstruction techniques

| Techniques | Database | Sensing matrix | Recovery method | Results | Encoding complexity | Remark |
|---|---|---|---|---|---|---|
| Mamaghanian [1] | MIT-BIH | Sparse binary | BPDN | PRD= 2-9 CR= 71% | Sub-optimal | Extends node lifetime up to 76%, slow decoding |
| Polania [97] | MIT-BIH | Gaussian | SOMP-PKS | PRD=2.57 CR=7.23 | High | QRS detection required, faster decoding |
| Mamaghanian [98] | MIT-BIH | Sparse binary | IHT | PRD=5.5 M=160 | Optimal | - |
| Dixon [41] | MIT-BIH | Bernoulli | Mixed | SQNR>60dB CR>16 | - | - |
| Polania [99] | MIT-BIH | Gaussian | BSBL | PRD≈1.9 CR≈13 | High | QRS detection required |
| Zhang [42] | DaISy/OSET | Sparse binary | BSBL-BO | Corr≈0.83 CR≈60% | Low | Works for low-sparse signals, faster |
| Sharma [44] | CSE | Gaussian | BP | PRD=10.19 CR=18.31 | High | Ignores spatial correlation, slower |
| Zhang [61] | DaISy/OSET | Sparse binary | BSBL-FM | PRD=3.78 CR=60 | Low | faster, saves 76.3% power |
| Mamaghanian [34] | PTB | Sparse binary | $\ell_1/\ell_2$ | PRD=9 CR=72.7 | Optimal | Extends node life-time by 26% |
| Polania [100] | MIT-BIH | Bernoulli | $\ell_1$-PKS | SNR≈23 dB M≈500 | Sub-optimal | - |
| Zhang [46] | MIT-BIH | Sparse binary | WLM | PRD=3.64 M=192 | Very low | Faster, saves 41.86% measurements |
| Polania [45] | MIT-BIH | Sparse binary | MMB-IHT | PRD=3.74 M=125 | Low | Exploits inter-beat correlation |

al. [1]. Authors have presented a comparative study between traditional wavelet transform-based ECG compression techniques and CS-based approach. The potential of CS is established and quantified for low-complexity and energy-efficient data reduction in the WBAN-enabled ECG monitors. Authors have presented a hardware implementation of both techniques, i.e., CS-based and traditional wavelet-based telemonitoring systems, on a Shimmer platform. It is shown that signal adaptive DWT is

able to compress the ECG data up to 90%, whereas non-adaptive CS-based approach leads to 71% compression for "good" signal reconstruction. Authors have also presented a power consumption analysis of both techniques, which shows that apart from being 95.69% faster, CS-based encoding approach also saves 27.09% power compared to DWT at the same compression ratio. In terms of WBAN deployment duration, CS extends the lifetime of body sensors by 76% and 46% for "good" and "very good" signal reconstruction quality, respectively. Later, similar hardware-based study was done by Chen et al. [47] who further established and demonstrated the real time compression ability of CS on a hardware platform by proposing an efficient CS architecture. Balouchestani et al. [43] have presented a low sampling CS approach using an efficient sensing matrix selection procedure. Using a dynamic thresholding approach a robust low-complexity detection algorithm is also presented and an increment of 1% for sensitivity as well as 0.15% for the prediction level is claimed.

Various design considerations have been studied by Dixon et al. [41] for the CS-based data acquisition and reconstruction systems. Authors have presented front-end circuit designs for both 'analog CS' and 'digital CS' systems. CS recovery for ECG and electromyogram (EMG) signals is analyzed using various sparse recovery algorithms and measurement/sensing matrices. A compression ratio greater than 16X for ECG and EMG signals is reported with signal-to-quantization noise ratios greater than 60 dB.

When signal is not sparse or low sparse, Bayesian learning-based CS techniques are known to be more effective compared to the traditional convex optimization and greedy algorithms [38, 39, 42, 61, 101]. Bayesian learning-based sparse recovery algorithms give superior joint sparse reconstruction performance due to their specific feature that global minimum is always the sparsest solution unlike $\ell_1$ minimization based algorithms [101]. Moreover, they are having fewer local minima than some classic joint sparse recovery algorithms. A block sparse Bayesian learning (BSBL)-based approach is proposed by Zhang et al. for fetal-ECG [42] telemonitoring application. Here, the authors have emphasized the retention of fetal-ECG signals in the non-sparse maternal ECGs during CS recovery. Furthermore, a sensing matrix with only two nonzero entries is introduced for CS encoding in order to achieve minimum energy consumption during compression process. Liu et al. [61] have proposed a variant of BSBL approach for fetal-ECG and epilepsy EEG signals. A hardware implementation using filed programmable gate array (FPGA) is presented to demonstrate the energy saving by the proposed

method. Their study shows that energy consumption and dynamic power consumption of the proposed approach is only 23.7% and 68.7% of those of the wavelet compression procedure, respectively.

Recent advancement in the CS field is to exploit prior knowledge in the tradition CS recovery algorithms in order to improve the recovery performance at a given number of compressed measurements [102, 103]. In these approaches, prior knowledge about support information is incorporated in the existing recovery algorithms to boost their performance. For ECG signals, there are several studies where such signal specific CS studies have been done [45, 46, 97, 100]. Polania et al. [97] have first presented a ECG signal specific recovery algorithm. In a joint recovery approach, authors have proposed to exploit the known support about the wavelet coefficients falling in approximation subband, which are mostly nonzero. This information is used in simultaneous OMP algorithm to simultaneously recover the successive heart beats together using less number of measurements. Authors claimed it to have better performance than the DWT-based SPIHT algorithm at higher compression ratios. A Bayesian learning-based approach [99] was also proposed by the same authors to exploit inter-beat correlations in CS-based ECG compression applications. Concept of structured sparsity is introduced for CS ECG recovery [98, 104], where sparsity pattern of ECG signals in wavelet domain is exploited to improve the CS recovery performance. Polania and Barner [100] have exploited the decay characteristics of detail subband coefficients in traditional $\ell_1$-norm minimization algorithm and claimed to have improved SNR values compared to the traditional BPDN CS recovery. In [45], authors have explored the correlation information between successive heart beats for support estimation of one beat and then using this prior knowledge in the recovery algorithm to accurately recover the next heart beat. Greedy algorithm CoSaMP and iterative hard thresholding (IHT) have been modified to incorporate the common support information. In a similar approach, Zhang et al. [46] have exploited the prior knowledge about amplitude decay characteristics of ECG in the wavelet domain in the traditional $\ell_1$-norm minimization algorithm for better signal reconstruction. Authors have also proposed low complexity sensing matrix, where the position of nonzero entry can be made adaptive, which allows the authors to claim 58% saving in energy consumption in encoding process. A saving of 41.86% and 21.88% in the number of measurements compared to BP and BSBL techniques, respectively is also reported by the authors.

In a recent work [74], clustering problem in long-term ECG monitoring is addressed. An advanced

$K$-means clustering algorithm for large scale ECG data based on CS theory in combination with the $K$-singular value decomposition is proposed. Performance of the proposed method is validated using PCA and linear correlation coefficient dimensionality reduction methods, which is followed by data sorting using K-nearest neighbors and probabilistic neural network classifiers. The method claims a classification accuracy of 99.98%, increasing 11% classification accuracy compared to the existing algorithm. It also claims to reduce 13% clustering energy consumption by increasing the classification performance. One of the major limitations with all the works discussed above is that they all have single channel ECG processing capabilities and hence, not suitable for joint processing of MECG signals.

## 2.3 Joint CS Framework for Multi-channel ECG Signals

There are two CS models reported in the literature, which have been used for ECG signals. One is single measurement vector (SMV) model for single channel ECG processing and other is a multiple measurement vector (MMV) model employed for multi-channel ECG signals. The CS model discussed previously in subsection 2.1 is called SMV model. The MMV model [105, 106] is an extension of traditional SMV CS model and deals with multidimensional signals. The required condition for the MMV model is that, all the signals under the ensemble must share a common sparsity profile, i.e., each should have a common support set. The joint wavelet representation of MECG signals shows row or joint sparsity as shown in Figure 2.3. Here, very small amplitude wavelet coefficients from each lead are neglected and best $k-$ term approximation is shown. **Dots** in the plot represent the indices of nonzero wavelet coefficients in various subbands. This joint sparsity enables MMV CS modeling of MECG signals for simultaneous compression/reconstruction. Let $\boldsymbol{X} = [\boldsymbol{x}_1,\ \boldsymbol{x}_2,\ \boldsymbol{x}_3,\ \ldots,\ \boldsymbol{x}_L] \in \mathbb{R}^{N\times L}$ be the data matrix whose columns represent the $L$ channels of $N$-dimensional signals (say, different channels of MECG signals). Therefore, if different channels have joint sparsity or row-sparsity structure in a common basis $\boldsymbol{\Psi}$, i.e., the significant information of data matrix $\boldsymbol{X}$ is confined to a few nonzero rows only in transform domain, then compressed measurements in an MMV CS model are given by:

$$\boldsymbol{Y} = \boldsymbol{\Phi}\boldsymbol{X} \tag{2.15}$$

where $\boldsymbol{\Phi}$ is a sensing matrix and $\boldsymbol{Y}$ is a measurement matrix of $L$ measurement vectors.

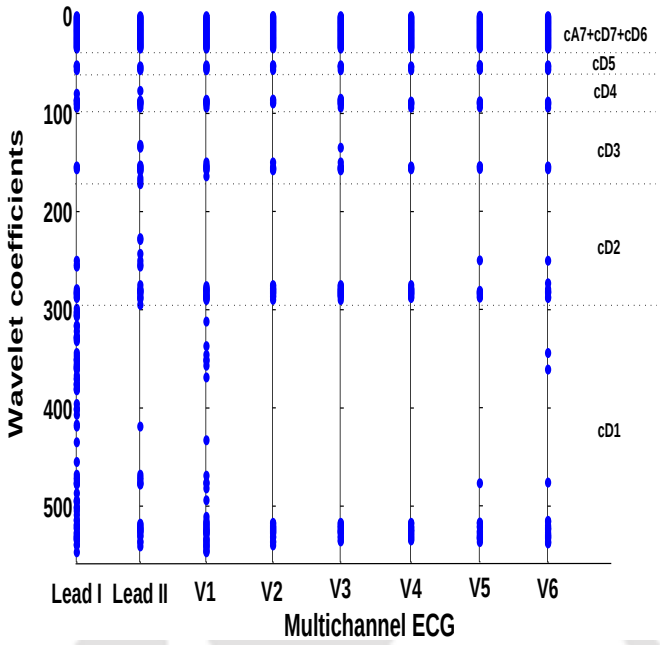


**Figure 2.3:** Joint sparse plot depicting the similar support of the best $k$-term approximation of MECG signals in wavelet domain. Black dots represent the indices of nonzero wavelet coefficients in various subbands for 7 level wavelet decomposition.

To solve MMV CS problem (2.15), joint sparse recovery algorithms are required, which can simultaneously recover signals from all the channels. Mixed-norm minimization-based algorithms are important type of joint sparse recovery algorithms [106, 107], where a combination of two norms e.g., $\ell_1/\ell_1$, $\ell_1/\ell_2$, $\ell_1/\ell_\infty$-norms, is generally used. These algorithms can be seen as an extension of SMV-based $\ell_1$-norm minimization algorithm. Similar extensions have been proposed for other SMV recovery algorithms also, e.g., OMP is extended to simultaneous OMP (SOMP) [108], CoSaMP is extended to CoSOMP [99, 104], etc. So far, SMV-based CS modeling has been extensively used for single channel ECG signals [1, 41, 44–46]. However, the MMV CS model is not well explored for ECG signals. Also, noting the importance of multi-channel ECG signals and their correlated structure, MMV modeling of MECG would be more beneficial in CS-based data compression in WBAN applications. So far, limited research is available in MMV ECG modeling, giving scope for further research in this field.

Mamaghanian et al. [34] have recently presented a work in the area of MECG telemonitoring using a MMV-based approach. Authors have used a mixed norm minimization (MNM)-based joint CS recovery technique to simultaneously recover all the channels exploiting the inter-channel correlation.

There is also a comparative study presented in this work over the gains of MMV CS and SMV CS for ECG signals in terms of power efficiency and reconstruction accuracy. Their hardware-based study shows that it is possible to increase the compression efficiency of WBAN system by 7%, and overall power consumption can be reduced by 22% following MMV CS approach over SMV for MECG signals. Though, the work highlights the importance of joint MECG processing through MMV model, it reported higher PRD values ($> 9$) when low signal measurements are available (at compression ratio $> 72.7\%$). To demonstrate this unsatisfactory performance at low measurements ($M$), we conducted an experiment and analyzed the clinical quality of the reconstructed MECG signals. Original MECG signals extracted from lead aVR and V5 of data-set s056lrem taken from PTB database [2] are shown in Figure 2.4 (a) and (d) in their original form. Assuming the wavelet domain joint sparsity of MECG signals, first $N = 512$ samples from all the channels are jointly CS encoded using a sensing matrix $\Phi$ of size $125 \times 512$. A modest value of number of measurements $M = 125$ is chosen for the CS reconstruction. First 2048 samples of the corresponding jointly reconstructed lead aVR and V5 signals are shown in Figures 2.4 (b) and 2.4 (e). The reconstruction error, defined as the difference between original and reconstructed signals, is shown in Figures 2.4 (c) and 2.4 (f). The degraded signal quality is clearly visible in terms of noisy reconstruction and loss of clinical components, encircled in Figures 2.4 (b) and 2.4 (e). The bigger circles in the reconstruction error plots highlight the large errors incurred in QRS features of ECG, which are having high diagnostic importance. The traditional MNM recovery algorithm used in this work leverages only the group sparsity structure of MECG signals, which might not be sufficient for their successful recovery, especially at low number of measurements (high compression ratios).

There is one more work reported in the literature which deals with MECG signals using CS framework. Sharma in [44] has presented a CS-based encoder for MECG signals. This work presents a multiscale processing of MECG signals in a CS framework. The CS-based data reduction procedure is applied over sparse subband signals, especially in high frequency wavelet subbands in order to retain the vital clinical ECG information present in low frequency subbands. The major drawback of this method is that it ignores the correlated signal information among different channels as it suggest to process subband signals from each channel individually. Also, it has higher computational complexity as it involves additional processing blocks in form of wavelet decomposition and subband matrix

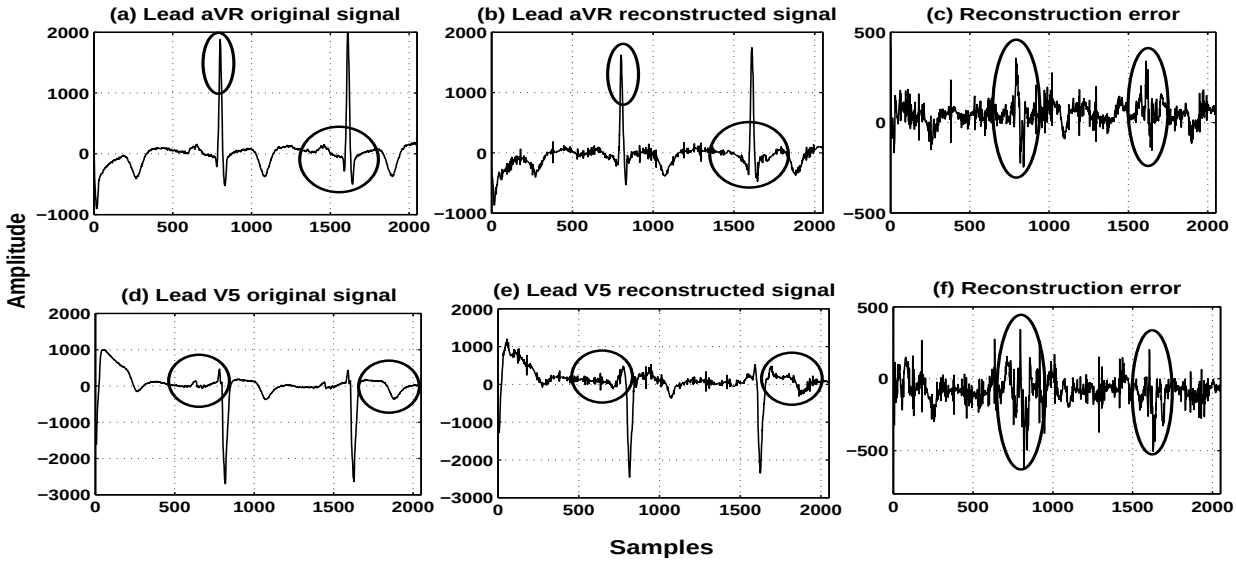


**Figure 2.4:** Joint reconstruction of MECG signals showing loss of clinical features when using traditional or non-weighted mix-norm minimization algorithm at $M = 125$. (a), (d) Original signals from lead aVR and V5. (b), (e) Jointly reconstructed signals from corresponding leads (c), (f) Reconstruction error signal. Data-set s056lrem taken from PTB data base.

formation prior to CS operation.

The importance of MECG signals in clinical practices and unavailability of efficient methods to deal with them in telemonitoring applications, motivated us to explore new approaches for effective CS implementation for MECG signals.

## 2.4 ECG Signal Distortion Measures

The quality of processed ECG signals is a direct measure of efficiency and applicability of a signal processing system. To assess/quantify the quality of processed ECG signals, there are subjective and objective quality measures. Subjective quality measure is evaluated through visual perception of different people, while standard mathematical formulations are used to quantify the errors in objective quality measures. The range of few major distortion metrics and the corresponding signal reconstruction quality is given in Table 2.2.

The Mean Opinion Score ($MOS$) is a widely used subjective measure. Here, the visual quality of the signal is used to evaluate the $MOS$. Visual inspection of diagnostic features such as amplitudes, durations and shapes of the ECG waves is done by cardiologists to assess the clinical relevance of

**Table 2.2:** Distortion metrics and corresponding signal quality

| Metrics | Signal reconstruction quality | | | |
|---|---|---|---|---|
| | Excellent/Very good | Very good | Good/Underminable | Bad |
| PRD | 0-2% | 2- 9% | 9-16 | $> 16\%$ |
| WDD | 0-2.3% | 2.3- 12% | 12-18% | $> 18\%$ |
| WEDD | 0-4.5% | 4.5-6.9% | 6.9-11.1% | $> 11.1\%$ |
| WWPRD | 0-7.4% | 7.4-15.4% | 15.4-25.1% | $> 25.1\%$ |
| SNR | $> 34$dB | 34-20.9dB | 20.9-15.9dB | $< 15.9\%$dB |
| MOS | 0-10% | 10-25% | 25-40% | $> 40\%$ |

processed signals. The $MOS$ for $l$-th ECG feature is given by [88]

$$MOS(l) = \frac{1}{N_c} \sum_{c=1}^{Nc} R(c) \tag{2.16}$$

where $N_c$ is number of evaluators and $R(c)$ is the rating given to the $c$-th ECG feature. $MOS$ for overall signal is given by the average of all $MOS$ ratings of all the clinical features. Depending on $MOS$ ratings (on a scale of 5), $MOS$ errors for ECG segments and overall signal is defined as [88]

$$MOS_e(l) = \frac{5 - MOS(l)}{5} \times 100 \tag{2.17}$$

$$MOS_e = \frac{5 - MOS}{5} \times 100 \tag{2.18}$$

where $MOS_e(l)$ and $MOS_e$ are the $MOS$ errors (in percentage) for an ECG segment and overall ECG signal, respectively.

Objective quality measures can be divided into two categories, i.e., non-diagnostic distortion measure (e.g., MSE, RMSE, PRD, SNR, StdErr, Maximum Error (MaxErr), etc.) [109] and diagnostic distortion measures (e.g. WDD, WPRD, WWPRD, WEDD, etc.) [79–81].

### Non-diagnostic distortion measures

Those metrics, which, irrespective of the signal, measure the overall difference (error) between original and processed/reconstructed signal are termed as non-diagnostic distortion measures [109]. Following measures fall in this category.

If original signal sequence is $x(n) = \{x(1), x(2), x(3), ..., x(N)\}$, and processed signal sequence is

$\widetilde{x}(n) = \{\widetilde{x}(1), \widetilde{x}(2), \widetilde{x}(3), ..., \widetilde{x}(N)\}$, the mean square error (MSE) is given as

$$\text{MSE} = \frac{1}{N}\sum_{n=1}^{N}[x(n) - \widetilde{x}(n)]^2 \tag{2.19}$$

where, $N$ is the number of the samples.

Normalized mean square error (NMSE) between the original and the processed ECG signals is defined as

$$\text{NMSE} = \frac{\sum_{n=1}^{N}[x(n) - \tilde{x}(n)]^2}{\sum_{n=1}^{N}[x(n)]^2} \tag{2.20}$$

In order to make the error independent of the original signals, the normalization factor is required. Root mean square error (RMSE) is another metric defined as

$$\text{RMSE} = \sqrt{\frac{1}{N}\sum_{n=1}^{N}[x(n) - \tilde{x}(n)]^2} \tag{2.21}$$

However, RMSE does not capture well the quality of ECG signals. Its normalized version, i.e. normalized RMSE (NRMSE), is expected to overcome this limitation and is defined as

$$\text{NRMSE} = \sqrt{\frac{\sum_{n=1}^{N}[x(n) - \tilde{x}(n)]^2}{\sum_{n=1}^{N}[x(n)]^2}} \tag{2.22}$$

Another widely used distortion measure is percentage root mean square difference (PRD), which is very often used for performance evaluation of ECG compression algorithms [110, 111]. It is defined as

$$PRD = \sqrt{\frac{\sum_{n=1}^{N}[x(n) - \tilde{x}(n)]^2}{\sum_{n=1}^{N}[x(n)]^2}} \times 100 \tag{2.23}$$

Signal-to-noise ratio (SNR) or reconstruction SNR (R-SNR) is also a global error measure, which is often used as performance measure in various ECG signal processing applications. It is defined as

$$R\text{-}SNR = 20\log_{10}\sqrt{\frac{\sum_{n=1}^{N}[x(n)]^2}{\sum_{n=1}^{N}[x(n) - \tilde{x}(n)]^2}} \tag{2.24}$$

Other similar distortion measures include, normalized cross-correlation (NCC), maximum amplitude error (MAX) or peak error (PE), normalized maximum amplitude error (NMAX), standard error (StdErr), etc.

### Diagnostic distortion measures

Though the aforementioned distortion measures give an idea about the distortion being incurred during various ECG processing, ECG signal should also be evaluated from clinical point of view to assess diagnostic distortion. There are few diagnostic distortion measures reported in the literature for this purpose. The error measures that capture the distortion in diagnostically relevant ECG features are called diagnostic distortion measures. This includes weighted diagnostic distortion (WDD) [79], wavelet based weighted PRD (WWPRD) [80] and wavelet energy based diagnostic distortion (WEDD) [81]. They are defined as follows.

$$WDD(\%) = \Delta\beta^T . \frac{\Lambda}{tr[\Lambda]} . \Delta\beta \times 100 \tag{2.25}$$

where $\Delta\beta$ is the normalized difference between the diagnostic feature vectors of original and reconstructed ECG signals, while $\Lambda$ is a diagonal weighting matrix. Duration, amplitude, and slope features are generally used for the $WDD$ calculation. These features are concatenated to form the feature vector $\beta$. The duration features included the $R$-$R$ interval, $P$ wave duration, $QRS$ interval, $QT$ interval, $PR$ interval, and $QT_p$ interval. For the amplitude features, amplitudes of the prominent ECG waves, such as $P$ wave, $R$ wave, $T$ wave, $QRS$ positive amplitude, and $QRS$ negative amplitude are considered. The $ST$ slope is taken as the slope feature. The $WDD$ measure is very helpful in quantifying the distortions incurred in clinically important ECG features. However, it is difficult to evaluate $WDD$ measure for every ECG signal. This is because it involves a complex procedure of delineation of ECG segments, which may not be accurately possible for every ECG morphology. Later, people have explored more simple diagnostic distortion measures, such as $WWPRD$ and $WEDD$.

The $WWPRD$ metric is defined as:

$$WWPRD = \sum_{j=1}^{S+1} w_j WPRD_j \tag{2.26}$$

where $w_j$ is the weight for the subband $j$, $S$ is the number of wavelet decomposition levels and $WPRD_j$ is the $PRD$ of subband $j$, and it is defined as

$$WPRD_j = \sqrt{\frac{\sum_{k=1}^{N_j}(w_{j,k} - \tilde{w}_{j,k})^2}{\sum_{k=1}^{N_j} w_{(j,k)}^2}} \tag{2.27}$$

where $w_{j,k}$ is an original coefficient, $\tilde{w}_{j,k}$ is a filtered coefficient and $N_j$ is the number of coefficients within subband, $j$. The weight $(w_j)$ is given as [112]

$$w_j = \frac{\sum_{k=1}^{N_j} |w_{(j,k)}|}{\sum_{j=1}^{S+1} \sum_{k=1}^{N_j} |w_{(j,k)}|} \quad , \quad j = 1, 2, 3, ..., S+1 \tag{2.28}$$

The $WEDD$ metric is defined as:

$$WEDD(\%) = \sum_{j=1}^{S+1} w'_j WPRD_j \text{ where } w'_j = \frac{\sum_{k=1}^{N_j} {w^2}_{j,k}}{\sum_{i=1}^{S+1} \sum_{k=1}^{N_j} {w^2}_{i,k}} \tag{2.29}$$

where $WPRD_j$ is the $PRD$ value at $j$-th subband.

Sometimes, classification accuracies are also used as diagnostic distortion measure to establish the clinical information preservation in the reconstructed ECG signals [36]. Higher percentage of classification implies better preservation of diagnostically important ECG features in the reconstructed or recovered ECG signals.

## 2.5 Databases

The performance evaluation of the works carried out in the present thesis is done using publicly available MECG databases. This includes Physikalisch-Technische Bundesanstalt (PTB), Massachusetts Institute of Technology-Boston's Beth Israel Hospital (MIT-BIH) database, St. Petersburg Institute of Cardiological Technics (INCART), and Noise Stress Test Database (NSTDB) [2,3]. Commercially available Common Standards for Electrocardiography (CSE) [4] database [4] is also used. The PTB and INCART contain various diagnostic MECG signals from 290 and 32 patients sampled at 1 kHz and 257 Hz, respectively, with 16-bit resolution. The MIT-BIH and NSTDB are 2-channel databases, where NSTB is a noisy database created from MIT-BIH. MIT-BIH contains 48 records of 2-channel arrhythmic ECG signals with $f_s = 360$ Hz and 11-bit resolution. CSE is also a 15-channel diagnostic database containing mainly noisy ECG signals with $f_s = 500$ Hz and 10-bit resolution.

## 2.6 Motivation for the Present Work

In recent years, CS has emerged as a low-complex and energy-efficient data compression framework for WBAN-enabled ECG telemonitoring applications [1,45,46]. In these resource-constrained applications, CS allows significant savings in the energy cost of the system by reducing the required digital signal

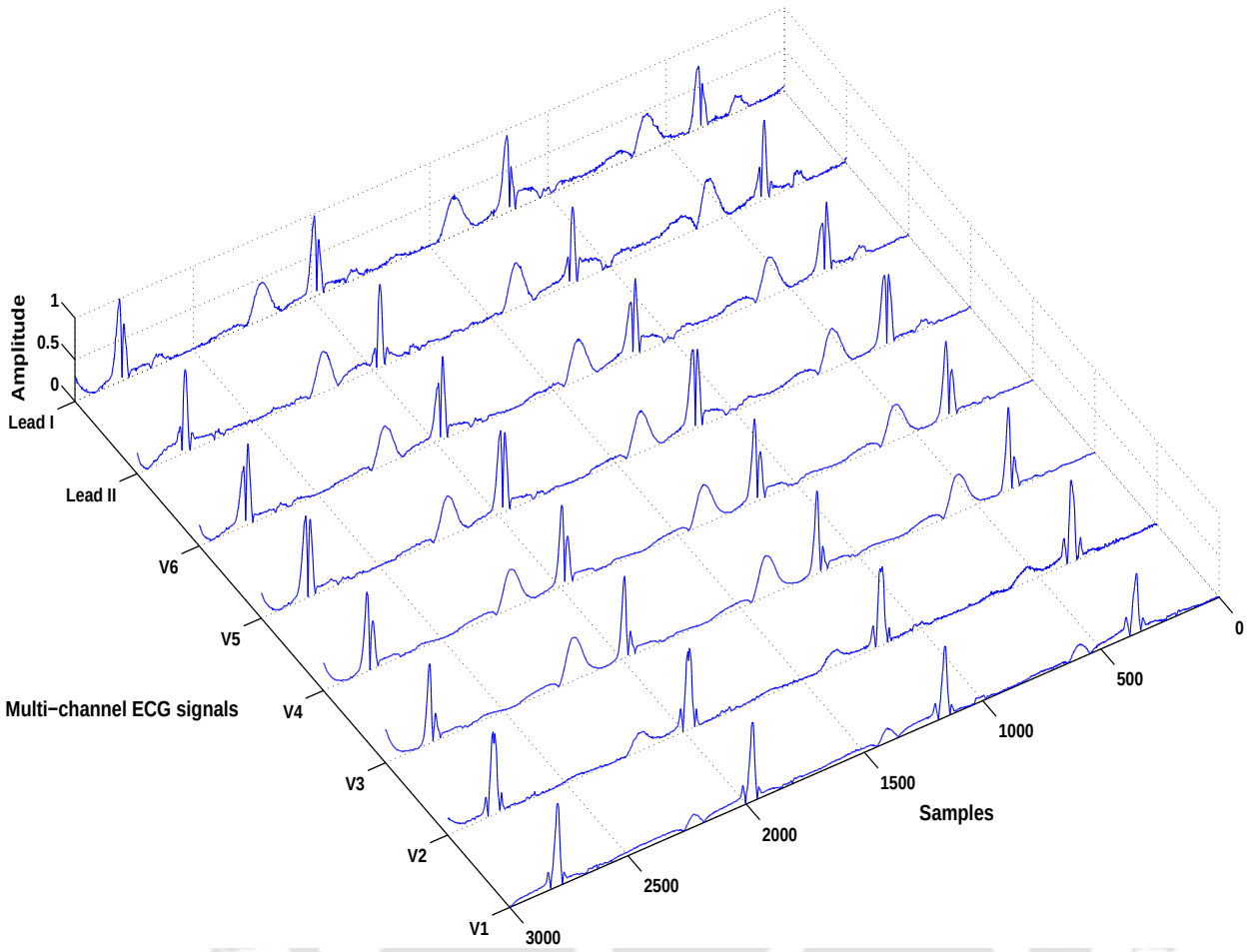


**Figure 2.5:** Multi-channel ECG signals from the eight fundamental leads showing spatially and temporally correlated time-domain information

processing resources (computation and memory) and circuitry requirement. The multi-channel ECG system carries detailed cardiac information captured through different spatial angles. Diagnostic clues about any pathological condition of cardiovascular system may appear in more than one leads. Because of this reason, MECG signals are preferred over single channel ECG by cardiologists for all diagnostic purposes. Existing telemonitoring systems are mostly based on single channel ECG [1, 42, 45, 46, 97, 99, 104]. If these systems could be extended efficiently for MECG signals, health monitoring could be made more effective and reliable. This motivated the study of CS-based telemonitoring system for multi-channel ECG signals. Different cardiac events captured by multi-channel ECG leads are from different narrow angles in three dimensional space. The same electrical pulse originating from sinus node creates PQRST morphologies in each lead. This generates huge source of spatio-temporal

redundancies in multi-channel ECG system. This motivated to propose an eigenspace CS approach, where different type of redundancies/correlations can be exploited using joint PCA-CS for effective MECG data encoding.

Because of shared cardiac information across different channels in time domain (shown in Figure 2.5), there also exist similar transform domain signal variations (Figure 2.2) resulting in common signal support. The indices of nonzero wavelet coefficients are called supports and the set of indices at which there are nonzero coefficients in all the channels together is called common support set. Figure 2.3 shows nonzero coefficients in each channel with dots. Most of the coefficients (accept a few in non-diagnostic $cD1$, $cD2$, $cD3$ subbands) form a common support set. These observations motivated us to explore a joint CS framework, which allows simultaneous MECG data compression/reconstruction by exploiting common support information. Exploitation of common support is expected to significantly boost the recovery performance of existing single channel ECG telemonitoring systems at a given number of measurements (or compression ratio), or equivalently, reduce the number of measurements (or increase the compression ratio) at a given signal quality.

The CS-based signal recovery leverages on wavelet domain sparsity of ECG signals. Though, irrespective of the signal, CS allows a universal data encoding, signal-adaptive CS encoding/decoding is expected to deliver better performance [45, 46]. This has motivated to develop new signal adaptive joint sparse recovery algorithms by incorporating clinically relevant MECG information in the joint CS recovery problem formulation through different weighting schemes. The weighting approach emphasizes important wavelet coefficients/subbands and is expected to help in precise support estimation and improve the joint MECG recovery at reduced number of measurements. Reduction in the number of measurements while retaining the diagnostic quality may further help in reducing the on-chip computations and improving the overall power efficiency of CS-based WBAN-enabled telemonitoring systems.

## 2.7 Plan of the Thesis

Within the CS framework of data compression/reconstruction, three problems have been dealt in this thesis. First problem deals with effective MECG encoding, while the rest two problems deal with joint recovery of MECG signals using minimum number of measurements. Investigations done in this thesis

have been planned in the following ways:

- To explore eigenspace CS for MECG signals. CS methodology is investigated in eigenspace, where spatial correlation among different ECG channels is exploited through PCA, and CS is applied over resulting principle eigenspace MECG signals. This Joint PCA-CS approach is discussed in **Chapter 3**. Application of PCA over MECG data is expected to retain diagnostically important ECG features in a few principal eigenspace signals whose dimensionality can be further reduced using CS by exploiting their sparsity either in eigenspace itself or in any other sparsifying domain. CS recovery performance for eigenspace MECG signals is further investigated in other sparsifying transforms, such as DWT, discrete cosine transform (DCT), and discrete Fourier transform (DFT) for better sparse recovery. Joint PCA-CS approach enables effective exploitation of spatio-temporal redundancies in MECG system.

- To minimize the computation burden at the encoder by exploring a low-complexity joint CS encoder and an efficient decoder. **Chapter 4** investigates a weighted mixed norm minimization (WMNM)-based joint CS recovery approach, which exploits spatial or inter-channel correlation between different channels at the decoder and allows simultaneous recovery of all the ECG channels. A simple matrix multiplication with random sparse binary sensing matrix having binary entries (with a very few ones), is done to jointly compress all the ECG channels directly and WMNM is employed to retrieve them back together. WMNM algorithm is based on a coefficient-level weighting strategy, which emphasizes the diagnostically important high amplitude wavelet coefficients and helps minimize the required number of measurements during CS recovery. The proposed approach transfers most of the load to the resourceful decoder side and is expected to reduce the computation burden and energy consumption at the encoder along with improved signal recovery.

- To study the multi-scale wavelet structure of MECG signals and exploit it in the WMNM-based joint CS recovery problem. This analysis is presented in **Chapter 5**. Grossly segmented clinically relevant ECG features in different wavelet subbands are captured using different parameters such as subband energy, entropy, amplitude decay, etc. This information is incorporated in the optimization problem formulation of WMNM-based joint CS recovery through different

subband-based weighting schemes. Such a weighting approach is expected to emphasize coefficients in wavelet subbands having high diagnostic importance during joint CS reconstruction. Insignificant coefficients in non-diagnostic subbands are deemphasized simultaneously, resulting in a sparser, and consequently, better CS recovery performance at reduced number of measurements. Diagnostic accuracy of the reconstructed MECG signals is validated through a post-reconstruction classification task. Additionally, a block-sparsity-based joint CS recovery is also explored in this chapter to exploit the spatio-temporal correlated MECG structure.

भारतीय प्रौद्योगिकी संस्थान गुवाहाटी
Indian Institute of Technology Guwahati

# 3

# Multi-channel ECG Data Compression Using Compressed Sensing in Eigenspace

Contents

Previous chapters highlighted the importance of multi-channel ECG (MECG) signals and their role in the detailed and reliable diagnosis of cardiac diseases. The MECG signal acquisition in continuous telemonitoring applications generates large amount of data. Since, these are resource-constrained applications with limited power and bandwidth, wireless transmission of such a large amount of data to healthcare centers is expensive. This necessitates efficient data reduction before transmission. The related reviews discussed in **Chapter** 2 showed that CS can be a better option for this purpose due to its simple and power-efficient data reduction ability compared to traditional wavelet-based methods. The inherent inter-channel correlation among different channels needs to be exploited from data reduction perspective. In existing CS-based ECG compression works [1, 45, 46, 97], mainly temporal correlation is considered. This is because of the design of these algorithms to process individual ECG channels. In this chapter, we investigate a joint principal component analysis (PCA)-CS approach, where all ECG channels are processed together in order to exploit the spatio-temporal redundancies from across the channels for effective data encoding.

The organization of the chapter is as follows: Section 3.1 envisages the feasibility of the joint PCA-CS approach and its advantages. Section 3.2 discusses about the different steps involved in the proposed methodology. Performance evaluations are presented in Section 3.3. Section 3.4 analyses the diagnostic features of the reconstructed ECG signals, especially in noisy conditions. Performance comparison results are presented in Section 3.5 followed by discussions on some practical issues in Section 3.6. Summary of the chapter is given in Section 3.7.

## 3.1 Analysis of Eigenspace MECG Signals

PCA has been previously used for dimensionality reduction, noise elimination, beat detection, classification, signal separation and feature extraction [88, 113–115]. It has also been employed to synthesize 12-channel MECG system using reduced 3-lead system for remote health monitoring applications [116–118]. For CS-based applications, the data-adaptive transformation feature of PCA makes it a good sparsifying basis [50, 119]. PCA has been used jointly with CS for distributed signals to learn optimal transformation through online estimation of the signal statistics [119]. For synthetic aperture radar (SAR) signals, it has been used as a sparsifying transform to compressively measure the SAR raw data [50]. Joint PCA-CS feasibility in above applications motivated us to explore PCA in the CS

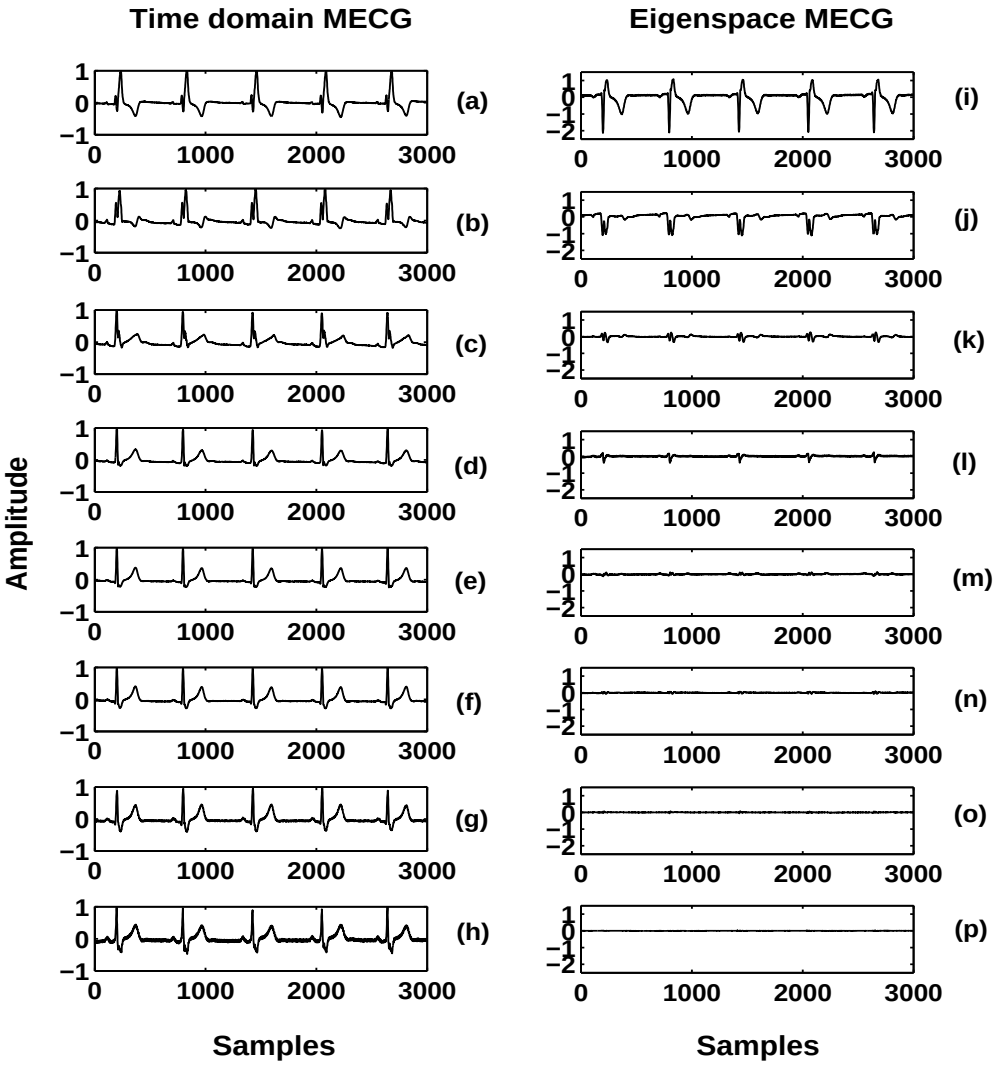


**Figure 3.1:** Time-domain MECG signals from eight independent channels: Lead I, II, V1, V2, V3, V4, V5, V6 are shown in plots (a) to (h), respectively. PCA transformed eigenspace MECG signals are shown in plots from (i) to (p).

framework in this chapter for MECG signals. PCA over MECG signals helps capture the diagnostic information spread across twelve channels into few eigenspace signals (reduced leads) by exploiting the inter-channel correlation structure of the MECG signals. The eigenspace transformed MECG signals are shown in Figure 3.1. It can be observed that important ECG features are confined within few eigenspace signals. The dimensionality of the retained eigenspace MECG signals can be further reduced using CS exploiting their sparsity either in eigenspace itself or in any other transform domain.

Processing the ECG signals from different channels jointly through PCA helps remove the redundant channel information while producing sparse eigenspace signals, which can be further compressed using CS approach. This feature is generally ignored in existing CS-based works that deal with each channel individually [1, 45, 46, 97]. The proposed joint PCA-CS approach, however, requires covariance matrix of the data during the reconstruction at decoder side. Noting the small size of covariance matrix ($8 \times 8$, if 8 independent MECG channels are considered), it can be sent as a side information along with the data with little effect on the resource cost of the system. After PCA transformation, the transformed eigenspace MECG signals retain morphological similarity with the time-domain ECG signals (Figure 3.1), and thus, still contain intra-signal correlated structure. This correlation can be further exploited, in addition to the inter-channel correlation, by choosing a suitable sparsifying basis during CS reconstruction in the proposed eigenspace CS approach. It can sparsify eigenspace signals and the required number of compressed measurements can thus be reduced further. Reduced number of measurements help CS to compress the MECG data further without compromising with the clinical quality of the reconstructed ECG signals.

## 3.2 Proposed Joint PCA-CS Approach

In this work, ECG signals from only eight independent channels have been considered in order to reduce the computational burden at the encoder. This includes six pre-cordial leads (V1, V2, V3, V4, V5, V6) and two limb leads (Lead I and Lead II). The dependent leads (aVR, aVL, aVF and Lead III) can be derived at the decoder using the limb leads. The proposed method is suggested as follows. First, the algorithm extracts the principal components after eigenvalue decomposition of the MECG signals. Principal components are selected based on a suitable threshold to avoid loss of vital clinical information across the channels. Then by randomly projecting these sparse eigenspace signals using a random sparse binary sensing matrix, compressed measurements are obtained that can be further quantized and encoded to get the compressed bit streams. The block diagram of the proposed method is shown in Figure 3.2. Details of each block are discussed in subsequent subsections.

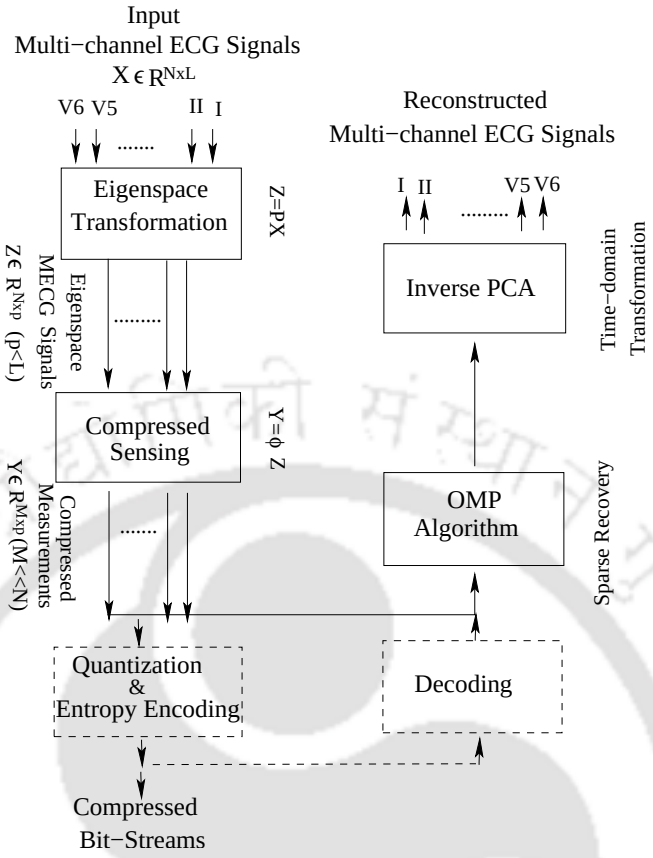


**Figure 3.2:** Block diagram of the proposed method

### 3.2.1 Eigenspace transformation

Eigenspace transformation of ECG data is done using the principal components obtained by eigenvalue decomposition of the MECG data matrix. If the data matrix $X = [\boldsymbol{x}_1\ \boldsymbol{x}_2\ \boldsymbol{x}_3\ ...\ \boldsymbol{x}_L] \in \mathbb{R}^{N\times L}$ contains the $L$ ECG channels of length $N$ as column vectors, then its covariance matrix $\boldsymbol{C}$ is given by:

$$\boldsymbol{C} = \frac{1}{N}([\boldsymbol{X} - \overline{\boldsymbol{X}}]^T[\boldsymbol{X} - \overline{\boldsymbol{X}}]) \tag{3.1}$$

where $\boldsymbol{C}$ is the covariance matrix and $\overline{X}$ contains the mean values of each channel data. Eigenvalue decomposition of the covariance matrix gives the eigenvalues and corresponding eigenvectors of covariance matrix $\boldsymbol{C}$ as:

$$\boldsymbol{C} = \boldsymbol{V}\boldsymbol{\Lambda}\boldsymbol{V}^T \tag{3.2}$$

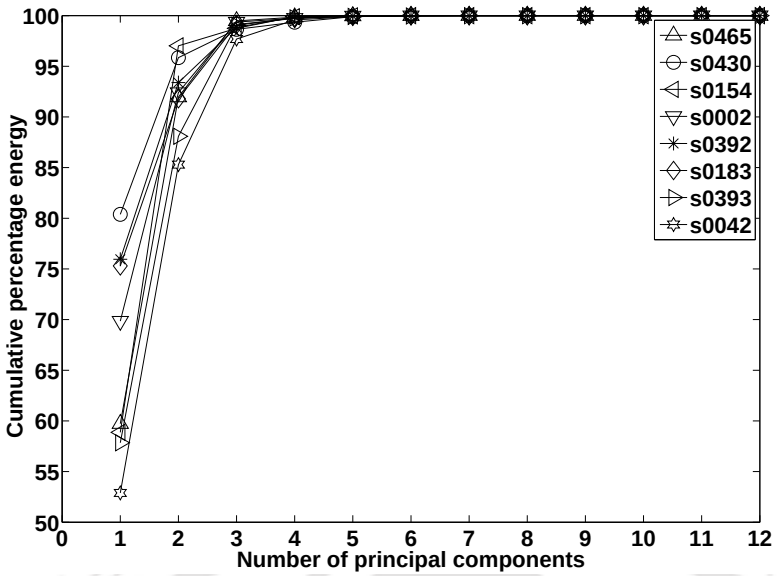


**Figure 3.3:** Cumulative percentage energy distribution across the principal components

where matrix $\boldsymbol{V} = [\boldsymbol{v}_1\ \boldsymbol{v}_2\ \boldsymbol{v}_3\ ...\ \boldsymbol{v}_L] \in \mathbb{R}^{L\times L}$ constitutes the eigenvectors and $\lambda_i = diag(\boldsymbol{\Lambda})\ , i = 1, 2, ..., L$, are the eigenvalues of the matrix $\boldsymbol{\Lambda}$. The eigenvectors corresponding to the largest eigenvalues are the principal components (PCs). They capture the directions of maximum variance present in the signals. The selection of the PCS is done on the basis of energy captured by the eigenvalues which corresponds to the clinical information in ECG signals [120]. For selection of $p$ out of total $L$ number of eigenvalues, an energy-based threshold is defined as:

$$T_s = \frac{\sum_{i=1}^{p} \lambda_i}{\sum_{i=1}^{L} \lambda_i} \times 100 \geq 99.5\% \tag{3.3}$$

The threshold limit of 99.5% of total energy is heuristically chosen by a simulation-based analysis on a number of datasets taken from the PTB and CSE databases. The variation of cumulative sum of energy of PCs w.r.t. number of PCs is shown in Figure 3.3 for a few datasets. It is observed that the selection of the number of PCs that captures 99.5% of the total energy, or more ensures retention of the vital clinical components of MECG in the reconstruction. The transformation matrix $\boldsymbol{P}$ is given

by,

$$\boldsymbol{P} = [\boldsymbol{v}_1\ \boldsymbol{v}_2 \ldots \boldsymbol{v}_p], \quad p < L \tag{3.4}$$

Matrix $\boldsymbol{P} \in \mathbb{R}^{L \times p}$ transforms the time-domain MECG signals to eigenspace as

$$\boldsymbol{Z} = (\boldsymbol{X} - \overline{\boldsymbol{X}})\boldsymbol{P} \tag{3.5}$$

where $\boldsymbol{Z} = [\boldsymbol{z}_1\ \boldsymbol{z}_2\ \ldots\ \boldsymbol{z}_p] \in \mathbb{R}^{N \times p}$ constitutes the principal eigenspace MECG signals. MECG signals transformed in eigenspace are shown in Figure 3.1. It can be noted that clinically relevant features in PCA transformed signals $\boldsymbol{Z} = [\boldsymbol{z}_1\ \boldsymbol{z}_2\ \ldots\ \boldsymbol{z}_p]$ are sparsely localized. This suggests that the compressed measurements can be directly taken over $\boldsymbol{Z}$. Furthermore, retained eigenspace signals $\boldsymbol{Z}$ can be represented in a more sparse form using a suitable sparsifying transform as it still contains inter- and intra-beat redundancies analogous to time-domain ECG heart-beats (refer to Figure 3.1). A sparser representation helps improve the signal reconstruction further at a given number of compressed measurements.

### 3.2.2 Compressed measurements of eigenspace signals

The compressed measurements of eigenspace MECG signals are obtained as $\boldsymbol{y} = \boldsymbol{\Phi z} = \boldsymbol{\Phi\Psi\alpha} = \boldsymbol{\Theta\alpha}$, where $\boldsymbol{\Theta} = \boldsymbol{\Phi\Psi}$ and $\boldsymbol{y}$, $\boldsymbol{\alpha}$ represent the compressed measurement vector and sparse coefficient vector, respectively. If the eigenspace itself is taken as the sparsifying basis, then $\boldsymbol{\Psi} = \boldsymbol{I}$ (unity matrix). In case any other basis is chosen for further sparsification of eigenspace signals, $\boldsymbol{\Psi}$ is chosen accordingly. Compressed measurements of all the eigenspace signals can be obtained as $\boldsymbol{Y} = [\boldsymbol{y}_1\ \boldsymbol{y}_2 \ldots \boldsymbol{y}_p] = \boldsymbol{\Theta Z}$ where $\boldsymbol{\Theta} \in \mathbb{R}^{M \times N}$ $(M < N)$ is the sensing matrix which transforms higher dimensional sparse signals into lower dimensional compressed measurement vectors $\boldsymbol{y}_i \in \mathbb{R}^M, i = 1, .2, .., p$. A random sparse binary matrix [34] is used as the sensing matrix as it requires the least number of computations during signal encoding and hence, suitable for practical applications.

### 3.2.3 Quantization and encoding

After linear measurement of the sparse ECG signal vectors, the compressed measurement vectors in $\boldsymbol{Y}$ are quantized and further encoded in a lossless manner to produce the compressed signal that is to be stored or transmitted. An uniform quantizer is used for the quantization purpose. Any lossless encoding technique can be used for the encoding of the quantized coefficients. Huffman coding provides

optimal codes without any loss of the data and hence, have been used here for the encoding purpose.

### 3.2.4 Data recovery

Huffman decoding is done to retrieve the compressed measurements at the decoder. The corresponding sparse eigenspace signals in $\boldsymbol{Z}$ are recovered using a sparse recovery algorithm, which are then projected over the inverse PCA transformation matrix $P^T$ to get back the $L$ channel MECG signals. For transform domain recovery such as DWT, DCT, etc., the corresponding sparsifying basis $\boldsymbol{\Psi}$ is used in the sparse recovery algorithm. It is to be noted that the covariance matrix/eigenspace transformation matrix $\boldsymbol{P}$ and the mean of the MECG data are required at the decoder for the signal recovery. They need to be sent as the side information along with the compressed data. However, sending $\boldsymbol{P} \in \mathbb{R}^{L \times p}$, which is usually a small size matrix (having maximum $8 \times 8$ elements when $p = L(= 8)$, i.e., all PCs are retained), will not be resource-consuming as it constitutes only a small fraction of the total data sent.

CS recovery is an underdetermined or ill-posed problem [40], which is solved using a convex optimization approach (2.14) as discussed in Chapter 2. Beyond the convex optimization solutions, there are other sparse recovery algorithms like greedy algorithms. Orthogonal matching pursuit (OMP) [95] is one such algorithm. In the greedy algorithms, the columns of measurement matrix $\boldsymbol{\Theta}$ $(= \boldsymbol{\Phi\Psi})$ and $\boldsymbol{y}$ that have got the maximum correlation with the measurement vector are selected iteratively in a greedy fashion. This contribution of $\boldsymbol{\Theta}$ is then subtracted from $\boldsymbol{y}$ and the process is repeated on the residue. OMP is relatively faster with a low computational complexity and produces a better signal-to-noise ratio as compared to $\ell_1$-minimization, and therefore, has been used in this work. The sparse recovery directly gives eigenspace MECG signals $[\boldsymbol{z}_1, \boldsymbol{z}_2, ...\boldsymbol{z}_p] \in \boldsymbol{Z}$. Matrix $\boldsymbol{P}$ is used for transforming eigenspace MECG signals back to time-domain signals as follows:

$$\widehat{\boldsymbol{X}} = \widehat{\boldsymbol{Z}}\boldsymbol{P}^{\boldsymbol{T}} + \overline{\boldsymbol{X}} \tag{3.6}$$

where $\widehat{\boldsymbol{Z}}$ constitute the reconstructed eigenspace signals, $\boldsymbol{P}^T$ is the inverse eigenspace transformation matrix, and $\widehat{\boldsymbol{X}}$ is the recovered MECG data matrix in time-domain. Dependent channels of the standard 12-channel MECG system can be derived after reconstructing the independent channels at the decoder.

## 3.3 Performance Evaluation

The performance evaluation of the proposed method is carried out using the publicly available PTB database [2, 3] and commercially available CSE database [4]. Each data record of both databases contains 15-channels of ECG signals including 3 frank leads. Out of these, $L = 8$ independent channels have been processed in this work. Experiments are conducted batch-wise in the form of a data matrix $\boldsymbol{X} \in \mathbb{R}^{3000\times 8}$ [44] composed of blocks of 3000 samples taken from of the eight independent channels. A random sparse binary sensing matrix $\boldsymbol{\Phi} \in \mathbb{R}^{M\times 3000}$ with binary entries (i.e., 0s and 1s) is generated, using which the sparse eigenspace MECG signals are projected to obtain the compressed measurements. Each column of $\boldsymbol{\Phi}$ contains only $d = 35$ non-zero values equal to 1 at random positions [34]. Results are averaged over 50 iterations with different realization of random matrix $\boldsymbol{\Phi}$ in each iteration.

### 3.3.1 Performance measures

The overall performance evaluation of the proposed method is carried out using different performance metrics that includes compression ratio ($CR$), percentage root mean square difference ($PRD$) and signal to noise ratio ($SNR$) [34]. Diagnostic distortion measures such as wavelet energy-based diagnostic distortion ($WEDD$) [81] and wavelet weighted PRD ($WWPRD$) [80] are also used to assess clinical fidelity. Average value of $PRD$ across the channels is calculated as [121]:

$$Average\ PRD\ (APRD) = \frac{\sum_{i=1}^{L} PRD_i}{L} \tag{3.7}$$

The average values of $WEDD$ and $WWPRD$, abbreviated as $AWEDD$ and $AWWPRD$, are calculated in the same way as $APRD$ is calculated in (3.7). $CR$ is used to quantify the compression efficiency of the proposed method and is defined as:

$$CR = \frac{b_{\text{orig}}}{b_{\text{comp}}}, \quad \text{or} \quad CR(\%) = \frac{b_{\text{orig}} - b_{\text{comp}}}{b_{\text{orig}}} \times 100 \tag{3.8}$$

where $b_{\text{orig}}$ and $b_{\text{comp}}$ are the number of bits required for original and compressed signal, respectively.

### 3.3.2 Recovery results in different sparsifying basis

Experiments are conducted to investigate the PCA transformation as a sparsifying domain for MECG signals in order to realize joint PCA-CS. The MECG signals transformed in PCA domain are shown in Figure 3.1. From the plot it is clear that the first four eigenspace signals that capture most of the diagnostically relevant features (with $T_s \geq 99.5\%$) are sufficient to represent twelve channel information. Measurements obtained after random projection are further quantized and entropy-encoded to obtain the compressed bit streams. The performance of the proposed method can be further enhanced by finding a suitable transform that can represent eigenspace signals in a sparser form. Eigenspace MECG signals have relatively low sparsity in eigenspace itself (54.31%), which gives higher reconstruction error ($APRD = 8.219$ at $CR = 5.96$). However, CS reconstruction is known to be improved substantially in sparser domains [40]. Better sparse representation can be achieved for eigenspace MECG signals due to their redundant structure, analogous to the quasi periodical structure of time-domain MECG (Figure 3.1). To exploit this sparsity, it is necessary to perform the CS reconstruction for eigenspace MECG signals in some other suitable transform/sparsifying domain. Transformations such as, DWT, DCT, and DFT are experimented by changing the sparsifying basis $\mathbf{\Psi}$ to the respective transformation matrix in the OMP recovery algorithm. The performance of the proposed algorithm in all the above three domains in terms of different metrics for same datasets is shown in Table 3.1. The DWT basis outperforms DFT and DCT as the sparsifying. It produces best sparse approximation for eigenspace signals, which is verified by the minimum overall recovery distortions (at approximately the same $CR$ value). The sparsity is enhanced significantly (up to 80%) in the wavelet domain compared to sparsity in the eigenspace (54.31%) itself. On the other hand, DCT and DFT have sinusoids as their basis functions that may not be suitable for better representation of eigenspace MECG signals, leading to their poor performance. From the above experiments, it can be concluded that the proposed framework of compressed sensing for eigenspace MECG signals results in better signal reconstruction in the wavelet domain. Therefore, the CS recovery is performed exploiting the wavelet domain sparsity of eigenspace MECG signals.

**Table 3.1:** Performance evaluation of the proposed technique in different sparsifying domains for eigenspace MECG signals

| PTB dataset-s0002_rem | | | | | CSE dataset-M01_002 | | | | |
|---|---|---|---|---|---|---|---|---|---|
| Sparsifying basis | Performance metrics | | | | Sparsifying basis | Performance metrics | | | |
| | CR | APRD | AWEDD | AWWPRD | | CR | APRD | AWEDD | AWWPRD |
| DWT | 15.7 | 6.71 | 2.59 | 12.34 | DWT | 8.72 | 13.81 | 10.25 | 22.5 |
| DFT | 15.74 | 34.9 | 33 | 139.7 | DFT | 8.40 | 45.33 | 39.21 | 79.34 |
| DCT | 15.3 | 7.89 | 6.0 | 24.98 | DCT | 8.76 | 19.03 | 15.73 | 29.65 |

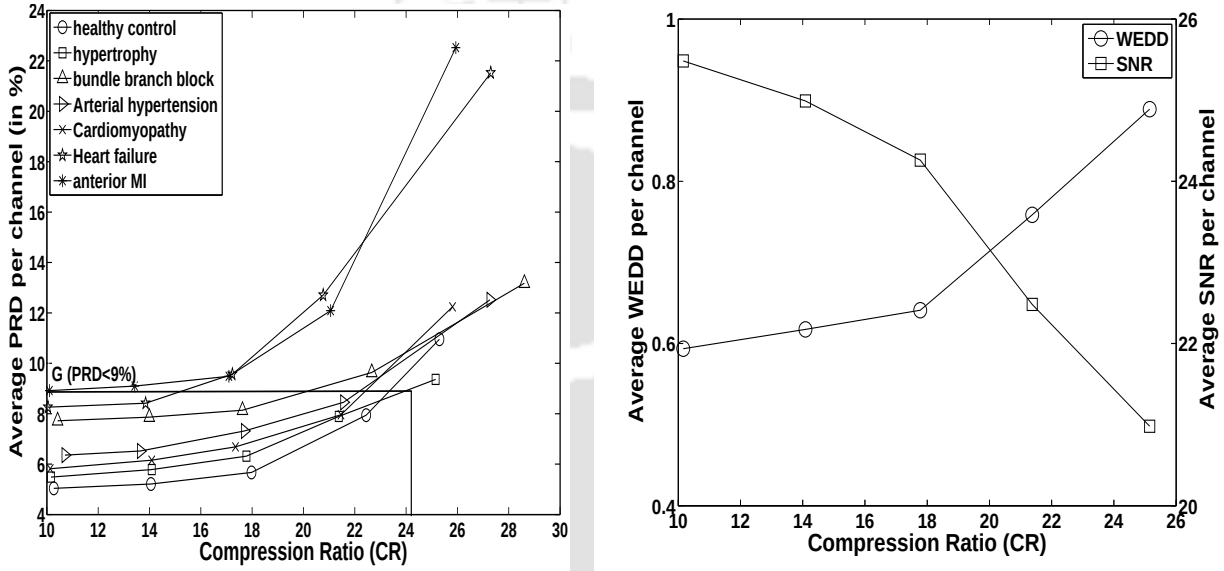


(a) (b)

**Figure 3.4:** (a) Evaluation of the proposed technique in terms of compression ratio (CR) at different distortion levels (average PRD) for different type of ECG signals exhibiting various pathological conditions. (b) WEDD and SNR variation with CR for dataset s0443 exhibiting hypertrophy. MECG datasets taken from PTB database.

### 3.3.3 Compression performance analysis

To study the variation of compression efficiency of the proposed encoder at different distortion levels, plots between $CR$ and average $PRD$ is shown in Figure 3.4(a) for the ECG signals associated with different pathological conditions. Here, average distortion values are calculated as the mean value per channel of a particular disease dataset. $PRD$ values less than 9% and $WEDD$ values less than 11.12% correspond to *good* quality signal reconstruction [1,79,81]. It is denoted by level 'G' in Figure 3.4(a). It is evident that most of the signals fall in this category. Best performance is achieved for the dataset s0443_rem having highest $CR = 25.15$ at $APRD = 8.9$. This dataset produces least distortion

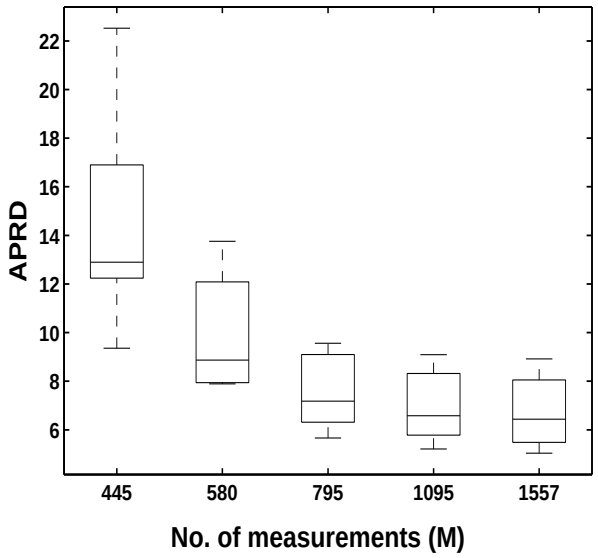


**Figure 3.5:** Box plot showing the variance of average output PRD per channel across all datasets of PTB database at different number of compressed measurements ($M$) for signal length N=3000

in terms of $WEDD$ and $SNR$ too. Variation of $WEDD$ and $SNR$ with $CR$ is shown in Figure 3.4(b) for dataset s0443_rem. Across all the MECG datasets from PTB database, lead V3 is found to have the least average value of $PRD = 5.24\%$ at $CR = 17.76$.

The variance of distortion i.e., APRD across individual datasets is shown in Figure 3.5 in the form of box plot at different number of compressed measurements ($M$). The edges of the box plots denote the $25th$ and $75th$ percentiles with the central line as median. Extreme values in the individual box plot depict the minimum and maximum $APRD$ values obtained at a particular value of $M$ for different datasets. Low value of distortion is achieved at a higher number of measurements as the median value decreases with $M$ but at the cost of $CR$ which holds inverse relation with $M$. Average distortion per channel saturates at around $M = 1000$ and $APRD$ does not depreciate much after that, as can be seen in last two box plots. This situation occurs because in the presence of a sufficient number of measurements, additional measurements do not add any extra information, and reconstruction accuracy remains almost the same.

Apart from the above case studies, average performance results are also calculated across the two databases (PTB and CSE) considered in this work. Reconstruction is performed at average $CR = 13.91$ and 10.39 and quantitative values of corresponding distortion metrics are given in Table

**Table 3.2:** Average value of distortion measures (both clinical, WEDD and WWPRD and non-clinical, PRD and SNR) for all the channels of MECG signals taken from PTB and CSE databases at average $CR = 13.91$ and 10.39, respectively. Average results are calculated over all the 549 data records of PTB database and 125 datasets of CSE database.

| Channels (Leads) | PTB Database | | | | CSE Database | | | |
|---|---|---|---|---|---|---|---|---|
| | PRD | WEDD | SNR | WWPRD | PRD | WEDD | SNR | WWPRD |
| I | 5.04 | 1.25 | 24.63 | 8.35 | 11.17 | 6.52 | 19.47 | 27.99 |
| II | 4.90 | 0.64 | 24.48 | 4.29 | 8.41 | 5.07 | 23.19 | 20.27 |
| III | 6.49 | 1.02 | 22.21 | 6.90 | 7.78 | 4.78 | 23.31 | 18.62 |
| aVR | 4.72 | 0.97 | 25.08 | 5.93 | 9.35 | 5.41 | 21.75 | 23.45 |
| aVL | 5.98 | 0.95 | 23.00 | 6.96 | 9.75 | 6.03 | 20.57 | 23.72 |
| aVF | 5.32 | 0.55 | 23.37 | 4.22 | 7.92 | 4.88 | 23.77 | 18.62 |
| V1 | 6.58 | 3.30 | 22.23 | 9.26 | 8.67 | 5.84 | 22.18 | 20.10 |
| V2 | 4.98 | 2.97 | 24.80 | 7.78 | 12.44 | 9.40 | 19.47 | 21.73 |
| V3 | 4.53 | 2.49 | 25.39 | 7.05 | 9.67 | 7.25 | 20.82 | 17.59 |
| V4 | 4.87 | 2.35 | 25.12 | 6.31 | 10.39 | 7.81 | 20.66 | 18.58 |
| V5 | 5.28 | 3.34 | 24.48 | 7.62 | 9.40 | 7.11 | 20.95 | 18.12 |
| V6 | 6.17 | 2.42 | 23.14 | 6.90 | 9.66 | 7.52 | 20.65 | 19.87 |

3.2. In an average sense too, the values of non-diagnostic distortion measures ($PRD$, $SNR$) as well as diagnostic distortion measures ($WEDD$, $WWPRD$) either fall in *very good* or *good* categories of reconstruction in all the channels. For CSE database, the error is relatively higher as compared to PTB. As a result, relatively low $CR$ value is achieved for CSE database than that achieved for PTB at a given distortion level. This may be because the low sampling frequency (500 Hz) of the CSE database as compared to PTB database (1 kHz) makes the MECG signals in the CSE database less compressible than the signals in the PTB database.

To analyze the data compression achieved in different stages of the proposed method, the compression achieved by different steps involved in the proposed encoding technique is calculated. Quantified values of $CR$ at each step, i.e., PCA, CS, and entropy encoding, are given in Table 3.3 for 10 different datasets, 5 each from PTB and CSE databases. For total average $CR = 18.86 : 1$ at $APRD = 8.44$, average contributions of the PCA, CS, and entropy encoding steps are found to be 4.62, 3.66, and 1.11, respectively for the PTB database. In the case of CSE database average contributions of three steps are 3.14, 2.61, and 1.21, respectively for total average $CR = 10.05 : 1$ at $APRD = 9.46$. So, both PCA and CS operations contribute almost equally in the compression efficiency of the proposed joint PCA-CS approach. Entropy encoding step enhances the CR further that is achieved by PCA

**Table 3.3:** CR obtained at different stages of the proposed algorithm

| Database | Datasets | CR at different stages | | | Final CR |
|---|---|---|---|---|---|
| | | PCA | CS | Entropy coding | |
| PTB | s0423rem | 3.98 | 3.71 | 1.12 | 16.65 |
| | s0404lrem | 5.31 | 3.30 | 1.09 | 19.29 |
| | s0027lrem | 5.31 | 3.71 | 1.11 | 22.01 |
| | s0275lrem | 5.31 | 3.71 | 1.11 | 22.06 |
| | s0029lrem | 3.25 | 3.90 | 1.12 | 14.33 |
| | **Average** | **4.62** | **3.66** | **1.11** | **18.86** |
| CSE | MO1_003 | 2.74 | 2.70 | 1.12 | 8.28 |
| | MO1_004 | 3.65 | 2.55 | 1.21 | 11.29 |
| | MO1_005 | 2.92 | 2.47 | 1.24 | 8.96 |
| | MO1_018 | 2.74 | 2.16 | 1.33 | 7.95 |
| | MO1_024 | 3.65 | 3.17 | 1.19 | 13.79 |
| | **Average** | **3.14** | **2.61** | **1.21** | **10.05** |

and CS operations.

It is to be noted that the eigenspace MECG signals (Figure 3.1) have varying information content (decreasing from top to bottom), and hence, varying sparsity. Highly sparse and low-informative signals can be acquired in very few CS measurements and hence could undergo through intensive compression. This flexibility in selecting the number of measurements can be used to control the data rates in telemonitoring applications. Data rates can be increased or decreased according to the extent of accuracy required at the healthcare centers.

## 3.4 Diagnostic Assessment of ECG Features

In a lossy compression technique, the loss of information is inevitable. Clinical feature assessment, therefore becomes important in order establish the compression efficiency of an encoding technique. The diagnostic quality of the reconstructed MECG signals is tested for several normal, pathological and noisy MECG signals. Open source OSET toolbox [122] is used to identify the QRS complex (an important ECG feature) in all the recovered signals, to ensure the feature preservation.

### 3.4.1 Noiseless scenario

In this section, the performance of the proposed method is evaluated on clean MECG signals which belong to normal as well as pathological classes. Healthy control or normal ECG signals posses

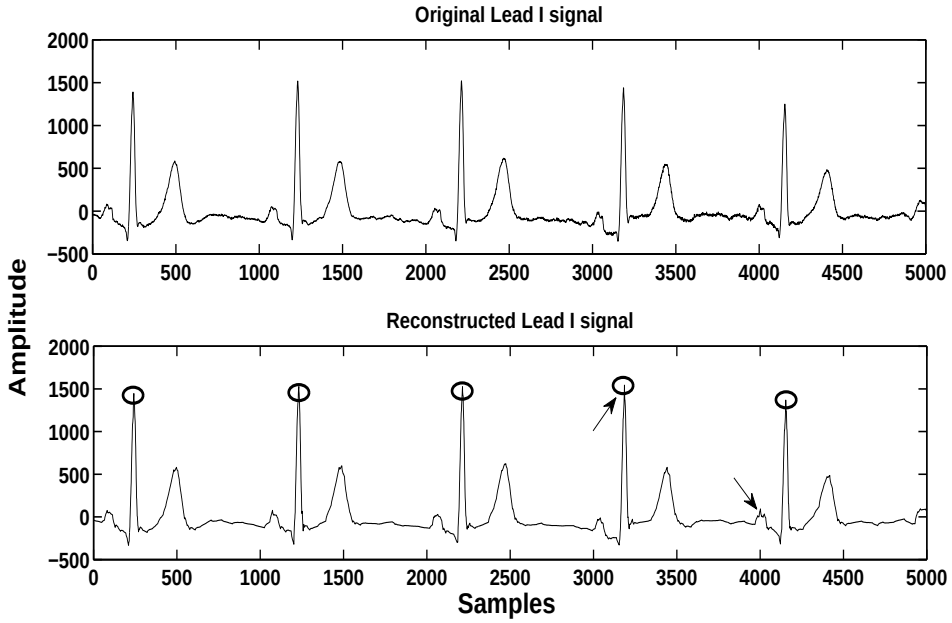


**Figure 3.6:** Original and reconstructed signal of Lead I taken from a healthy patient from PTB dataset s0465 at CR=13.18 and at sparsity constraint $K\_target = 208$ with identified R waves in the reconstructed signal. Alterations in the clinical segments are marked by arrows in the reconstructed waveform.

normal ECG rhythms (Figure 3.6) and their diagnostic information lies only in PQRST morphology. Figure 3.6 shows a Lead I plot from the dataset s0465_rem with its original and reconstructed signals; along with identified QRS complexes. The reconstruction is achieved from its compressed form at $CR = 13.18$. The quality of the reconstruction clearly shows the retention of the important clinical features of a normal ECG with little distortion in P wave and a slight loss in the amplitude of QRS complex (shown by arrows in the reconstructed signal).

In case of a pathology, the heart rhythms get altered and clinical information of the ECG signals may lie anywhere in the signal unlike the normal sinus rhythms. This reduces the sparsity of the signal both in the time-domain as well as in transformed domain. A pathological ECG signal exhibiting antero-septal myocardial infarction is shown in Figure 3.7(a). It is taken from Lead I of dataset s0410lrem from PTB database. Here, the diagnostic features are spanned over the entire signal waveform without any isoelectric line. For these types of pathological signals too, a satisfactory reconstruction with good clinical fidelity is obtained with a relatively low $CR$ (=12.74 at 8-bit quantization). Figure 3.7(b) shows a different pathological case taken from Lead III of dataset s0007rem

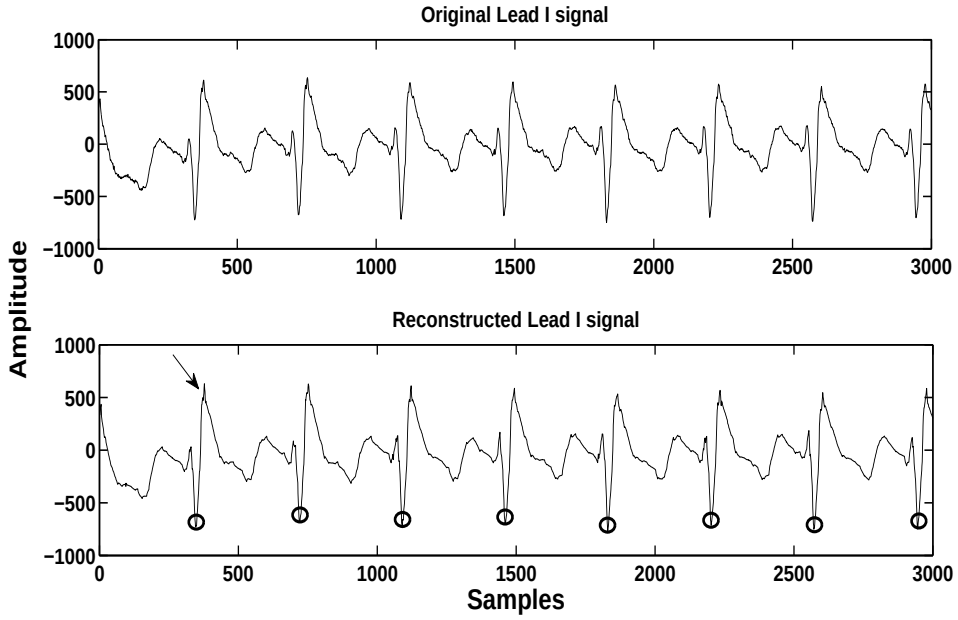


(a)

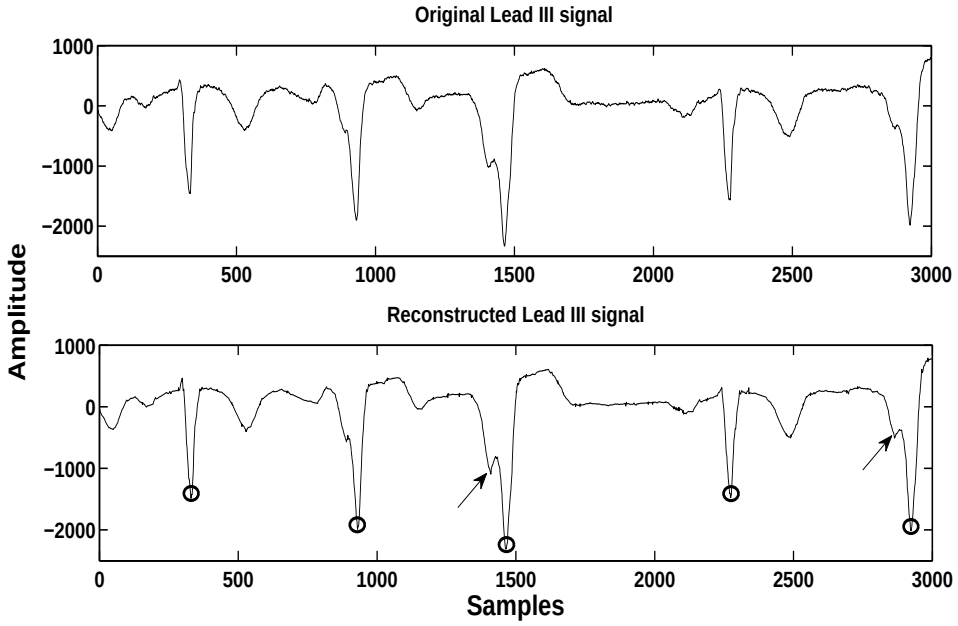


(b)

**Figure 3.7:** (a) Original signal of Lead I taken PTB dataset s0410lrem exhibiting antero-septal myocardial infarction and its reconstructed version at CR=12.74 (b) Original and reconstructed signal of Lead III taken from PTB dataset s0007rem exhibiting irregular pathological beats at CR=13.1 with identified R waves in the reconstructed signals. Sparsity constraint is put at $K\_target = 208$. Alterations in the clinical segments are marked by arrows in the reconstructed waveforms.

with highly irregular heart-beats. When reconstructed at $CR = 13.1$, it shows a good quality recovery with a marginal loss in the amplitude that occur for a couple of notches present in the QRS complex (shown by arrows). In all the above CS reconstruction, sparsity constraint is taken as $K\_target = 208$ in the OMP algorithm.

### 3.4.2 Noisy scenario

The signal reconstruction ability of the proposed encoder is also assessed for cases of noisy MECG signals. As noise remains present in nearly all practical applications, this case study becomes important. Two types of noisy signals are analyzed in this experiment: ECG signals with naturally present noise, and ECG signals with artificially-added noise. Figure 3.8 depicts both of these reconstructions. A noisy dataset $M01\_014$ from CSE database with mostly powerline noise, a very common noise present in the ECG during its acquisition, is compressed by the proposed encoder. Reconstruction is performed at $CR = 7.76$ and waveforms are shown in Figure 3.8(a). In the other experiment, clean pathological data-set $s0154\_rem$ exhibiting palpitation has been corrupted by artificially adding 10 dB additive white Gaussian noise (AWGN). Recovered signal at $CR = 9.1$ and average $PRD$ ($APRD$)=10.6 % is shown in Figure 3.8(b). As evident from the recovered signals in both the cases, important clinical features of ECG are almost preserved and noise level is significantly reduced. Nominal alterations are noted in the reconstructed waveforms (indicated by arrows). This experiment also establishes the denoising ability of the proposed algorithm in addition to good signal retrievability at high $CR$ values. The denoising feature of the algorithm can be attributed partly to the rejection of insignificant PCs that are mainly noise-dominated [120], and partly to the controlled selection of columns of $\mathbf{\Phi}$ (also called atoms or bases) during CS reconstruction. The number of atoms (sparsity constraint) is reduced to $K\_target = 35$ in the sparse recovery algorithm OMP so as to select only highly correlated atoms, leaving behind uncorrelated noisy atoms.

Therefore, it can be concluded that the proposed algorithm is applicable for all variants of MECG signals having different morphologies. The compression efficiency may vary with different signals, but diagnostic features are maintained in each case. This makes the reconstructed signals usable for clinical purposes. To quantify the visual quality of reconstructed MECG signals, a subjective quality measure called mean opinion score (MOS) is used. It is a qualitative-based distortion measure [79, 88]

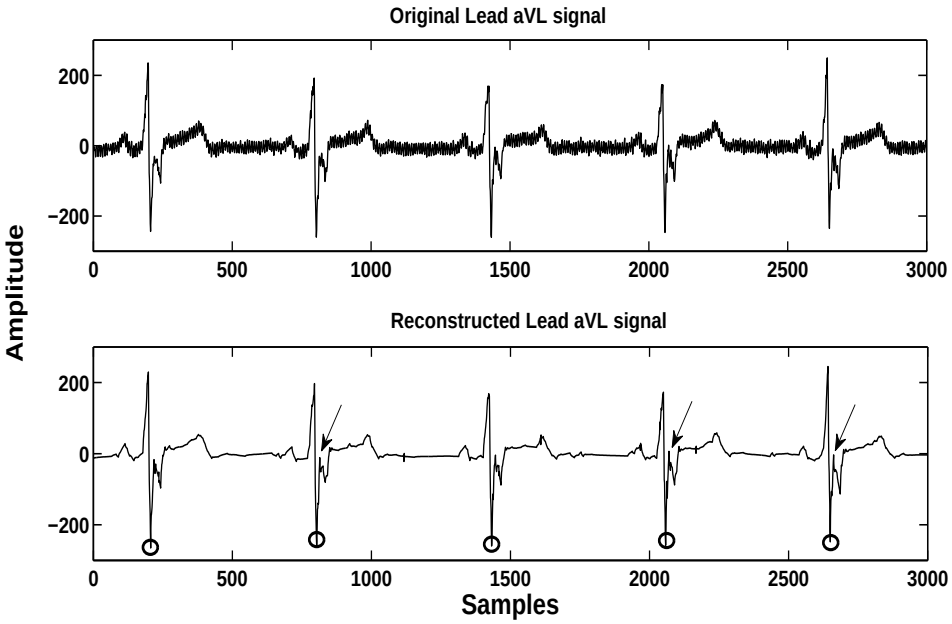


(a) Denoising of a noisy ECG signal

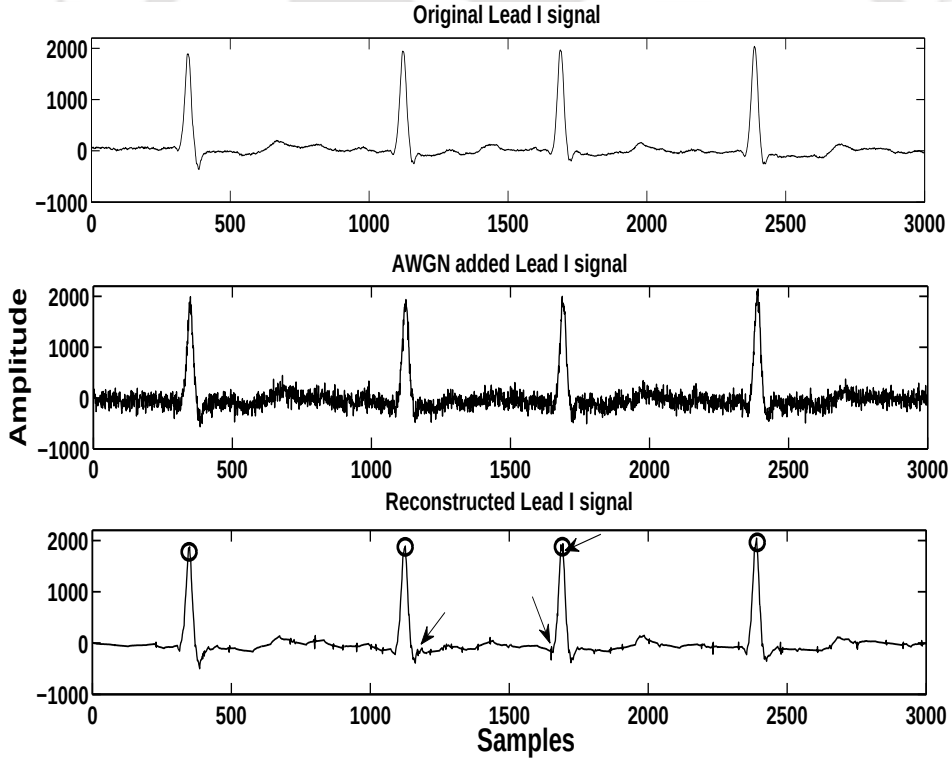


(b) Denoising of a AWGN added ECG signal

**Figure 3.8:** Demonstration of the denoising ability of the proposed technique. (a) Original noisy ECG signals and reconstructed (denoised) signal from Lead aVL of dataset M01_014 of CSE database at CR=7.76 and sparsity constraint $K\_target = 108$. (b) Originally clean signal from Lead I added with 10 dB additive white Gaussian noise (AWGN) and corresponding reconstructed (denoised) signal at CR=9.12 and $K\_target = 35$. The PTB Dataset s0154_rem exhibiting coronary heart-disease was used . Circles show the identified R waves while arrows indicate the altered clinical segments in the reconstructed waveforms.

**Table 3.4:** MOS Error (in %) in ECG signals from different channels.

| M OS error for different diagnostic features of ECG | | | |
|---|---|---|---|
| Features/Segments of ECG signal | Lead I | Lead aVL | Lead V5 |
| P-wave | 8 | 10 | 4 |
| PR-segment | 10 | 16 | 8 |
| PR-interval | 4 | 8 | 4 |
| QRS-complex | 12 | 8 | 12 |
| ST-segment | 8 | 16 | 6 |
| T-wave | 6 | 8 | 2 |
| Overall ECG signal | 8 | 11 | 6.66 |

that measures visual distortions in the recovered signal. The evaluators for this subjective study include two doctors, and ten research scholars and project engineers working in the area of biomedical signal processing. Different diagnostic features of ECG, such as P-wave, PR-segment, PR-interval, QRS-complex, ST-segment and T-wave are evaluated in a semi-blind test, where the evaluators are provided with the originals and reconstructed versions of the ECG signal and are asked to find the similarities between them. The quality rating used for this evaluation is as follows: 1 (bad), 2 (almost tolerable), 3 (tolerable), 4 (good), and 5 (excellent) [79,88]. The average MOS error in percentage for the ECG signals from the Lead I, Lead aVL, and Lead V5 for dataset M01_014 is given in Table 3.4. According to MOS rating [79], all the diagnostically-important features of ECG fall into the category of *very good* signal reconstruction. MOS error for overall ECG signal is also calculated and Lead V5 was found with least MOS error of 6.66%.

## 3.5 Comparison with the State-of-the-art Techniques

A detailed performance comparison of the proposed technique is done with the existing CS-based ECG data compression techniques and the results are shown in Table 3.5. The channel-wise distortion incurred during the entire encoding and the reconstruction process is compared in terms of same distortion measures as used in the respective works. One of the recent CS-based work reported for ECG signals is based on multi-scale CS for efficient MECG data encoding [44]. When compared with this method in terms of $PRD$, $SNR$, and $WEDD$ at almost same $CR$ level ($\approx 10.26:1$), the proposed technique displays significant improvement (Table 3.5). The improvement in the distortion levels is

achieved due to the removal of redundant information across the channels using PCA before applying CS on the resultant eigenspace signals. However, [44] does not exploit the inter-channel correlation. It encoded and decoded all channels individually, corresponding to high frequency wavelet subband matrices, resulting in a poor compression efficiency, or equivalently, higher distortions at a given $CR$ level. Another work reported in [34] presents a power-efficient data reduction technique based on joint CS (JCS) for MECG signals exploiting the idea of joint sparsity. On comparison of the proposed method with the JCS method, substantial gain in the compression performance is achieved with less output distortions. At $CR \approx 8:1$, approximately the same as reported in [34], significant gain in the reported reconstruction $SNR$ is obtained in each channel's ECG signal. This performance gain is mainly due to exploitation of different correlations in MECG signals by the proposed method, which helps increase the overall compression efficiency. On the other hand, JCS only targets inter-channel correlations. A joint sparsity-based single-channel ECG compression work is presented in [97]. This is implemented here for MECG signals for comparison purpose with the help of the source code provided by the authors. We have used the same distributed CS (DCS) approach with simultaneous OMP technique as in [97]. However, the concept of DCS did not work well for MECG since it gives high $PRD$ and $WEDD$ values.

The present work is also compared with another multi-scale PCA (MSPCA)-based MECG compression technique proposed by Sharma et al. [88]. Significantly reduced distortions are achieved for all channels at the same reported $CR = 5.98$ for the same dataset. The improved performance gain was expected due to the exploitation of sparsity of eigenspace MECG signals using CS framework in the proposed work that was ignored in [88]. CS-based single-channel ECG compression works reported in earlier studies [1, 46] show lower compression efficiencies. Individual channel processing in these works does not allow to exploit the inherent inter-channel correlation that exists among different channels. This leads to low CR, or high distortion at a particular CR as compared to the proposed work as shown in Table 3.5.

**Table 3.5:** Performance comparison table

| Techniques | Metrics | Leads | | | | | | | | | | | | Average | CR | Database |
|---|---|---|---|---|---|---|---|---|---|---|---|---|---|---|---|---|
| | | Lead I | Lead II | Lead III | aVR | aVL | aVF | V1 | V2 | V3 | V4 | V5 | V6 | | | |
| MCS [44] | PRD | 20.26 | 19.51 | 21.97 | 17.91 | 23.84 | 23.75 | 14.66 | 13.97 | 17.73 | 18.91 | 19.35 | 15.88 | 17.29 | 10.26:1 | CSE |
| | WEDD | 8.09 | 6.46 | 8.16 | 6.44 | 10.24 | 9.29 | 4.72 | 4.02 | 6.01 | 6.43 | 6.51 | 5.28 | 6.80 | | |
| **Proposed** | PRD | 11.17 | 8.41 | 7.78 | 9.35 | 9.75 | 7.92 | 8.67 | 12.44 | 9.67 | 10.39 | 9.40 | 9.66 | **9.55** | 10.39:1 | |
| | WEDD | 6.52 | 5.07 | 4.78 | 5.41 | 6.03 | 4.88 | 3.84 | 3.40 | 4.25 | 3.81 | 2.11 | 3.52 | **4.46** | | |
| JCS [34] | SNR | 22 | 23 | 24 | 19 | 21 | 22 | 19 | 21 | 22 | 24 | 27 | 27 | 22.58 | 8.00:1 (87.50%) | PTB |
| **Proposed** | SNR | 36.74 | 44.32 | 41.53 | 42.22 | 39.31 | 43.97 | 34.73 | 34.71 | 35.29 | 34.75 | 35.96 | 35.34 | **38.23** | 8.37:1 (88.05%) | |
| DCS [97] | PRD | 23.78 | 23.74 | 15.27 | 12.35 | 42.86 | 10.06 | 16.92 | 11.21 | 7.78 | 8.20 | 8.41 | 7.36 | 15.66 | 5.98:1 | |
| | WEDD | 19.00 | 18.21 | 11.06 | 8.81 | 37.49 | 6.86 | 12.27 | 8.84 | 5.50 | 5.87 | 5.96 | 5.25 | 12.09 | | |
| MSPCA [88] | PRD | 18.76 | 20.74 | 12.51 | 12.85 | 35.80 | 8.08 | 9.82 | 11.74 | 14.08 | 10.33 | 7.63 | 6.82 | 22.16 | 5.98:1 | CSE:M01_014 |
| | WEDD | 8.26 | 5.87 | 6.28 | 5.54 | 27.18 | 9.23 | 9.57 | 8.34 | 10.97 | 6.38 | 4.27 | 4.19 | 8.84 | | |
| **Proposed** | PRD | 17.3 | 13.3 | 12.4 | 8.51 | 27 | 4.71 | 7.8 | 11.4 | 8.2 | 6.27 | 6 | 4.43 | **10.61** | 5.97:1 | |
| | WEDD | 1.08 | 1.76 | 1.81 | 5.68 | 8.92 | 2.41 | 4.03 | 7.95 | 5.53 | 4.9 | 3.49 | 1.5 | **4.08** | | |
| Mamaghanian [1] | PRD | - | - | - | - | - | - | - | - | - | - | - | - | 5.53 | 4.54:1 | PTB |
| **Proposed** | | - | - | - | - | - | - | - | - | - | - | - | - | **3.34** | 4.27:1 | |
| WLM [46] | PRD | - | - | - | - | - | - | - | - | - | - | - | - | 6.34 | 8.09:1 | PTB |
| **Proposed** | | - | - | - | - | - | - | - | - | - | - | - | - | **4.38** | 8.66:1 | |

**Table 3.6:** Computational cost of the proposed method in terms of average execution time required by the algorithm for encoding and decoding.

| Measurements (M) | Execution time (s) at each stage of the algorithm | | | | | |
|---|---|---|---|---|---|---|
| | Eigenspace transformation | CS encoding | Total | CS recovery | Inverse PCA | Total |
| 400 | 0.0087 | 0.0035 | 0.0122 | 0.3525 | 0.0043 | 0.3568 |
| 700 | 0.0129 | 0.0051 | 0.0180 | 0.5402 | 0.0054 | 0.5456 |
| 1000 | 0.0112 | 0.0082 | 0.0194 | 0.6168 | 0.0058 | 0.6226 |

## 3.6 Practical Considerations

This section discusses the proposed method in the context of some of the practical issues. The sensing matrix responsible for data reduction in the CS operation is taken to be a random sparse binary matrix having binary entries, i.e., 0s and 1s only. This replaces the multiplication operation with a simple addition operation reducing the computation burden at the encoder.

In order to analyze the computational cost of the proposed method, the average execution time (CPU time) required in each stage of the algorithm is calculated. The simulation is done on MATLAB R2010a using 3.20GHz Intel Core i5 system with 8GB RAM. Average time elapsed in each of the encoder and decoder module for one MECG data packet $\boldsymbol{X} \in \mathbb{R}^{300\times 8}$ is given in Table 3.6 for different number of measurements ($M$). It can be observed that the PCA module adds only a marginal delay in encoding and decoding process while most of the CPU time is consumed by the CS module. CS decoding being a computationally intensive task takes the highest CPU time (0.3525 $s$) for $M = 400$. CS encoding that involves a simple matrix multiplication operation takes the least time ($0.0035s$). Encoding and decoding time increases when more number of measurements are used for CS recovery. This experiment helped us to infer that the use of PCA with traditional CS-based compression techniques can boost up the compression efficiency with little increase in the computational cost of the system.

For PCA implementation, certain statistical features of the data (mean and covariance) are required and hence they need to be estimated at the run time. To realize joint PCA-CS practically, a training and monitoring-based approach is usually adopted [50, 119]. Here too, the joint PCA-CS framework is implemented in two phases: training and monitoring. Statistical features are calculated in the training

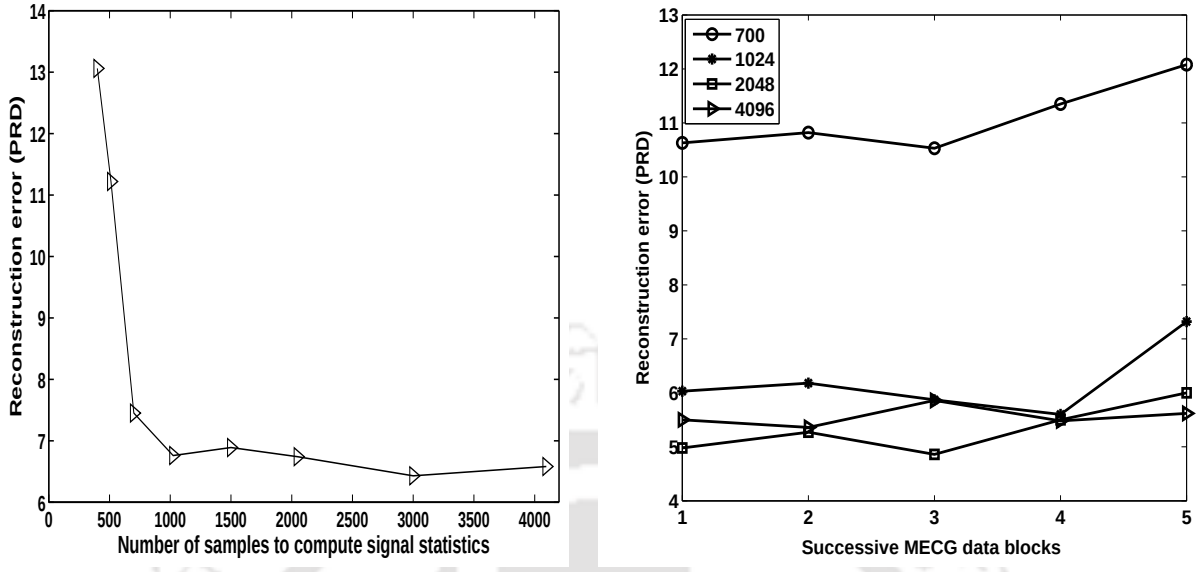


**Figure 3.9:** Reconstruction error analysis. (a) Variation of output signal reconstruction error in terms of PRD w.r.t. number of samples used to compute signal statistics (means, covariance). (b) Output distortion variation in terms of PRD for reconstruction of successive MECG data blocks using same eigenspace transformation matrix $\boldsymbol{P}$. Different plots show the distortion variation in cases when different number of samples are used to compute signal statistics.

phase to find mean $\bar{\boldsymbol{X}}$ and transformation matrix $\boldsymbol{P}$, which are further used in the monitoring phase for compressive measurement. To find the optimum number of training samples for computation of signal statistics, the output reconstruction error in terms of $PRD$, is simulated at a fixed number of CS measurements. Figure 3.9(a) shows the error variation with respect to varying number of training samples. It can be observed that the error trend decreases with an increase in number of samples. Hence, sufficient number of training samples should be included to compute signal statistics. Also, the error fluctuation minimizes and almost settles to a minimum at higher number of training samples.

Unlike other non-stationary signals, the training module may not be required to update quite frequently for ECG signals, thus minimizing the number of computations at the encoder. ECG signals, though considered non-stationary [121], are slowly varying in nature. Because of this, the statistical features of MECG do not change significantly over time for patient-specific applications, until a sudden arrhythmia is reported. Therefore, PCA transformation matrix $\boldsymbol{P}$, once calculated with sufficient number of training samples, may be used for subsequent incoming data blocks. Training module may

not need to be updated at each instance of the data acquisition. A simulation study is conducted to support this statement. Simulation results for dataset $s0443\_rem$ are depicted in Figure 3.9(b). Five successive data blocks of the dataset are reconstructed after joint PC-CS operation with the same eigenspace transformation matrix $\boldsymbol{P}$ for each block. It may be noted that the output reconstruction error, in terms of $PRD$, slightly fluctuates, but remains approximately same for a number of incoming blocks. Significant change is only noticed after four to five blocks. Thus, in a scenario involving tolerable error, this observation remains valid. Matrix $\boldsymbol{P}$ can be recalculated after some time to follow the statistical changes in the data, if any. This may help in lessening the computational burden at the encoder at a cost of marginal increase in error. Hence, despite the computational cost incurred in the training phase, PCA can be successfully employed with CS to produce substantial improvement in terms of compression efficiency as compared to the existing CS-based MECG data compression techniques (TABLE 3.5).

### 3.6.1 Evaluation of computational complexity

To calculate the computational cost of the proposed method, the algorithmic complexity of PCA and CS needs to be calculated. The PCA operation consists of two steps: covariance matrix calculation and eigenvalue decomposition. So, the computational complexity of PCA will depend on these two operations. For a data matrix $X \in \mathbb{R}^{N \times L}$, covariance calculation involves $NL^2$ number of multiplications. On the other hand, eigenvalue decomposition involves a worst-case multiplication complexity of $O(L^3)$ [123]. Therefore, total complexity involved with PCA operation is $O(NL^2 + L^3)$. The standard joint CS-based algorithms show the complexity of the order of $O(dNL)$ [34] when random sparse binary sensing matrix $\boldsymbol{\Phi}$ is used with $d$ number of 1s in each column. Therefore, the total complexity involved with the proposed joint PCA-CS approach is $O(NL^2 + L^3 + dNL)$.

We have also compared the computational complexity of the proposed method with the existing CS-based methods. The performances of these methods have already been compared with the proposed method in the previous section. Complexity is calculated in terms of order of the signal length ($N$) and execution time, and shown in Table 3.7. A recent CS-based technique with a DWT-based preprocessing is reported in [44]. This follows a multi-scale CS (MCS) approach for MECG signal encoding. This method has computational complexities of DWT and CS together. The complexity

**Table 3.7:** Comparative study of †computational cost of the proposed method and existing methods. Execution time is the average CPU time required by the algorithms for encoding and decoding of one MECG data frame $\boldsymbol{X} \in \mathbb{R}^{3000\times 8}$

| Techniques | Complexity order | Encoding time (s) | | | Decoding time (s) | | |
|---|---|---|---|---|---|---|---|
| | | Data compression | Quantization & encoding | Total | Huffman decoding | Time-domain recovery | Total |
| MCS [44] | $O(NlogN + dNL)$ | 0.0102 | 1.0107 | 1.0209 | 2.7271 | 8.6482 | 11.3753 |
| JCS [34] | $O(dNL)$ | 0.0081 | 1.2502 | 1.2583 | 4.3704 | 11.9402 | 16.3106 |
| DCS [97] | $O(dNL)$ | 0.0093 | 1.3541 | 1.3634 | 6.0345 | 0.0276 | 6.0621 |
| MSPCA [88] | $O(NlogN + NL^2 + L^3)$ | 0.0211 | 1.1371 | 1.1582 | 5.6405 | 0.0274 | 5.6679 |
| Mamaghanian [1] | $L \times O(dN)$ | 0.0188 | 1.2421 | 1.2609 | 4.6620 | 21.2817 | 25.9437 |
| WLM [46] | $L \times O(dN)$ | 0.0196 | 0.9843 | 1.0039 | 4.0405 | 18.8602 | 22.9007 |
| **Proposed** | $O(NL^2 + L^3 + dNL)$ | 0.0235 | 0.5242 | **0.5477** | 2.1234 | 0.2879 | **2.4113** |

†All computations are done on the same computing platform having 3.20GHz i5 system with 8GB RAM.

of DWT is $O(N\log N)$ [124] and for CS it is $O(dNL)$ [34]. So, the total complexity of the method is $O(N\log N + MN)$. There are two traditional CS-based methods: joint CS (JCS) [34] and distributed CS (DCS) [97], which are used for MECG data compression. The encoding steps are same in both cases, while the decoding algorithms are different. Both the JCS and DCS have same data encoding complexity, i.e., $O(dNL)$. A CS framework for single-channel ECG data compression was employed in [1,46]. Both the above techniques have ability to perform individual channel CS processing. Therefore, for $L$ ECG channels, their complexity level is $L \times O(dN)$. The comparison is also done with a multi-scale PCA (MSPCA)-based work [88], which uses PCA at each wavelet scale to exploit inter-channel correlation for MECG data compression. It has combined algorithmic complexity of DWT and PCA, i.e., $O(N\log N + NL^2 + L^3)$, as given in Table 3.7.

Therefore, by observing the algorithmic complexity of different methods in terms of the signal length $N$ and the number of channels $L$, it may be concluded that, though the performance of the proposed method is superior to the existing methods (Table 3.5), this performance gain comes at the cost of a moderate increase in the computational complexity. However, this additional theoretical complexity of the proposed joint PCA-CS approach is not significant enough to be noticeable in practical applications. This is because, practically, the signal length $N(= 3000)$ and number of channels $L(= 8)$

may not be large enough to significantly affect the computational cost of the system. To support this statement, we compared the average execution time required by each of the aforementioned algorithms for encoding and decoding of same MECG data block $\boldsymbol{X} \in \mathbb{R}^{3000\times 8}$ using same computing platform. Results are shown in Table 3.7. It is observed that the proposed method requires relatively higher time at the data compression stage compared to the traditional CS-based methods, JCS, DCS, MCS, but has comparable execution time with the rest of the methods. Also, if we include the quantization and entropy encoding time with data compression time, then the proposed method performs better than the rest of the techniques. Overall, the MECG data can be encoded nearly twice as fast by the proposed method ($0.5477s$) compared to other techniques (Table 3.7). Similarly, the proposed method requires less than half of the time ($2.4113s$) required to decode the same data block as compared to the fastest MSPCA technique ($5.6679s$). The DCS (0.0274) and the proposed technique ($0.2879s$) use greedy algorithms for sparse recovery. The greedy algorithms are relatively faster than the convex optimization-based CS recovery algorithms employed in the rest of the CS-based techniques. Additionally, in the quantization and entropy encoding/decoding phases, all the techniques have to process data corresponding to all eight channels, whereas the proposed method needs to process only principal eigenspace signals, which decreases the overall encoding and decoding time.

### 3.6.2 Power consumption analysis

In this section, analysis of power consumption by the proposed method and other existing methods is carried out by following a power model reported in [125]. This model was employed in several earlier studies [37, 58] for comparative power consumption analysis in remote monitoring applications with CS-based compression systems. It is shown that the total power in such systems is contributed by three different types of powers:

$$P_{total} = P_{sense} + P_{proc} + P_{trans} \tag{3.9}$$

The power consumed in signal sensing $P_{sense}$ comprises of two factors: amplification ($P_{amp}$) and analog-to-digital conversion ($P_{ADC}$). Therefore, for $L$ number of channels, it is given by: $P_{sense} = L(P_{amp}+P_{ADC})$. Processing power ($P_{proc}$) involves two types of powers, $P_{PCA}$ and $P_{CS}$ corresponding to PCA and CS operations. Again, $P_{CS}$ comprises random number generation ($P_{RNG}$) and matrix

multiplication operations ($P_{mul}$). Hence, $P_{proc} = P_{PCA} + P_{RNG} + P_{mult}$. Transmission or communication power ($P_{trans}$) depends on the communication protocol, which makes it difficult to model it uniquely. In general, it is given as $P_{trans} = LJf_sR$, where $J$, $f_s$ and $R$ are transmission power per bit, sampling frequency, and number of bits per sample, respectively. The proposed method reduces the transmission power by $1/CR$ times by compressing the data to be transmitted. Thus, the total power consumption in the proposed system is given by:

$$P_{total} = L(P_{amp} + P_{ADC}) + P_{PCA} + P_{RNG} + P_{mult} + (1/CR)LJf_sR \tag{3.10}$$

Now, if $P_{sys}$ is the power consumed by the proposed system when there is no data communication, then the transmission power in (3.9) will be zero, i.e., $P_{trans} = 0$. From (3.9) and (3.10),

$$P_{sys} = P_{sense} + P_{proc} = L(P_{amp} + P_{ADC}) + P_{PCA} + P_{RNG} + P_{mult} \tag{3.11}$$

Furthermore, if the proposed system consumes $P_{nocomp}$ amount of power when data is transmitted without any compression, then the term $1/CR$ will vanish from (3.10), and $P_{nocomp}$ will be given as:

$$P_{nocomp} = L(P_{amp} + P_{ADC}) + P_{PCA} + P_{RNG} + P_{mult} + LJf_sR \tag{3.12}$$

To get an idea of power cost of the proposed system, we followed the steps suggested in [37,58,125], where the authors referred to hard values of different types of powers involved in (3.10), from different studies for approximate power calculation. A hardware-based study done in [126] reported that a CMOS amplifier with gain 67.7 dB consumes $P_{amp} = 0.274\ \mu W$ power during ECG signal amplification. The ADC power is taken from [127] as $P_{ADC} = 0.2\ \mu W$ for 12-bit resolution ($R$) and sampling frequency $f_s = 500$ Hz. For $P_{PCA}$, we have referred to the work in [128], which proposed an efficient low power VLSI architecture for PCA implementation. Their study shows that PCA operation consumes 152 $\mu W$, 282 $\mu W$, and 521 $\mu W$ power for 16, 32, and 64 features or channels, respectively. It can be seen that $P_{PCA}$ scales almost linearly with the number of channels. Therefore, the average power consumption per channel comes out to be 9.50 $\mu W$, 8.81 $\mu W$, and 8.14 $\mu W$, respectively in each case. Taking average of the three cases, $P_{PCA}$ per channel is 8.82 $\mu W$. The values of $P_{RNG} = 3\ \mu W$ [129] does not scale with the channels as the same random sensing matrix $\mathbf{\Phi}$ is used for each channel. The power $P_{mult} = 352\ \mu W$ is taken from [125], which is the maximum power in worst case scenario for the

systems having 64 or less channels assuming the DSP chip from TI MSP430 family. Authors in [130] estimated the transmission energy per bit ($J$) to be 5 $nJ$.

Taking the above state-of-the-art figures, total power consumed by the system is given as: $P_{sys} = 8 \times (0.274 + 0.2) + 8 \times 8.82 + 3 + 352 = 429.35\ \mu W$ and power consumption during data transmission (without compression) is given as: $P_{nocomp} = 3.79 + 70.56 + 3 + 352 + 240 = 669.35\ \mu W$. On the other hand, there is $P_{total} = 3.79 + 70.56 + 3 + 352 + 240/18.86 = 442.07\ \mu W$ power consumption when data is transmitted in compressed form using the proposed compression algorithm. So, a power saving of 33.95% can be achieved by the proposed method as compared to the case when data is transmitted in raw form (without compression).

Following the same power model (3.9), power consumption is also calculated for other existing methods [34, 44, 88, 97]. Taking the same value of $CR$ as reported in the above works, power in different studies is given by: $P_{MCS} = L(P_{amp} + P_{ADC}) + P_{DWT} + P_{RNG} + P_{mult} + (1/CR)LJf_sR = 3.79 + 8 \times 100 + 3 + 352 + 240/10.26 = 1182.2\ \mu W$ (Taking $P_{DWT} = 100\ \mu W$ per ECG channel [131]),

$P_{JCS} = 3.79 + 3 + 352 + 240/8 = 388.79\ \mu W$,

$P_{DCS} = 3.79 + 3 + 352 + 240/5.98 = 398.92\ \mu W$,

$P_{MSPCA} = 3.79 + 800 + 70.56 + 240/5.98 = 1269.5\ \mu W$,

$P_{Mamaghanian} = 3.79 + 3 + 352 + 240/4.54 = 411.65\ \mu W$,

$P_{WLM} = 3.79 + 3 + 352 + 240/8.09 = 388.45\ \mu W$.

From this study, it can be concluded that the proposed method (442.07 $\mu W$) saves significant amount of power (65.18%) as compared to the DWT-based preprocessing methods (1269.5 $\mu W$) [88]. However, it consumes a little higher (12.13%) amount of power as compared to the CS-based techniques (388.45 $\mu W$) [46]. If we see the overall power to compression ratio (PCR) i.e. power required for unit compression, then the proposed method is found to have lower PCR (23.44) than the CS-based techniques (48.01 for WLM). This is due to higher compression efficiency of the proposed method as compared to the CS-based techniques (Table 3.5).

It must be noted that the authors in [37, 58, 125] have used the power calculation formula (3.10) for theoretical power calculations only. Different values of power incurred in different processes are taken from other studies, e.g., the value of $J$ is taken for a particular processor family. Its value may change for some other processor. We have also used the model (3.10) only for the comparative study,

keeping the same parameters in all the cases.

## 3.7 Summary

In this chapter, a joint PCA-CS approach is investigated for MECG signals. PCA over MECG signals facilitates the application of CS framework in eigenspace. PCA is used to decorrelate the mutually-correlated 12-channel ECG signals, and capture their clinical features in reduced-dimension eigenspace signals. Sparse eigenspace signals are then randomly projected on to a sparse binary sensing matrix to obtain the compressed measurements. Using orthogonal matching pursuit (OMP) and inverse PCA, original data is successfully recovered while preserving the important clinical features. The algorithm is evaluated on a data compression platform for a variety of pathological, noisy and normal MECG datasets. Higher data compression performance is achieved for the proposed method compared to state-of-the-art CS-based techniques because of exploitation of spatio-temporal redundancies present in MECG system. Higher compression efficiency at reduced signal distortion helps reduce the overall volume of the data to be transmitted, thus saving the transmission power cost.

भारतीय प्रौद्योगिकी संस्थान गुवाहाटी
Indian Institute of Technology Guwahati

# 4

# Weighted Mixed Norm Minimization-based Joint Compressed Sensing

Contents

As we observed in the previous chapter that joint processing of all ECG channels is advantageous over individual channel processing due to their spatially shared information. Therefore, channel-by-channel processing of MECG is not optimal in terms of the computational cost as well as the system performance. A joint principal component analysis (PCA)-compressed sensing (CS) approach was introduced in Chapter 3 to deal with all the channels together. PCA was used to decorrelate the spatially correlated MECG signals and the resulting principle sparse eigenspace signals were gone through further dimensionality reduction using CS. In this chapter, to reduce the processing steps at the encoder in order to minimize the computational resources, we explored new ways to process correlated MECG signals in the CS framework. A new CS model called multiple-measurement-vector (MMV) model [106] is employed, where all the channels' data is compressed simultaneously using a simple matrix multiplication with a random sparse sensing matrix having very few nonzero entries (of unity magnitude). The inter-channel correlation information is exploited at the decoder to recover all the ECG channels simultaneously. In this way, most of the processing steps and corresponding computational requirements are transferred from encoder to decoder. It is very important from the energy saving point of view, as in telemonitoring applications decoding is performed at hospitals/healthcare centers, which are more resourceful than the encoders, which are highly resource-constrained. The MMV CS model has not been well explored for ECG signals as most of the existing CS-based works employ the traditional single-measurement-vector (SMV) model [1, 41, 44, 46], which allows only single channel processing.

In addition to employing a low-complexity encoder, a joint CS recovery algorithm based on weighted mixed-norm minimization (WMNM) is also proposed in this chapter. WMNM exploits the wavelet domain joint sparsity of MECG signals for their simultaneous reconstruction. Recently, a similar traditional (non-weighted) mixed-norm minimization (MNM)-based recovery algorithm [34] is reported for a CS-based MECG data compression/reconstruction task. It is to be noted that when the number of measurements is low (at higher compression ratios), the performance of the traditional MNM algorithm was observed to be unsatisfactory. While reviewing this work in Chapter 2, this fact is demonstrated through reconstruction results in Section 2.3. The amplitude dependence of the MNM algorithms, similar to traditional $l_1$-norm minimization algorithms, might be the reason behind this under-performance [132, 133]. Due to the amplitude dependence, the nonzero rows corresponding

to the higher coefficients in joint sparse representation are penalized more than those corresponding to the lower coefficients during the optimization procedure [132]. Hence, the MNM algorithm used in [34] is unable to preserve the clinically important higher wavelet coefficients during joint MECG recovery. The problem gets more pronounced when the number of measurements is less, which results in higher reconstruction error. To address this issue in SMV formulations, methods based on iterative re-weighting were proposed [132, 134]. These algorithms received significant attention due to their improved performance over their non-weighted counterparts. Thus, it can be concluded that the weighting approach allows more flexibility and enables easy incorporation of additional constraints in the joint optimization problems [134]. This motivated us to use a coefficient-level weighting approach in the traditional MNM-based recovery algorithms. This is expected to further improve their recovery performance, especially at low measurement rates.

The proposed weighting strategy in WMNM algorithm intends to prioritize the higher amplitude ECG wavelet coefficients whose indices form the row support of jointly sparse MECG signals during the joint CS-based reconstruction. The insignificant lower amplitude coefficients are de-emphasized simultaneously. These coefficients correspond to the indices that are more likely to fall outside the row support of jointly sparse MECG signals, and therefore are expelled from the row support in the final solution. It enhances the sparseness of the solution and reduces the number of measurements required for accurate recovery. The traditional MNM-based algorithms lack this flexibility. Additionally, a pre-defined weighting rule based on the prior knowledge about MECG wavelet representation is also explored that exploits prior structural knowledge about the common support of diagnostically relevant MECG wavelet coefficients to determine the weights.

This chapter is organized as follows: Section 4.1 discusses about the conditions of simultaneous reconstruction under MMV modeling and how it is applicable to MECG signals. Section 4.2 discusses about the detailed joint CS processing steps followed by experimental results in Section 4.3. Comparative results are presented in Section 4.4. Issues related to practical applications of the proposed method are discussed in Section 4.5. Section 4.6 highlights the advantages of joint MECG processing through MMV CS over SMV CS. Summary of the chapter is given in Section 4.7.

## 4.1 Joint CS for Multi-channel ECG Signals

The spatially correlated structure of MECG signals enables the joint processing of all the channels in a joint CS framework. This spatial or inter-channel correlation generates common supports, which allows simultaneous compression/reconstruction of all ECG channels together.

In this chapter, a multiple-measurement-vector (MMV)-based CS model [106] is employed, which assumes a row-sparse or group/joint sparse structure for wavelet domain representation of MECG signals. The MMV, or row-sparse modeling of the MECG signals, helps exploit the natural group sparsity of different channels, which is present because of their correlated structure. However, strict joint sparsity is difficult to achieve in case of real world signals like MECGs. Though each channel share common support information, at the same time each channel conveys some unique pathological information. Due to this reason, sparsity is found to be varying slowly in each channel (Figure 2.3). But, the slow time-varying sparsity across the channels may not have noticeable effect on final reconstruction quality. One of the reasons for this is the high sparse nature of ECG signals from each channel in wavelet domain and their highly correlated structure. Due to these characteristic features, row sparsity of joint MECG wavelet representation could be ensured to be less than $(N + L)/2$, a required condition for MMV recovery [105]. Here, $N$ and $L$ are the number of wavelet coefficients in each channel and number of ECG channels, respectively. Also, varying support information of each channel that leads to time varying sparsity, is found mostly corresponding to high frequency subband coefficients as discussed in the motivation section of Chapter 2 and shown in Figure 2.3. Since these subband coefficients are not very important from clinical point of view [81, 109], the recovery results are expected to be least affected. Also, because of this, dynamic sparsity can be assumed to be approximately static in case of MECG and common support (row-sparse) assumption remains valid.

## 4.2 Proposed Joint CS Framework

The MECG signals taken from eight fundamental leads are jointly CS encoded using a random binary sensing matrix (with very few ones) at the encoder. The resulting compressed measurements are collected at the decoder where all the ECG channels are simultaneously reconstructed with the help of proposed recovery technique. The compressed measurements can be quantized and Huffman encoded to further enhance the compression efficiency of the system. The main contribution of this

work focuses on the joint reconstruction algorithm that uses a weighting strategy to emphasize the clinically relevant high amplitude wavelet coefficients while exploiting the underlying inter-channel correlations. The aim is to improve the diagnostic reconstruction quality of ECG signals at a reduced number of measurements. A block diagram is shown in Figure 4.1, which illustrates all the important steps involved in the proposed method. The detailed description of the proposed method is given in subsequent subsections.

### 4.2.1 Joint MECG compression

Joint CS or multi-channel CS enables simultaneous compression/reconstruction of all the ECG channels using an MMV modeling approach. Let $\boldsymbol{X} = [\boldsymbol{x}_1,\ \boldsymbol{x}_2,\ \boldsymbol{x}_3,\ \ldots,\ \boldsymbol{x}_L] \in \mathbb{R}^{N\times L}$ be the data matrix whose columns represent the $L$ channels of $N$-dimensional MECG signals. Furthermore, let us represent the ECG signals from all the channels using same orthonormal wavelet basis $\boldsymbol{\Psi} = [\boldsymbol{\psi}_1, \boldsymbol{\psi}_2, \boldsymbol{\psi}_3, \ldots, \boldsymbol{\psi}_N]$ as $\boldsymbol{X} = \boldsymbol{\Psi}\boldsymbol{A}$, where $\boldsymbol{A} = [\boldsymbol{\alpha}_1,\ \boldsymbol{\alpha}_2,\ \boldsymbol{\alpha}_3,\ \ldots,\ \boldsymbol{\alpha}_L] \in \mathbb{R}^{N\times L}$ is a matrix containing the wavelet coefficient vectors. Since the channels share common mutual information, most of the

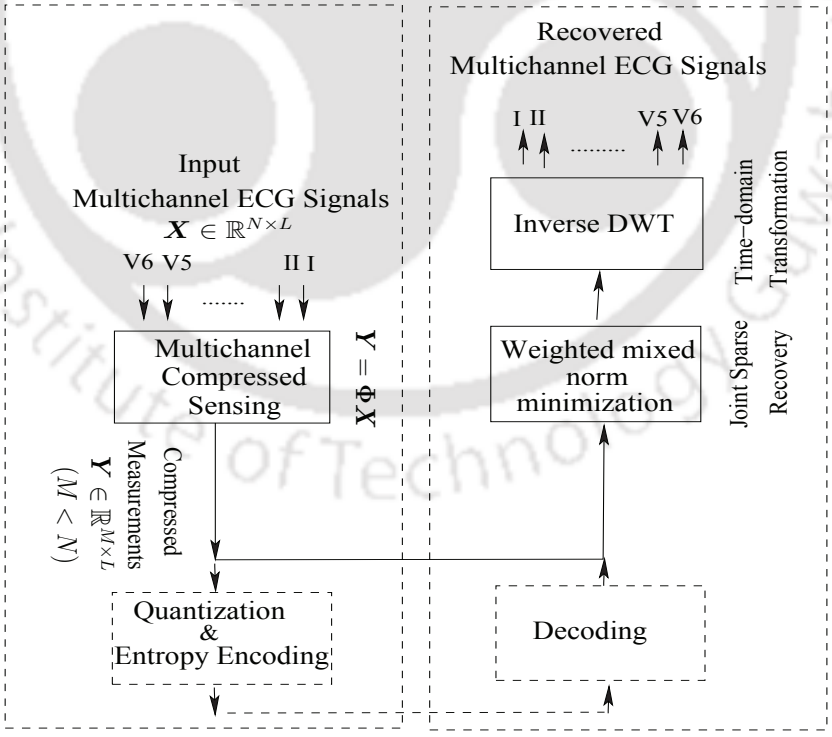


**Figure 4.1:** Block diagram of the proposed method

ECG signal information in all the channels lie only in the lower frequency wavelet subbands. Diagnostically relevant information present in the high frequency wavelet subbands is very small or almost negligible (refer to Figure 2.2). Therefore, $\boldsymbol{X}$ can be assumed to be row- or joint-sparse in the wavelet domain, wherein the information is confined to a few nonzero rows only. Following the MMV model of CS theory [106] as discussed in Chapter 2, compressed measurements corresponding to all time domain ECG channels are obtained using (2.15). Thus, unlike to eigenspace CS approach proposed in previous chapter, here directly the time-domain MECG signals are jointly compressed through CS, reducing the computational burden of the encoder. The compressed measurements can be quantized and entropy encoded to remove the redundancies further as shown in Figure 4.1. An uniform quantizer is used for the quantization purpose followed by Huffman encoding.

Now, to exploit the wavelet domain row-sparsity of MECG signals, joint CS recovery at the decoder is performed in the wavelet domain using the sparsifying bases $\boldsymbol{\Psi}$ in (2.15). The recovery equation can be given as:

$$\boldsymbol{Y} = \boldsymbol{\Phi}\boldsymbol{\Psi}\boldsymbol{A} \triangleq \boldsymbol{\Theta}\boldsymbol{A} \tag{4.1}$$

where $\boldsymbol{\Theta} = \boldsymbol{\Phi}\boldsymbol{\Psi}$. The problem formulated in (4.1) can be viewed as an MMV problem intended to simultaneously recover signals of all the ECG channels in $\boldsymbol{X}$, using their compressed measurements in $\boldsymbol{Y}$ at the decoder. The sensing matrix $\boldsymbol{\Phi} \in \mathbb{R}^{M \times N}$ used here is a binary sparse random matrix that satisfies a modified restricted isometric property ($RIP$), referred to as $RIP_p$ [1]. Sparse matrices are memory efficient and involve lesser computations, thus help minimize the computational cost at the encoder [46].

### 4.2.2 Joint MECG reconstruction using weighted mixed-norm minimization

The compressed measurements are sent to the remote healthcare centers, where the proposed weighted MNM-based joint sparse recovery algorithm is employed to jointly recover all ECG channels. This section discusses the development of the proposed MECG recovery approach.

Solution of the MMV problem in (4.1) in noisy case, $\boldsymbol{Y} = \boldsymbol{\Theta}\boldsymbol{A} + \boldsymbol{V}$, is achieved by solving the following standard MNM-based convex optimization problem [106]:

$$\underbrace{\min}_{\boldsymbol{A}} \|\boldsymbol{A}\|_{p,q} \qquad \text{such that} \qquad \|\boldsymbol{Y} - \boldsymbol{\Theta}\boldsymbol{A}\|_F \leq \varepsilon \tag{4.2}$$

where $\boldsymbol{V}$ is the additive measurement noise, $\varepsilon$ is the noise tolerance limit, and $\|.\|_F$ is the Frobenius norm. The term $\|\boldsymbol{A}\|_{p,q}$ denotes the $\ell_{p,q}$ mixed-norm of coefficient matrix, $\boldsymbol{A}$, and is defined as:

$$\|\boldsymbol{A}\|_{p,q} = (\sum_{j=1}^{N} \left\|\boldsymbol{A}^{\rightarrow j}\right\|_p^q)^{1/q} \tag{4.3}$$

where $\boldsymbol{A}^{\rightarrow j}$ denotes the $j$-th row of $\boldsymbol{A}$, and $\|.\|_p$ is the $p$-th norm defined as $\left(\sum_i \left|\boldsymbol{A}_i^{\rightarrow j}\right|^p\right)^{1/p}$.

Corresponding to three different sets of values for $p$ and $q$, i.e., $(p,q) = \{(1,1),\ (2,1),\ (\infty,1)\}$, three cases of (4.2) are analyzed. In all these cases, the final sparsity inducing-norm is kept the same (i.e., $\ell_1$-norm), while the inner-norm is varied. The $\ell_2$-norm promotes denser solutions than the $\ell_1$- and $\ell_\infty$-norms [106]. Hence, the mixed-norm with $p = 2, q = 1$ results in better joint reconstruction performance and is employed in this work for further studies. Hereafter, the mixed-norm is referred to as a combination of $\ell_1$- and $\ell_2$-norms, denoted by $\ell_{2,1}$. The $\ell_{2,1}$-mixed-norm acts as a group-sparsity inducing norm and exploits the fact that the nonzero sparse coefficients of all the ECG channels are naturally grouped together. Dense solution is promoted by taking $\ell_2$-norm over each row of $\boldsymbol{A}$ and then the outer $\ell_1$-norm, i.e., sum of $\ell_2$-norm of each row, forces the selection of only few rows. Thus, the $\ell_{2,1}$-mixed-norm, also referred to MNM, exploits the inter-channel correlation of the MECG signals while promoting row-sparsity. In the following, we propose a weighted MNM algorithm to jointly recover MECG signals.

In [135], it was assumed that the coefficients of an optical spectrum signal follow a Laplacian distribution due to their sparse characteristics. This assumption was further adapted for wavelet coefficients of single channel ECG signals due to their wavelet domain sparse behavior [46]. In an MMV approach for MECG signals, sparsity is enforced on the dense coefficients obtained after taking the $\ell_2$-norm on each row of $\boldsymbol{A}$ for a row-sparse solution. The dense coefficient vector is given as:

$$\boldsymbol{A}^{\ell_2} = \left[\left\|\boldsymbol{A}^{\rightarrow 1}\right\|_2, \left\|\boldsymbol{A}^{\rightarrow 2}\right\|_2, \left\|\boldsymbol{A}^{\rightarrow 3}\right\|_2, \ldots, \left\|\boldsymbol{A}^{\rightarrow N}\right\|_2\right]^T \tag{4.4}$$

where

$$A_j^{\ell_2} = \left\|\boldsymbol{A}^{\rightarrow j}\right\|_2 = \sqrt{(\alpha_1^j)^2 + (\alpha_2^j)^2 + ... + (\alpha_L^j)^2}, \qquad j = 1, \ldots, N \tag{4.5}$$

Here, $\alpha_L^j$ denotes the $j^{th}$ wavelet coefficients of $L^{th}$ ECG channel. Thus, the vector $\boldsymbol{A}^{\ell_2}$ is a joint wavelet coefficient vector, which integrates information from all the channels. Taking a prior on the

entries of $\boldsymbol{A}^{\ell_2}$ that promotes row-sparsity, coefficient matrix $\boldsymbol{A}$ can be estimated following a maximum a *posteriori* (MAP) approach. We assumed entries $A_j^{\ell_2}, j = 1, ..., N$, to be independent and Laplacian distributed and additive noise $\boldsymbol{V}$ to be Gaussian of unknown variance $\sigma_n^2$ with independent and identically distributed (i.i.d.) entries. These assumptions are consistent with the assumptions taken in [46], where the Laplacian assumption was taken as a sparsity encouraging prior in SMV recovery. Here, the essence of MAP estimation is extended from SMV [46, 135] to MMV case to estimate $\boldsymbol{A}$ in (4.2). With standard deviation $\sigma_j$, Laplace distribution of the elements of $\boldsymbol{A}^{\ell_2}$ can be defined as:

$$p(A_j^{\ell_2}) = \frac{1}{\sigma_j\sqrt{2\pi}} \exp(-\sqrt{2}\frac{A_j^{\ell_2}}{\sigma_j}) \tag{4.6}$$

MAP estimation of $\boldsymbol{A}$ can be deduced by maximizing the posterior probability $p(\boldsymbol{A}^{\ell_2}|\boldsymbol{Y}, \boldsymbol{\Theta})$ with likelihood function $p(\boldsymbol{Y}|\boldsymbol{\Theta}, \boldsymbol{A}^{\ell_2}) \propto exp(-\frac{\|\boldsymbol{Y}-\boldsymbol{\Theta}\boldsymbol{A}\|_F^2}{2\sigma^2{}_n})$ for Gaussian noise. Using Bayes rule:

$$\begin{aligned}
\widehat{\boldsymbol{A}}_{MAP} &= \underbrace{\arg\max}_{\boldsymbol{A}} \; p(\boldsymbol{A}|\boldsymbol{Y}, \boldsymbol{\Theta}) \\
&= \underbrace{\arg\max}_{\boldsymbol{A}} \; (\log p(\boldsymbol{Y}|\boldsymbol{\Theta}, \boldsymbol{A}^{\ell_2}) + \sum_j \log p(\boldsymbol{A}_j^{\ell_2})) \\
&= \underbrace{\arg\min}_{\boldsymbol{A}} (\frac{\|\boldsymbol{Y}-\boldsymbol{\Theta}\boldsymbol{A}\|_F^2}{2\sigma^2{}_n} + \sum_j \frac{\sqrt{2}\boldsymbol{A}_j^{\ell_2}}{\sigma_j})
\end{aligned}$$

The above equation can also be written as,

$$\widehat{\boldsymbol{A}}_{MAP} = \underbrace{\arg\min}_{\boldsymbol{A}} \frac{1}{2}\left\|\boldsymbol{Y} - \boldsymbol{\Theta}\widehat{\boldsymbol{A}}\right\|_F^2 + \lambda \sum_j w_j \boldsymbol{A}_j^{\ell_2} \tag{4.7}$$

where $\boldsymbol{w} = [\frac{1}{\sigma_1^2}, \frac{1}{\sigma_2^2}, ..., \frac{1}{\sigma_N^2})]$, and $\lambda$ is a tuning parameter. This is a weighted version of (4.2) (with $p = 2, q = 1$) and is referred to as weighted MNM (WMNM). Under the Laplacian prior on $\ell_2$-norm of each row of $\boldsymbol{A}$ (i.e., entries of vector $\boldsymbol{A}^{\ell_2}$) and with the assumption that each entry has equal standard deviation $\sigma_j$, $j = 1, \ldots, N$, the standard (non-weighted) MNM algorithm in (4.2) can be seen as a special case of (4.7).

However, the same standard deviation assumption for all the entries of $\boldsymbol{A}^{\ell_2}$ does not reflect the reality. This is because the elements of $\boldsymbol{A}^{\ell_2}$ are the dense coefficients corresponding to different wavelet scales. Since, the magnitude of detail subband wavelet coefficients at different scales decays exponentially with increase in resolution level, it gives unequal standard deviation for each coefficient.

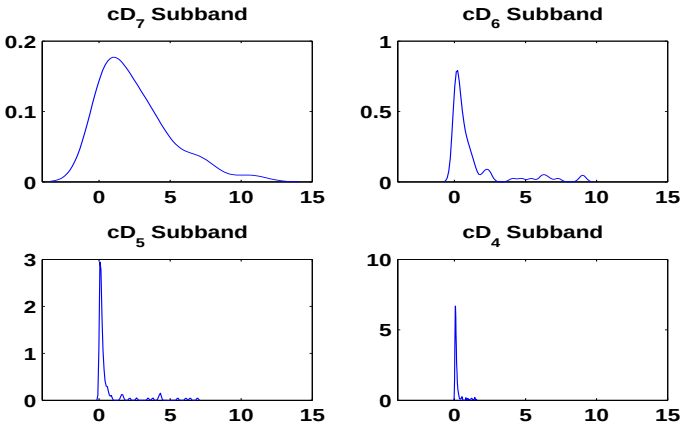


**Figure 4.2:** PDF plot of entries of $\boldsymbol{A}^{\ell_2}$ corresponding to four high frequency wavelet subbands

This statement can be supported by probability density function (PDF) plots of four detail subbands, given in Figure 4.2, where different standard deviations at each scale can be clearly observed. However, if the weight vector $\boldsymbol{w}$ can be constructed, there are many standard approaches available to solve the joint sparse reconstruction problem (4.7). Depending on the understanding of the underlying problem, there can be different ways to construct the weight vector $\boldsymbol{w}$. A proper selection of weights $w_j, j = 1, 2, \ldots, N$, in (4.7) can significantly improve the performance of (4.2). The weighted $l_{2,1}$-mixed-norm acts as the weighted $l_1$-norm over the vector resulted after $\ell_2$-norm of each row of $\boldsymbol{A}$. The weighted $l_{2,1}$-mixed-norm tries to find a local minimum of the concave penalty function that more closely approximates the $l_1$-norm to the $l_0$-norm, similar to the reweighted $l_1$ algorithm presented in [132]. This improves the overall joint recovery performance of non-weighted $l_{2,1}$-mixed-norm. Two different weighting rules are explored for WMNM. In the first case, the weights are based on $\ell_2$-norm of nonzero rows of $\boldsymbol{A}$ (adaptive weighted mixed-norm minimization (AWMNM)). In the second case, the weights are chosen based on the *a priori* information (binary weighted mixed-norm minimization (BWMNM)).

#### 4.2.2.1 Adaptive weighted mixed-norm minimization

In this approach, an adaptive weighted mixed-norm minimization (AWMNM) algorithm based on adaptive weighting strategy is proposed. It aims to perform a more democratic penalization of the nonzero rows of joint sparse matrix $\boldsymbol{A}$, and thus, reduces the amplitude dependence of the traditional

non-weighted $l_{2,1}$-mixed-norm. The weights are chosen according to an inverse relation to the $\ell_2$-norm (i.e., energy) of each row. The nonzero rows with higher energy (corresponding to the low frequency wavelet coefficients) are assigned small weights, while the nonzero rows with lower energy (i.e., high frequency wavelet coefficients) are assigned large weights. The justification for such a weighting is evident from (4.7). Here, it can be noted that small weights emphasize the nonzero rows associated mainly with the clinically important high amplitude wavelet coefficients. On the other hand, large weights de-emphasize such rows. Therefore, the rows from lower energy subbands (clinically less important) are pushed towards zero and their corresponding indices are more likely to be thrown out of the row-support of the final solution. This, in turn, leads to a row-sparse solution. The weight for the $j$-th row of source matrix $\boldsymbol{A}$ at $(t+1)$-th iteration is calculated using coefficients of the respective row estimated in the previous iteration as follows:

$$w_j^{t+1} = ((\widehat{\boldsymbol{A}}_j^{\ell_2})^t + \epsilon)^{p/2-1}, \ p \in [0, 2] \tag{4.8}$$

The weight exponent, $p$, is a user defined parameter that relates the weights to the energy of nonzero rows. For $p = 0$, the weights are in inverse relation to the subband energy. On the other hand, for $p = 2$, the weights become unity, i.e., a case of non-weighting. The parameter $\epsilon$ is a small nonzero scalar introduced to make the algorithm stable in the case of zero-valued coefficients. The performance of the algorithm is found to be fairly robust to the choice of $\epsilon$ (described later in Section 4.6). A more precise value of $\epsilon$ can be obtained by calculating the 10% of standard deviation for the $\ell_2$-norm of the nonzero rows.

Steps involved in the joint MECG reconstruction through the adaptive weighting are given in the Algorithm 1. The proposed weighting strategy is implemented by initializing the weights $w_j$, $j = 1, \ldots, N$, with unity. A weighted MNM problem is solved in each iteration and the weights are updated iteratively based on the solution of previous iteration. In ***Step* 1** at iteration $t = 1$, a non-optimal solution for the coefficient matrix $\boldsymbol{A}$ is obtained using the unity weights. The coefficients of the matrix $\boldsymbol{A}$ are now used to derive more accurate weights according to the relation given in (4.8), and are used in the next iteration. These weights are further used to estimate a more accurate $\boldsymbol{A}$ in the following iteration. This process is repeated until convergence, or until the maximum number of iterations is reached. For the convergence, the error should fall below a predefined threshold value ($\rho$). We have

**Algorithm 1** Proposed Weighted Mixed Norm Minimization (WMNM) Algorithm for the Joint CS MECG Recovery

**Initialize:** $\epsilon = 0.2$, $p = 0.2$, $\rho = 10^{-2}$, $w_j^t = 1,\ (j = 1\ to\ N)$, iteration count, t = 1. Set $t_{max} = 3$.
**Step 1.** Solve weighted $\ell_{2,1}$ mixed-norm minimization problem to jointly reconstruct the row-sparse MECG wavelet coefficient matrix $\widehat{\boldsymbol{A}}^{\boldsymbol{t}}$

$$\underbrace{\min}_{\boldsymbol{A}} \|\boldsymbol{A}\|_{w_j^t,2,1} \qquad \text{such that} \qquad \|\boldsymbol{Y} - \boldsymbol{\Theta}\boldsymbol{A}\|_F \leq \varepsilon.$$

**Step 2.** Determine the weights $w_j^t$, $j = 1, \ldots, N$ from (4.8) using the estimated matrix $\widehat{\boldsymbol{A}}^{\boldsymbol{t}}$.
**Step 3.** Update the weights with the currently estimated weights $w_j^t$

$$w_j^{t+1} = w_j^t$$

**Step 4.** Stop on convergence i.e., $\frac{\|A^t - A^{t-1}\|_F}{\|A^t\|_F} < \rho$ or if $t = t_{max}$. Else, go to ***Step* 1** and increment $t$.
**Step 5.** At $t = t_{max}$, recover time domain MECG signals using $\widehat{\boldsymbol{X}} = \boldsymbol{\Psi}^T \widehat{\boldsymbol{A}}^{\boldsymbol{t_{max}}}$ .

experimentally chosen $\rho = 10^{-2}$ and $t_{max} = 3$ for all the simulations. Thus, the adaptive weighting strategy produces more focal estimates of the signal as the optimization progresses. Consequently, the reconstruction quality of the MECG signals improves iteratively.

#### 4.2.2.2 Binary weighted mixed-norm minimization

In addition to the iterative reweighting strategy proposed in previous subsection, the weights $w_j, j = 1, \ldots, N$, can also be set on the basis of some prior structural knowledge about the MECG wavelet representation. In this case, the MECG recovery can be done in ***Step I*** of the algorithm 1. As discussed earlier, in the joint sparse approximation of MECG signals in the wavelet domain, most of the ECG features containing the important pathological information fall in the low frequency subbands [81]. The wavelet coefficients in these subbands are always expected to be nonzero. Consequently, the indices corresponding to those entries are highly likely to fall within the row support of jointly-sparse MECG signals. This prior support information can be used to determine a set of pre-defined weights. For $n$ levels of wavelet decomposition, we have considered three low-frequency subbands ($A_n$, $D_n$, $D_{n-1}$) as clinically relevant subbands since most of the ECG features lie in these subbands (constituting more than 80% of subband energy) [81]. Small weights are used for the entries corresponding to these subbands in order to preserve the corresponding indices in the row-support of the final solution. The likelihood of having only nonzero wavelet coefficients in other detail subbands is very low (refer to

Figure 2.3). This is because of the low energy and minimal diagnostic contents of these subbands. Hence, relatively large weights are used for the coefficients in rest of the detail subbands. Because of the large weighting factors, the indices corresponding to the insignificant coefficients are kept out of the row support in the final solution. This promotes sparseness of the solution at right positions. At the same time, it also improves the joint recovery without compromising with the diagnostic fidelity.

A simple case of binary weighting has been discussed in this paper. In this case, the weights corresponding to the coefficients in three lower frequency subbands are set to zero, while those corresponding to other detail coefficients are set to unity. This approach is referred to as binary-weighted MNM (BWMNM) in this work. The BWMNM not only makes the recovery non-iterative but also improves the recovery performance as compared to the traditional MNM.

The joint optimization problem in (4.7) can be cast as a semidefinite programming problem and could be solved using interior point methods [106]. Other faster algorithms like the class of proximal methods are also available to solve the problem (4.7) [34].

## 4.3 Joint Compression/Reconstruction Analysis

The performance evaluation of the proposed scheme is carried out on various publicly available MECG databases, such as PTB, INCART, NSTDB, MIT-BIH [2,3], and CSE [4]. From each of the processed channels, a window of signal length $N = 512$ [34] is extracted to construct a data-matrix $\boldsymbol{X} \in \mathbb{R}^{512\times 8}$. This data-matrix is termed as the data packet. Experiments are performed on 30 such data packets, taken from each of the datasets. The Daubechies-4 ($db4$) wavelets are employed as the sparsifying bases for the ECG signals. The number of levels in the wavelet decomposition is decided on the basis of sampling frequency and decomposition level relationship suggested in [80]. The compressed measurements are obtained by jointly encoding all the channels through a random sparse binary sensing matrix $\Phi \in \mathbb{R}^{M\times 512}$ with binary entries, i.e., $0s$ and $1s$. Each column of $\boldsymbol{\Phi}$ contains only $d$ number of nonzero values equal to 1 at random positions [46]. The value of $d$ is chosen in accordance with earlier studies [1, 45]. These studies suggest a value of $d = 0.025 \times N$ in order to have a good trade-off between the signal sensing capability and computational time. Different values of $M$ are used to get varied performances of the proposed algorithm. The results are averaged over 100 trials with different realization of the random sensing matrix $\boldsymbol{\Phi}$ in each trial.

**Table 4.1:** Performance comparison between the proposed and existing algorithms for joint CS recovery of MECG signals.

| Techniques | Measurements (M) | Metrics | Different ECG channels | | | | | | | | Database |
|---|---|---|---|---|---|---|---|---|---|---|---|
| | | | Lead I | Lead II | V1 | V2 | V3 | V4 | V5 | V6 | |
| MNM [34] | 100 | PRD | 22.83 | 39.72 | 26.25 | 31.06 | 29.85 | 28.43 | 26.15 | 24.93 | PTB ($s0043lrem$) |
| | | SNR | 12.83 | 8.03 | 11.63 | 10.17 | 10.50 | 10.92 | 11.65 | 12.06 | |
| | | WEDD | 20.15 | 39.61 | 24.93 | 32.41 | 33.02 | 34.16 | 31.70 | 22.06 | |
| | | QS | 0.65 | 0.37 | 0.57 | 0.48 | 0.50 | 0.52 | 0.57 | 0.60 | |
| **Proposed** | 100 | PRD | 10.27 | 29.16 | 9.92 | **6.92** | 6.87 | 7.41 | 7.90 | 11.70 | |
| | | SNR | 19.77 | 10.70 | 20.07 | **23.19** | 23.25 | 22.60 | 22.04 | 18.63 | |
| | | WEDD | 8.36 | 26.84 | 8.97 | **6.87** | 7.85 | 8.98 | 8.04 | 9.77 | |
| | | QS | 1.46 | 0.51 | 1.51 | **2.16** | 2.18 | 2.02 | 1.89 | 1.28 | |
| MCS [44] | 100 | PRD | 20.26 | 19.51 | 14.66 | 13.97 | 17.73 | 18.91 | 19.35 | 15.88 | CSE |
| **Proposed** | 100 | | 18.97 | 19.51 | 13.47 | 12.22 | 12.47 | **12.95** | 14.05 | 13.18 | |
| SGAP [136] | 200 | PRD | - | 2.8 | 3.4 | - | - | - | - | - | MITDB |
| **Proposed** | 200 | | - | 2.5 | **2.8** | - | - | - | - | - | |
| MBSBL-FM [137] | 200 | NMSE | -22.8 | - | - | - | - | - | - | - | DaISy |
| **Proposed** | 200 | (dB) | **-23.2** | - | - | - | - | - | - | - | |

The fraction of the common support [45] is found to be increased by limiting the total number of ECG channels to 8, instead of 15. It increased up to 15% in case of 8 channels as compared to 15 channels. This helps improve the recovery performance further. The rest of the supplementary channels of the standard 12 channels MECG can be synthesized after reconstructing the independent channels at the decoder using linear lead relations given in Chapter 1.

### 4.3.1 Performance measures

The performance evaluation of the proposed method is carried out using some of the widely used performance metrics, such as the percentage-root mean square difference ($PRD$), and reconstruction signal-to-noise ratio ($R\text{-}SNR$) [45]. Because of lesser clinical acceptability of the above defined distortion measures [1], we have also employed a few other metrics that are specifically used as diagnostic distortion measures for the ECG signals. These metrics include the weighted diagnostic measure ($WDD$), wavelet-energy-based diagnostic distortion ($WEDD$), and quality score ($QS$) [45, 79, 81]. The $QS$ metric measures the trade-off between $PRD$ and $CR$, and is defined as: $QS = CR/PRD$.

### 4.3.2 Evaluation of the reconstruction quality

The retention of the diagnostic features, such as P-R interval, QRS interval, ST segment, and R amplitude of the jointly reconstructed MECG signals, is of utmost importance in remote ECG monitoring applications. The objective of this section is to demonstrate the effectiveness of the proposed weighting strategies for improved recovery performance at a low measurement rate.

The MECG signals from the dataset $s0043lrem$ are jointly encoded using the sensing matrix of size $100 \times 512$. These are reconstructed at a lower number of measurements $M = 100$ using the proposed AWMNM with $p = 0$ and $t = 3$ iterations. Reconstruction is also performed using the traditional MNM technique when no weighting is done, i.e., with $p = 2$. The quantitative values of distortion metrics, $PRD$, $SNR$, $WEDD$, and $QS$, of different algorithms are listed in the Table 4.1 for the comparison purpose. A higher level of distortion can be noted in the reconstructed signals using the traditional method compared to the proposed method. The proposed technique shows a substantial reduction in the distortion level in each channel. The Lead V2 exhibits a maximum reduction in the $PRD$ value as highlighted in the table, which drops from a value of 31.06% to 6.92% (up to 77%). Furthermore, a gain of more than 100% is noted in the values of $SNR$ and $QS$ when joint weighted recovery is done using AWMNM as compared to the non-weighted recovery case. The AWMNM technique exploits the joint correlation of MECG wavelet coefficients while encouraging clinically important wavelet coefficients through weighting parameters. Consequently, the high amplitude wavelet coefficients from the rows of $\boldsymbol{A}$ are privileged and their support information is preserved in the row-support of the final solution. This helps improve the joint MECG recovery. It is reflected in terms of lower $PRD$ value and higher $SNR$ and $QS$ values, which fall in "good" category reconstruction [1]. The joint recovery performance is also compared with some other reported works in the related area, such as multi-scale CS (MCS) [44], simultaneous greedy analysis pursuit (SGAP) [136], and Bayesian-learning-based work (MSBL-FM) [137]. The proposed method outperforms the aforementioned works in terms of lower reconstruction distortions (refer to Table 4.1).

**Table 4.2:** WDD calculation using different ECG features for the healthy control (HC) and myocardial infarction (MI) classes. Both the datasets $s0274rem$ (HC) and $s0043lrem$ (MI) are taken from the PTB database.

| Class | Signals | Duration features | | | | | | | Amplitude features | | | | | WDD |
|---|---|---|---|---|---|---|---|---|---|---|---|---|---|---|
| | | $RR_{int}$ $(ms)$ | $P_{dur}$ $(ms)$ | $QRS_{int}$ $(ms)$ | $QT_{int}$ $(ms)$ | $PR_{int}$ $(ms)$ | $QTp_{int}$ $(ms)$ | $ST_{slope}$ $(mV/s)$ | $P_{amp}$ $(mV)$ | $R_{amp}$ $(mV)$ | $T_{amp}$ $(mV)$ | $QRS^{+}_{amp}$ $(mV)$ | $QRS^{-}_{amp}$ $(mV)$ | |
| HC | Original Lead I | 640 | 130 | 60.5 | 308.5 | 177.5 | 265 | 1.3 | 0.11 | 0.97 | 0.20 | 1.82 | -0.91 | |
| | Reconstructed Lead I | 640 | 130 | 72.5 | 321.5 | 170 | 281.5 | 1.5 | 0.08 | 0.94 | 0.20 | 1.79 | -0.90 | 13.12 |
| | Original Lead V6 | 640 | 130 | 57.5 | 307.5 | 137 | 273.5 | 2.4 | 0.12 | 1.11 | 0.15 | 1.57 | -0.54 | |
| | Reconstructed Lead V6 | 639 | 130 | 68.5 | 315.5 | 124.5 | 282 | 2.3 | 0.11 | 1.09 | 0.15 | 1.53 | -0.52 | 6.20 |
| MI | Original signal | 1109 | 130 | 61 | 380 | 200 | 345.5 | 0.5 | 0.12 | 1.05 | 0.14 | 1.17 | -0.17 | |
| | Reconstructed Lead I | 1110 | 130 | 79 | 392 | 191.5 | 366 | 0.47 | 0.12 | 1.08 | 0.13 | 1.16 | -0.15 | 15.95 |
| | Original Lead V5 | 1110 | 130 | 72 | 390 | 181.5 | 353.5 | 2.8 | 0.11 | 0.97 | 0.08 | 1.89 | -0.94 | |
| | Reconstructed Lead V5 | 1110 | 130 | 72 | 382 | 182 | 350 | 2.8 | 0.09 | 0.96 | 0.08 | 1.89 | -0.95 | 9.73 |

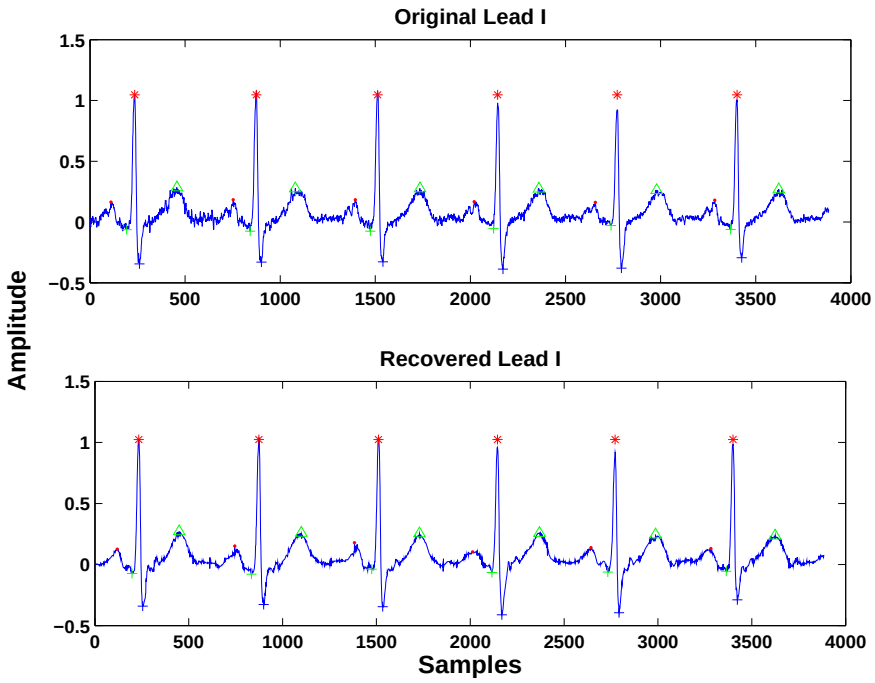


**Figure 4.3:** Detection and segmentation of important ECG clinical features in the original and reconstructed ECG signals for the WDD calculation. Features in the reconstructed signal suggest that they have been preserved in the compressed signal. Healthy control dataset s0274rem is used from PTB database.

The superiority of the joint MECG reconstruction obtained by the proposed method is also verified from the clinical point of view using measures, such as $WDD$ and $WEDD$. Values of $WDD$, given in Table 4.2, fall in the "very good" signal reconstruction category for lead V6 ($WDD = 6.20\%$) and lead V5 ($WDD = 9.73\%$) from healthy control (HC) (dataset $s0274rem$) and myocardial infarction (MI) classes (dataset $s0043lrem$), respectively [79]. However, "good" category reconstructions are achieved for lead I in both the classes. The different diagnostic ECG features, which are used to calculate the $WDD$ value are detected and shown in Figure 4.3 for the original and recovered signals of lead I from the HC class. These features mainly include the amplitude and duration features. These features are very important diagnostic characteristics for some of the life threatening heart diseases, such as bundle branch block (BBB), MI, etc. Therefore, quantifying the distortions in such features is necessary in order to clinically validate the reconstruction accuracy of the proposed method. These clinical features for both the HC and MI classes are also quantified in Table 4.2. It is seen that the

amplitude features are almost preserved in both the classes, but small deviations are noticeable in the duration features, especially in the case of $QT_{int}$, $PR_{int}$, and $QTp_{int}$. This may be the reason for a slightly higher $WDD$ value obtained in lead I. The $WEDD$ values (given in Table 4.1) for most of the channels fall in "good" reconstruction category [81]. A significant performance improvement is also achieved with the use of binary weighting in the BWMNM algorithm as compared to the traditional MNM recovery (discussed in the next section).

The reconstructed waveforms of the jointly recovered MECG signals are shown in Figures 4.4 and 4.5 for visual evaluation. The original and the reconstructed ECG signals corresponding to first 4096 time points from different channels are plotted together for better visualization. A case of HC is depicted in Figure 4.4, while Figure 4.5 shows a case of MI signal. For the HC dataset, the characteristic PQRST morphologies have been retained with the exception of a slight alteration at a few points when the AWMNM recovery is employed. On the other hand, severe distortions can be noted in the traditional MNM recovery (encircled in the waveforms). Figures 4.5(a) and 4.5(b) show the reconstruction results for the MI class using the traditional MNM and the proposed AWMNM, respectively, at the same number of measurements ($M = 100$). In the case of MNM, reconstructed ECG signals lose important clinical features, such as $ST$-segment, $Q$-wave, and $T$-wave (encircled) that are very crucial for detecting AMI progression in a patient. All the diagnostically relevant ECG features have been preserved using the proposed AWMNM method, except Lead II, which shows slight distortion (encircled), possibly due to its high noise content. Therefore, the proposed weighting strategy gives significant improvement in the reconstruction signal quality (verified clinically using $WDD$) when lesser measurements are available. This helps achieve low data rate, which is quite desirable in resource-constrained applications.

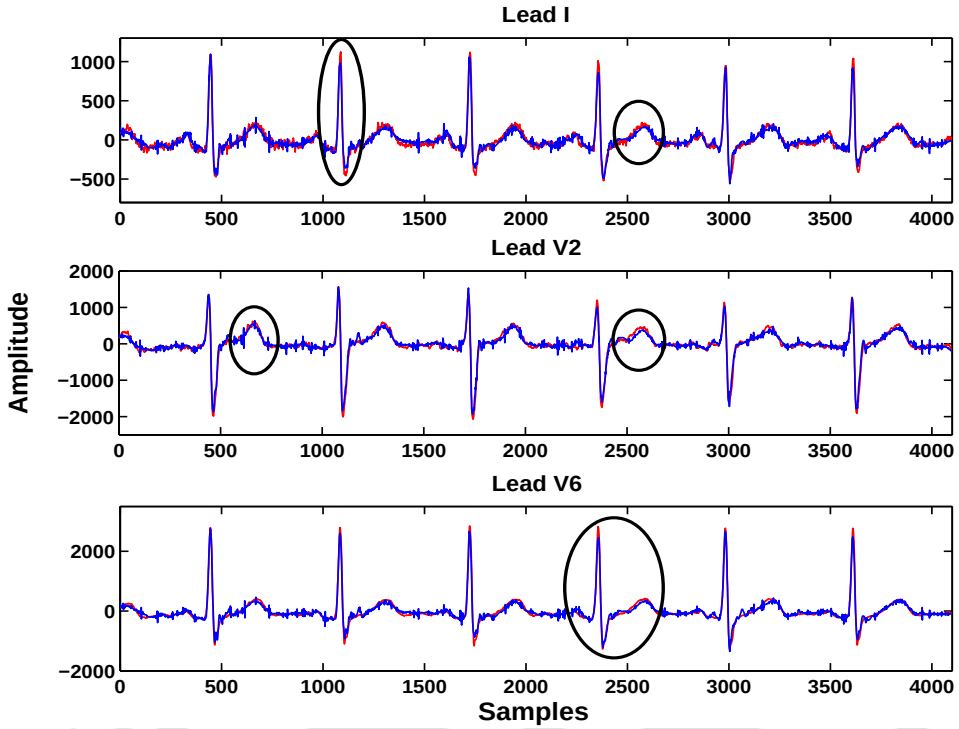


(a) Recovered results by traditional MNM

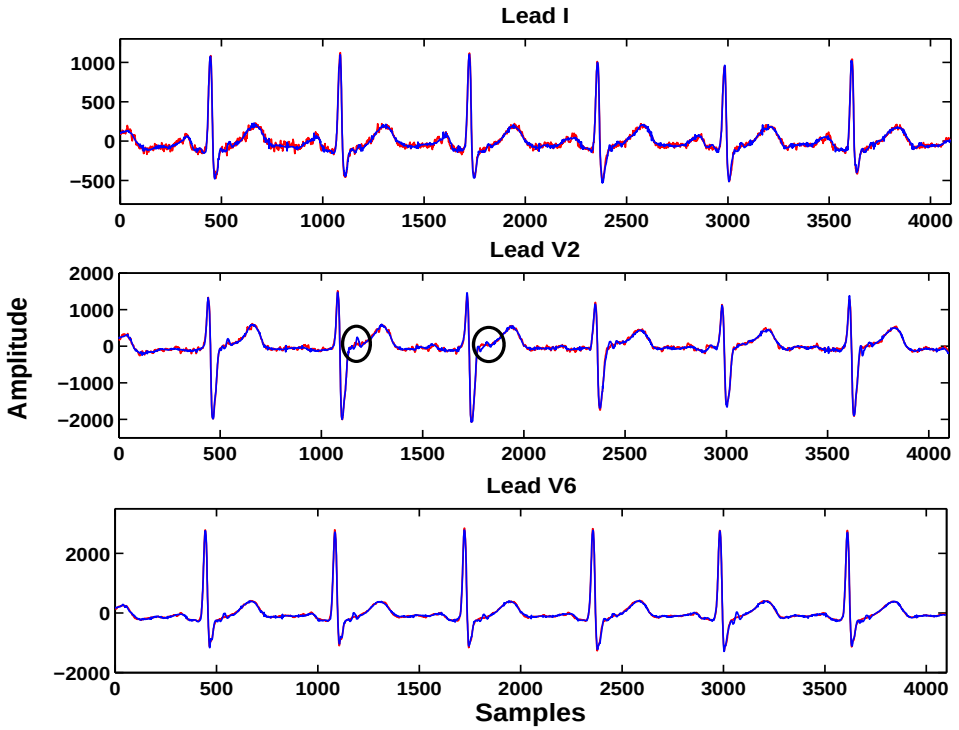


(b) Recovered results by weighted MNM (WMNM)

**Figure 4.4:** Original (in red color) and recovered (in blue color) signals (first 4096 samples, 4-sec data) (a) using the traditional non-weighted MNM technique ($p = 2$) and (b) using the proposed adaptive weighted MNM (AWMNM) technique ($p = 0$) after $t = 3$ iterations when the number of measurements $M = 80$. Dataset s0274rem of healthy control category is used from the PTB database.

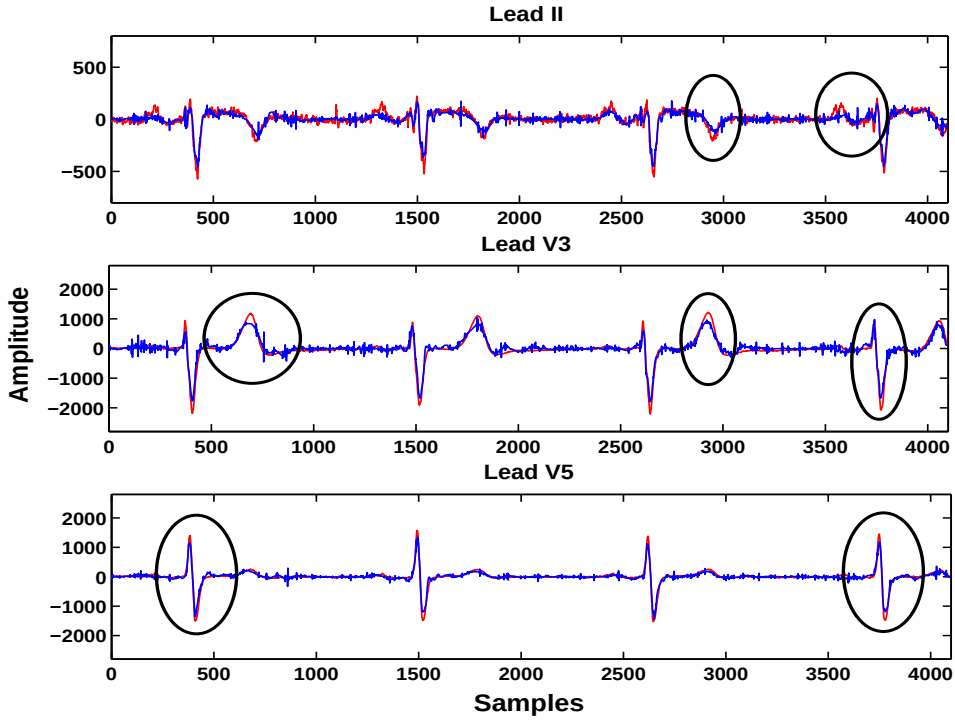


(a) Recovered results by traditional MNM

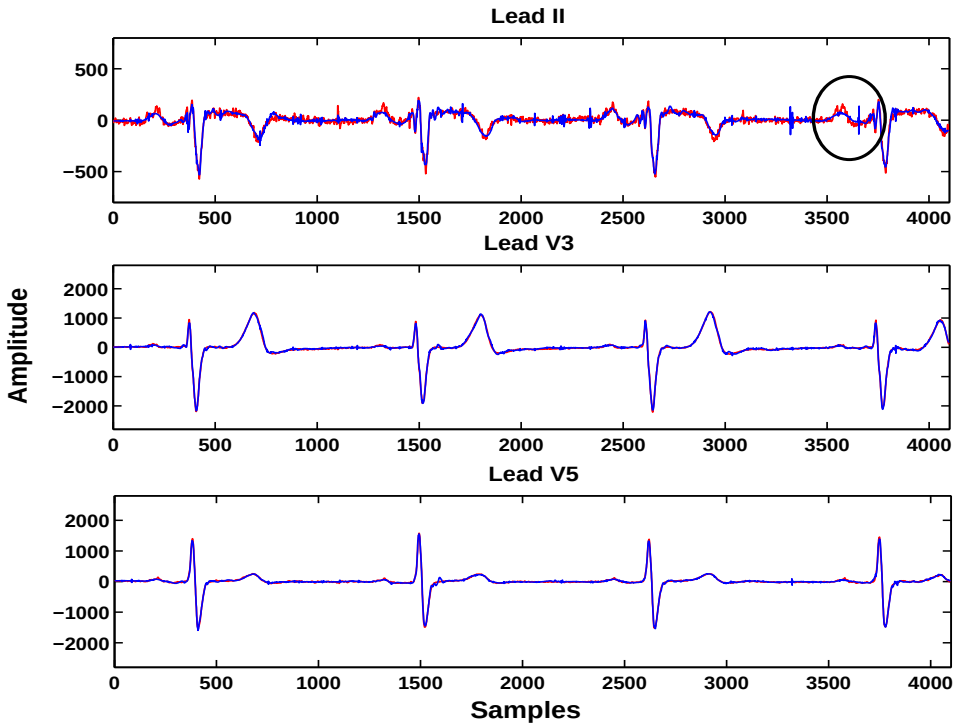


(b) Recovered results by weighted MNM (WMNM)

**Figure 4.5:** Original (in red color) and recovered (in blue color) signals (first 4096 samples, 4-sec data) (a) using the traditional non-weighted MNM technique ($p = 2$) and (b) using the proposed adaptive weighted MNM (AWMNM) technique ($p = 0$) after $t = 3$ iterations when the number of measurements $M = 100$. Dataset s0043lrem exhibiting anterior myocardial infarction (AMI) is used from the PTB database.

**Table 4.3:** Channel-wise average reconstruction results in terms of output PRD values for different types of normal and pathological cases using proposed techniques (AWMNM, BWMNM) at different number of measurements (M). Results are averaged over all the datasets available in that particular database.

| **Pathological class** | **Technique** | **Measurements** (M) | **Leads** | | | | | | | | **Database** |
|---|---|---|---|---|---|---|---|---|---|---|---|
| | | | Lead I | Lead II | V1 | V2 | V3 | V4 | V5 | V6 | |
| Healthy control | AWMNM | 150 | 8.35 | 6.49 | 4.64 | 4.11 | 4.10 | 4.28 | 7.75 | 6.95 | PTB ($f_s$=1 kHz) |
| Myocardial Infarction | | | 9.57 | 6.07 | 5.73 | 7.52 | 10.45 | 13.81 | 20.69 | 17.41 | |
| Hypertrophy | | | 10.14 | 8.53 | 7.07 | 7.28 | 7.49 | 8.84 | 10.97 | 9.67 | |
| Bundle branch block | | | 6.97 | 6.74 | 5.87 | 6.47 | 5.78 | 5.80 | 8.14 | 7.18 | |
| Average | | | 8.75 | 6.95 | 5.82 | 6.34 | 6.95 | 8.18 | 11.88 | 10.30 | |
| Arrhythmia | AWMNM | 120 | - | 5.88 | 6.14 | - | - | - | - | - | NSTDB ($f_s$=360 Hz) |
| | | 150 | - | 3.36 | 4.42 | - | - | - | - | - | |
| | BWMNM | 120 | - | 9.03 | 8.55 | - | - | - | - | - | |
| | | 150 | - | 5.37 | 4.98 | - | - | - | - | - | |
| Arrhythmia | AWMNM | 120 | 12.20 | 9.67 | 5.49 | 12.46 | 10.83 | 10.79 | 7.79 | 12.21 | INCART ($f_s$=257 Hz) |
| | | 150 | 6.92 | 5.65 | 3.42 | 5.71 | 5.94 | 5.23 | 4.38 | 7.22 | |
| | BWMNM | 100 | 6.06 | 13.19 | 9.88 | 13.92 | 11.80 | 11.28 | 13.59 | 13.54 | |
| | | 150 | 3.92 | 7.53 | 6.58 | 5.94 | 6.94 | 7.468 | 5.38 | 7.42 | |

The behavior of output distortion in terms of $PRD$ and parameter $p$, given by (4.8), is studied in Figure 4.6. The output $PRD$ variations for all the pathological datasets in PTB database are shown in the form of box plot in Figure 4.6(a) for different values of $p$. The edges of the boxes denote the 25th and the 75th percentiles with the central line as the median. The extreme values in the individual box depict the minimum and maximum $PRD$ values obtained at a particular value of $p$ and $M$ $(= 120)$ using different datasets. It can be noted that the overall output distortion increases with an increase in the value of $p$. This is indicated by the shift in the group median towards higher $PRD$ values as $p$ increases. In Figure 4.6(b), the oversampling ratio $M/K$ is plotted against the output $PRD$ at different values of $p$. Here also, it is quite evident that at small values of $p$ ($p = 0$ and $p = 0.5$), a lower output distortion is observed, which gradually increases as $p$ is increased. After $p = 1$, $PRD$ increases at a faster rate and becomes maximum at $p = 2$ when the weights become unity, i.e., a non-weighting case.

The distortion values in terms of the average $PRD$ in AWMNM recovery for the HC and three other major pathological classes from the PTB database are given in the Table 4.3 at measurements $M = 150$. The class-specific average results are calculated over 52 healthy control, 148 myocardial infarction, 7 hypertrophy, and 15 bundle branch block datasets available in the PTB database in order to analyze the inter-class performance variation of the proposed method. It is quite evident from the readings in Table 4.3 that the normal MECG signals have less reconstruction error as compared to the pathological cases. This is quite expected as the normal MECG signals are more correlated, and hence, more jointly sparse as compared to the pathological cases. In the latter case, joint sparsity may decrease because of the changes in the ECG morphologies in specific channels, leading to a degradation in the performance. The average results for the arrhythmic databases, such as NSTDB, and INCART are also evaluated. Quantified results are given in Table 4.3 at different values of $M$ for both the AWMNM and the BWMNM recovery cases.

## 4.4 Comparative Performance Analysis

The performance comparison of the proposed method is done with the state-of-the-art joint sparse recovery algorithms for the joint MECG recovery. These techniques include MNM [34], basis pursuit (BP) [1, 41], TMSBL [99], improved smooth $l_0$ (ISL0) [138], and simultaneous orthogonal matching

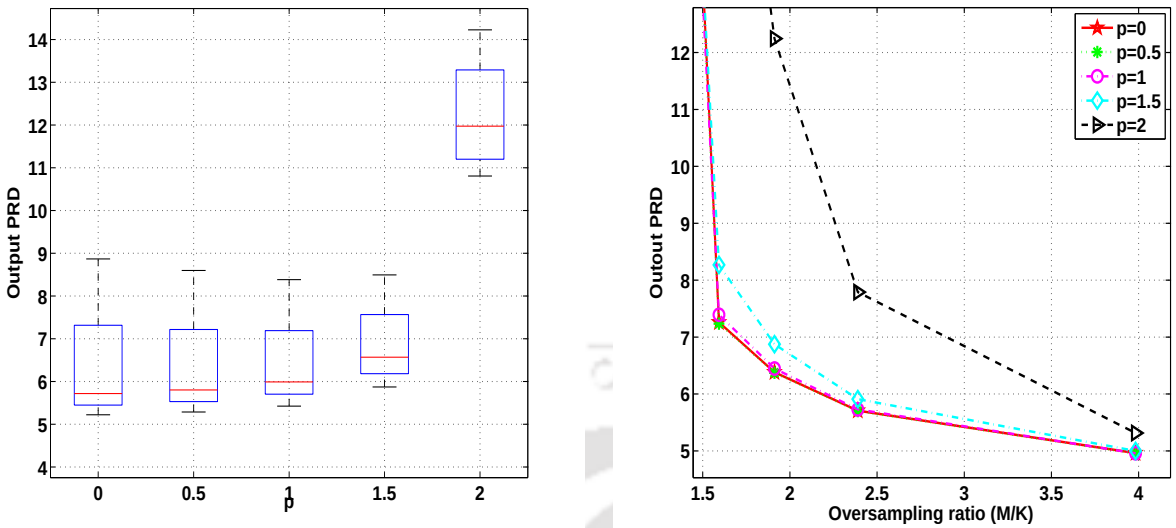


(a) (b)

**Figure 4.6:** (a) Box plot showing variations in output distortion for all the pathological classes with respect to $p$ in AWMNM when the number of measurements $M = 120$. (b) Output PRD variation with respect to the number of measurements $M$ at different $p$ values. Output PRD is averaged over all the datasets taken from the PTB database.

pursuit (SOMP) [97]. The comparative results in terms of $PRD$ and $SNR$, averaged over all the PTB records, are shown in Figures 4.7(a) and 4.7(b), respectively, at different $M$ and $CR$ values (using 8 bit of quantization).

First, we compare the performance of the proposed WMNM (AWMNM and BWMNM) with its non-weighted counterpart, i.e., the traditional MNM, which is a special case of AWMNM with $p = 2$ and iterations count $t = 1$. The MNM, as a joint sparse recovery algorithm, was earlier used by Mamaghanian et al. [34] for the joint CS reconstruction of the MECG signals. However, the trend of $PRD$ and $SNR$ in Figure 4.7, indicate that both the WMNM methods perform better than the MNM algorithm. The weighting of the jointly correlated coefficients with significant clinical importance grants special privilege to the bases corresponding to those coefficients. Consequently, those coefficients are encouraged to be preserved in all the channels even when lesser signal measurements are available. However, the MNM lacks this attribute as it only leverages the group sparsity leading to degradation in the performance at low measurements. The BP is a classic CS recovery algorithm for the SMV models and is implemented in this work using the SPGL1 software [139]. In the case of MECG signals, BP

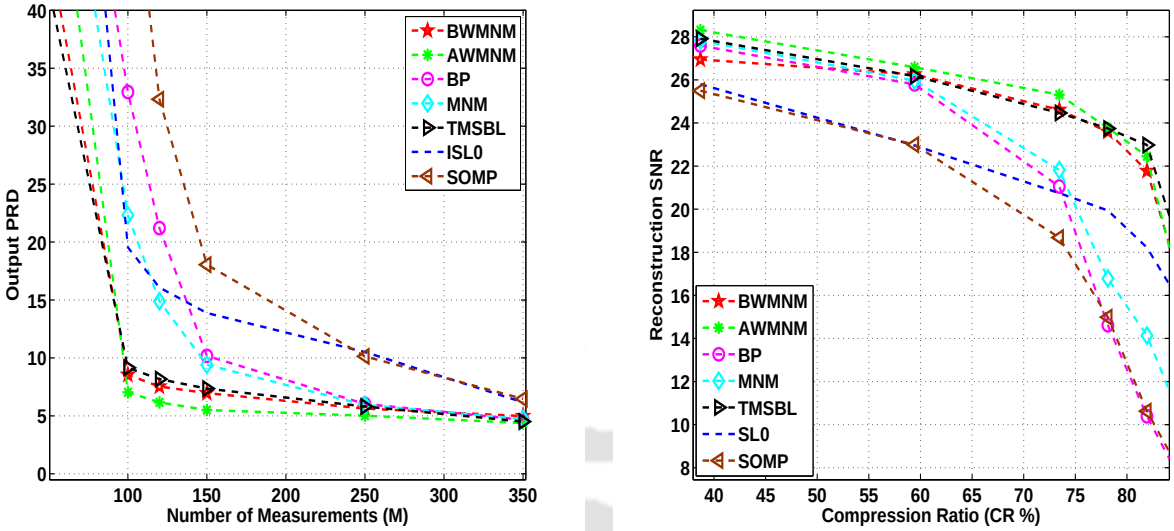


(a) (b)

**Figure 4.7:** Comparison plot of reconstruction distortions between proposed technique (BWMNM, AWMNM) and existing techniques. (a) Output PRD variation with number of measurements (M). (b) Reconstruction SNR (in dB) variation with compression ratio (CR). Results are averaged over all the datasets taken from the PTB database.

fails to exploit the inter-channel correlation efficiently, and hence performs poorly. Another algorithm similar to, but relatively faster than BP, is ISL0 [1]. The WMNM makes better utilization of the inter-channel correlation structure of MECG, and therefore, outperforms both the BP and ISL0. Apart from the convex optimization techniques discussed above, greedy algorithm like SOMP is also employed for comparison. This algorithm usually requires more measurements for accurate reconstruction. It was used in [97] for jointly recovering consecutive ECG cycles of the single channel ECG in a joint CS framework. For the multi-channel case, SOMP is outperformed by the proposed methods.

TMSBL is a recently proposed algorithm for the MMV recovery, and is based on the Bayesian learning approach. This technique is known to be very effective, especially when the nonzero rows of the source matrix $\boldsymbol{A}$ are highly correlated. It was previously applied to exploit the inter-beat correlation in the single channel ECG [99]. We have analyzed the performance of TMSBL for the MECG recovery. It is implemented in a low noise scenario ($SNR > 22\ dB$) for the PTB database using the source code provided by the authors. In the case of single channel ECG, different heart-beats

[1] Matlab scripts obtained by the first author through private communication

of the same channel are highly correlated. Consequently, the row vectors of the coefficient matrix $\boldsymbol{A}$ turn out to be correlated, and the algorithm performs better. But in the case of MECG signals, the correlation in each row of $\boldsymbol{A}$ is relatively low. This, in turn, might lead to moderate performance of the TMSBL for MECG signals. In the case of AWMNM, the assigned weights are adaptive in nature, unlike the BWMNM that uses static weights. This produces a more focal estimate of the signal as the algorithm progresses, but at the cost of extra iterations. Thus, it can be concluded that the BWMNM fares better in terms of the recovery speed. On the other hand, the AWMNM is preferable in terms of reconstruction accuracy.

## 4.5 Application Considerations

ECG telemonitoring is a resource-constrained application, which requires a low-complexity encoder with minimum energy consumption, and low memory requirements. This section discusses the proposed method from the perspective of such issues.

### 4.5.1 Energy consumption

To keep the computation burden during signal acquisition at minimum, a random sparse binary matrix $\boldsymbol{\Phi}$ is employed in this work. Unlike the densely populated Gaussian matrices, which suffer from heavy computation and memory storage problem in the WBAN applications, the binary sensing matrix offers least computation and faster hardware implementation. Instead of choosing the values of nonzero entries in the column of $\boldsymbol{\Phi}$ equal to $\pm 1/d$ [1], where $d$ is the number of nonzero entries, here binary values (0 or 1) are taken [46]. This saves further computations as the multiplication operations are now replaced with simple additions of the signal coefficients to get the signal measurements without changing the sensing ability of $\boldsymbol{\Phi}$. This, in turn, helps reduce the energy consumption during signal sensing at the encoder.

Regarding the energy consumption in the wireless data transmission, results shown in Figure 4.7(a) indicate that the proposed method can achieve good quality of reconstruction using only 20% of measurements. On the other hand, techniques, such as the BP and MNM need to increase the number of measurements up to 34% in order to meet the same reconstruction quality. The comparative compression performance analysis at 8-bit quantization is also shown in Figure 4.7(b). An improved

**Table 4.4:** Average runtime of the recovery algorithm of Figure 4.7 for jointly recovering one data packet ($\boldsymbol{X} \in \mathbb{R}^{\mathbf{512\times 8}}$) at different number of measurements (M).

| Techniques | Average Runtime(s) | | |
|---|---|---|---|
| | M=50 | M=100 | M=150 |
| BWMNM | 2.011 | 3.146 | 3.725 |
| AWMNM | 6.481 | 9.787 | 12.781 |
| BP | 5.011 | 5.346 | 6.012 |
| MNM | 1.991 | 2.918 | 3.810 |
| TMSBL | 18.972 | 39.235 | 65.057 |
| ISL0 | 0.0936 | 0.1882 | 0.2295 |
| SOMP | 0.0028 | 0.0036 | 0.0046 |

performance can be observed for both AWMNM and BWMNM as compared to most of the techniques. Thus, a higher data reduction (or a lower bit rate) can be achieved using the proposed technique, which results in transmission power savings in WBAN applications.

### 4.5.2 Computational requirements

The computational cost of the proposed method and other existing CS-based methods is studied in terms of average encoding and decoding time of the algorithms for one data packet ($\boldsymbol{X} \in \mathbb{R}^{\mathbf{512\times 8}}$). All simulations are done on the same platform using MATLAB R2010a environment running on a computer with 3.1GHz CPU and 4GB RAM. It is to be noted that the encoder is same in all the algorithms being compared. Therefore, all the algorithms take the same average time to encode a data packet. This average encoding time is found to be 0.163s, 0.257s and 0.334s when $M = 50$, 100, and 150, respectively.

The average runtime of the proposed and other existing algorithms in recovering one data packet, is given in Table 4.4 for different number of measurements (M). It can be noted that out of the two proposed WMNM algorithms, AWMNM and BWMNM, the latter has almost the same runtime as the standard MNM since the weights are set *a priori*. Though, the AWMNM technique performs better than all the other existing algorithms (refer Figure 4.7), this performance gain is obtained with a moderate increase in the computational cost. The AWMNM is an iterative algorithm, which solves a WMNM problem in each iteration with updated weights each time. The runtime, therefore, required by the algorithm is approximately $t_{max}$ times the runtime of the standard MNM algorithm [34]. Here, $t_{max}$ is the number of iterations used for the joint recovery (in all the simulations 3 iterations are

taken). The TMSBL, which performs close to that of the proposed algorithm, is found to be the slowest one in terms of runtime. The SOMP and ISL0 are the fastest algorithms, with the SOMP having least runtime followed by the ISL0. However, both of these algorithms exhibit inferior recovery performances (refer to Figure 4.7).

From the above studies, it can be concluded that there is a trade-off between the recovery speed and the reconstruction accuracy. The proposed CS framework using the joint WMNM recovery transfers the computational burden from the encoder to the decoder. By using a binary sensing matrix it further reduces the computations involved at the resource-constrained encoder while moderately increasing the computations at the decoder. It is noteworthy that the decoders are usually resourceful since the decoding is performed on high performance computers. Therefore, the computational complexity of the decoder is not an important issue in the case of WBAN-enabled health monitoring applications [46].

### 4.5.3 Memory requirements

The memory requirements of the proposed method are same as that of the existing standard CS-based works [34], since we have not added any additional steps in the encoding process. We have calculated the memory requirements during the data compression process at the encoder. CS involves a matrix-vector multiplication for the data reduction task [1, 46]. Therefore, we need to calculate the memory required to store the sensing matrix $\mathbf{\Phi}$, which is multiplied with the arriving data packets $\boldsymbol{X}$ in order to compress them [61, 137]. Unlike the DWT-based compressors that work in the batch mode, here the complete data packets are not required during the compression process [61]. With $y^{(0)} = 0$, the compressed measurement vector gets updated with each incoming data sample: $y^{(i)} = \boldsymbol{\phi}_i x_i + y^{(i-1)}$. If $\mathbf{\Phi}$ is a dense Gaussian matrix or a non-binary matrix [41, 44], the whole quantized matrix needs to be stored. This, in turn, increases the computational burden and the resource cost. However, in the proposed work, a binary sensing matrix is used with the entries being 0s and 1s only. This minimizes the computations (by replacing multiplication operations with additions) and also requires comparatively lesser memory to store. Each entry of $\mathbf{\Phi}$ will require a maximum space of 1-bit. Consequently, for a moderate size $\mathbf{\Phi} \in \mathbb{R}^{100\times512}$, the memory required will be $100 \times 512$ bits = 50 kB. The memory requirement can be further reduced if we store only the positions of 1s in each column of $\mathbf{\Phi}$ as suggested in [1, 45]. For a signal of length $N = 512$, memory space of 42 kB is required by taking

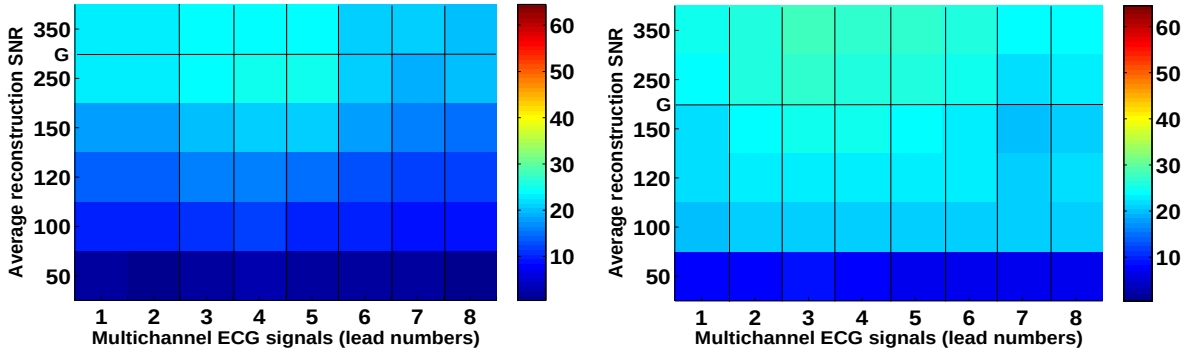


(a) Channel by channel recovery (SMV) (b) Joint recovery (MMV)

**Figure 4.8:** Averaged SNR (in dB) across all records for different value of measurements for all MECG channels. (a) Channel by channel reconstruction in SMV. (b) Joint reconstruction in MMV. Datasets are taken from PTB database.

twelve number of 1s (i.e., $d = 12$) in each column. In addition to the 42 kB memory that is required as read only memory (ROM), the random access memory (RAM) would also be required to temporarily store the compressed measurement vectors just before their transmission [61]. A hardware-based study is done in [61, 137] where the standard CS-based single channel and multi-channel compressors are implemented on field-programmable gate array (FPGA). Their results suggest that for a data packet of length $N = 512$ (same as that used in this work), CS requires 3 kB of RAM for single channel compression. Furthermore, this can be performed in parallel for multi-channel signals. It can be noted that the memory requirements would remain unchanged for all the CS-based algorithms used for comparison. This is because the same sensing matrix $\mathbf{\Phi}$ is employed in all the algorithms.

## 4.6 MMV Recovery Versus SMV Recovery

This section highlights the advantages of the joint CS reconstruction (MMV) over the traditional channel-by-channel CS reconstruction (SMV) of the MECG signals [1, 45, 46]. The comparison is done in terms of the number of measurements and the reconstruction signal quality. In the MMV approach, all the ECG channels corresponding to all the columns of $\boldsymbol{A}$ are jointly reconstructed using the proposed WMNM technique. On the other hand, in the case of SMV, individual channels are reconstructed separately using the popular $l_1$ minimization, as used in [1, 41]. Figure 4.8 shows the average reconstruction $SNR$ variation with the number of measurements ($M$) for the MECG signals

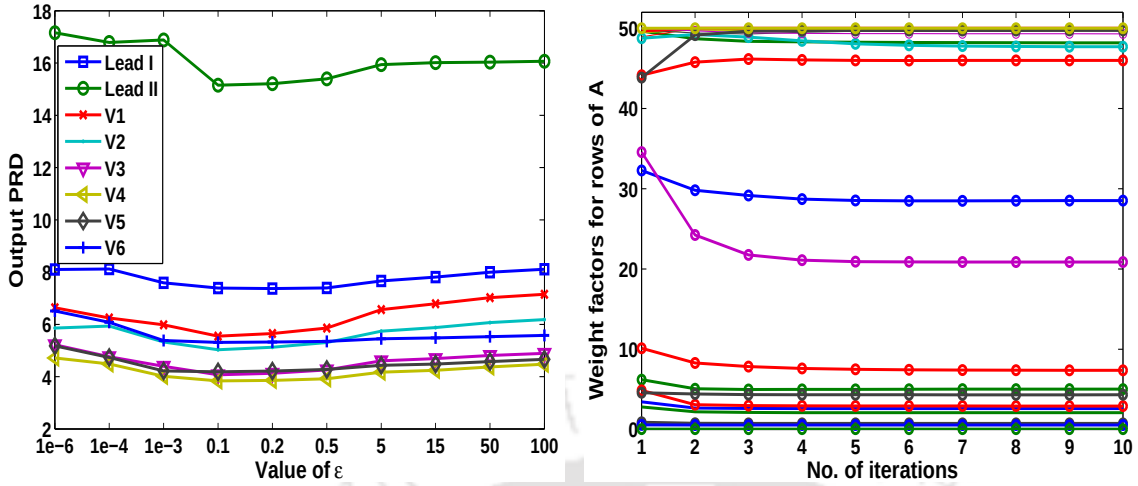


(a) (b)

**Figure 4.9:** Dependence of AWMNM on parameter $\epsilon$ and weighting factor $w$. (a) Variation of output PRD with respect to different values of $\epsilon$ in all MECG signals. (b) Variation of the weights for different entries forming the rows of coefficient matrix $\boldsymbol{A}$ at different iterations.

recovered through both the SMV and MMV approaches. The reconstruction quality is considered to be in "good" category if the $SNR$ value is greater than 22 $dB$ [1, 34, 79], and this point is marked with "G" in Figure 4.8. In SMV, "good" quality reconstruction is achieved at $M = 250$, while the same level of $SNR$ is reached at $M = 150$ in the case of MMV. This results in saving of the required number of measurements by 40%. Reduced number of measurements can enhance the overall energy efficiency of the system by reducing the computational burden and increasing the compression efficiency of the system [46]. In terms of reconstruction quality, MMV ($SNR = 25.4$ $dB$) outperforms SMV ($SNR = 23.1$ $dB$) as it gives an absolute improvement of 10% in $SNR$ at $M = 250$. It is quite clear from the above performance comparison that in the case of spatially correlated signals, like MECGs, the SMV approach may not be suitable and effective. The MMV approach that can exploit this correlation through the proposed WMNM technique is more suited for CS of MECG signals. This also validates the importance of correlation information in multi-channel-based CS ECG systems. In the MMV approach, the joint recovery technique AWMNM depends on various parameters like $\epsilon$, the weights $w_j, j = 1, 2, \ldots, N$, and the number of iterations $t$. Therefore, there is a need to study the variation in performance of the algorithm with respect to these parameters. The output PRD for all the channels of MECG is plotted against a wide range of $\epsilon$ values in Figure 4.9(a). A quite robust

performance is achieved in the selected range of values of $\epsilon$. The same can be observed in the given plot where a marginal variation in PRD values (w.r.t. change in $\epsilon$) is noticed in all the channels. For all the results reported in this work, we used $\epsilon = 0.2$. Figure 4.9(b) shows the variation in the weights during the optimization procedure at each iteration. For the sake of clarity, variations of first 50 weights only are shown in Figure 4.9(b). It can be observed that the weights get optimized at each iteration and attain a saturation level after 2 to 3 iterations. No further gain in the reconstruction accuracy is achieved, and the output distortion level gets saturated after 2 to 3 iterations. Hence, the proposed AWMNM approach does not overburden the decoder, and therefore, with a moderate increase in the computational cost, an improved quality of reconstructed MECG signals can be obtained.

## 4.7 Summary

In this chapter, a WMNM-based joint recovery algorithm is introduced for joint CS-based MECG data compression in telemonitoring applications. The ECG signals in different channels of MECG are highly correlated. The shared information across the channels is exploited here to jointly compress and reconstruct all the channels simultaneously. The proposed WMNM technique is based on a weighting strategy that helps maintain the diagnostic quality of reconstructed MECG signals even at higher compression ratios. The weighting scheme is such that it emphasizes clinically important high amplitude wavelet coefficients across the channels while de-emphasizing those with insignificant information, thus leading to a sparser solution. Joint recovery through the proposed method reduces the number of CS measurements needed for an accurate recovery, or equivalently, improves the joint reconstruction at a given number of measurements. Performance evaluations on various databases show that the proposed method can jointly recover MECG signals with a wide range of morphologies. Moreover, it is also observed that in the presence of the inter-channel correlated information, joint CS-based approach is more advantageous than the traditional CS-based approaches in terms of improved reconstruction quality at a lower number of measurements. The reduction in the number of measurements directly translates into the reduced volume of data to be transmitted. Higher data compression efficiency and low encoding complexity of the proposed method make it suitable for energy efficient continuous wireless telemonitoring of MECG signals.

भारतीय प्रौद्योगिकी संस्थान गुवाहाटी
Indian Institute of Technology Guwahati

# 5

# Exploiting Multi-scale Signal Information in Joint Compressed Sensing Recovery

Contents

In **Chapter** 4, we proposed a weighted mixed-norm minimization (WMNM)-based joint CS approach for multi-channel ECG (MECG) signals. It was observed that weighted joint CS recovery significantly improves the reconstruction results compared to non-weighted CS recovery at the same number of measurements. The weighting-based sparse recovery algorithms gives flexibility to adopt different weighting rules depending on the understanding of the problem and that in return, improves the estimation of latent data. This motivated us to explore new diagnostically relevant MECG features, which can be exploited in the weighting-based joint CS recovery algorithms to improve the signal reconstruction quality further even when fewer signal measurements are available. In this chapter, multi-scale wavelet structure of MECG signals is studied and this information is incorporated in joint CS recovery through a subband-based weighting approach. Observing the gross segmentation of clinical ECG features in different wavelet scales (as shown in Figure 5.1), subband-level weighting seems more intuitive compared to coefficient-level weighting introduced in Chapter 4 for categorically emphasizing diagnostically relevant ECG features lying in some particular subbands.

In this chapter, an improved family of WMNM algorithms is proposed for the joint CS reconstruction of MECG signals. In this family, various weighted versions of standard MNM algorithm are analyzed. In particular, two specific classes of WMNM algorithms are proposed which are referred to as subband weighted MNM (SWMNM) and prior weighted MNM (PWMNM). The former is an iterative reweighted version of standard MNM with similar iterative steps as in AWMNM proposed in previous chapter, but with a different weighting criterion. Here, the weighting rule is defined on the basis of diagnostic information contents of the wavelet subbands captured in the form of subband energy, subband entropy and subband amplitudes. The second algorithm, i.e., PWMNM is a non-iterative algorithm, which solves a weighted MNM using the weights designed in *a priori*. The *a priori* weight selection is based on the prior structural knowledge of MECG wavelet representation. Incorporation of clinically important information in the WMNM algorithm through the proposed subband-based weighting schemes is expected to reduce the number of compressed CS measurements ($M$) further (allows lower data rates) required for faithful signal reconstruction. Reducing $M$ without affecting the signal reconstruction quality of the system would directly help in lowering the on-chip computations and energy consumption, thus making the CS-based wireless body area network (WBAN)-enabled ECG telemonitoring systems more autonomous and cost-effective. Additionally, a

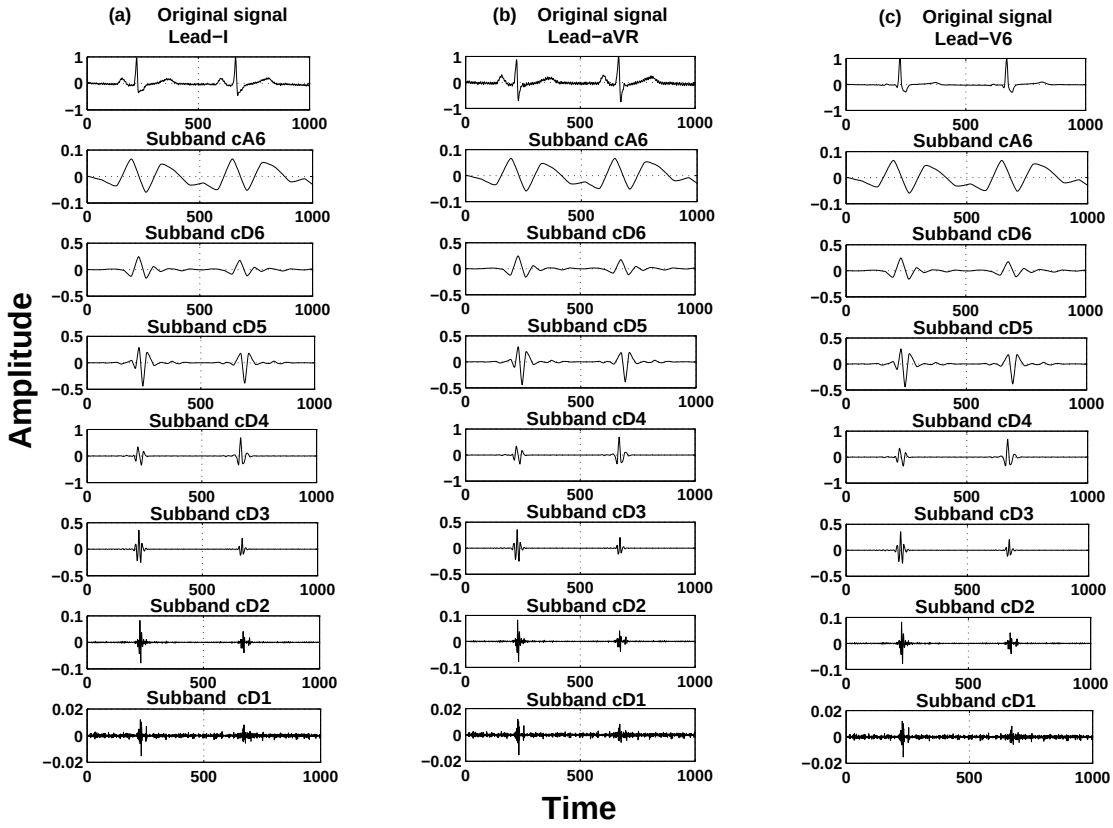


**Figure 5.1:** Grossly segmented ECG signal information/features in various wavelet subbands in three different leads

block-sparsity-based joint CS recovery is also explored in this chapter to exploit the spatio-temporal correlated MECG structure.

The organization of the chapter is as follows: Section 5.1 discusses about the diagnostic importance of multi-scale ECG features and ways to capture and incorporate them in the weighted CS recovery. Proposed methodology describing different weighting criterion is discussed in Section 5.2. Section 5.3 briefly presents performance measures used for the evaluation. Recovery performance under different proposed weighting schemes is discussed in Section 5.4. Evaluation of reconstruction and compression performance is presented in Section 5.5. Recovery results in noisy scenario and some practical issues are also discussed in this section. As an exploratory work, Section 5.6 discusses a block-sparsity-based joint CS recovery approach. Summary of the chapter is presented in Section 5.7.

## 5.1 Multi-scale Signal Information and Their Diagnostic Relevance

The ECG information gets grossly segmented at various wavelet scales as shown in Figure 5.1 for three different leads. Low frequency subbands constitute most of the clinically important ECG features. As can be observed in Figure 5.1, low frequency features, such as P wave, T wave, ST segment, and a major portion of the QRS-complex are present in approximation ($cA6$) and three detail subbands ($cD6$, $cD5$, and $cD4$). On the other hand, high frequency wavelet subbands are mainly noise dominated as can be observed in lower order detail subbands. A very similar subband level feature distribution can be observed in all three leads shown in Figure 5.1. Clinical relevance of the wavelet subbands have already been intensively studied and established in the literature [81, 88, 140, 141]. The clinically important ECG information can be captured at the subband level through different measures, such as entropy, energy, amplitude decay, etc. There are many diagnostic distortion measures, such as $WEDD$, $WWPRD$, etc. reported in the literature, where these measures have been used to quantify the diagnostic distortions in various ECG signal processing tasks [80,81,141]. These studies motivated us to capture the diagnostically relevant ECG features through the aforementioned measures and incorporate them in the joint CS reconstruction problem formulation using a new multi-scale weighting approach. This subband-based weighting scheme is expected to emphasize the clinically relevant wavelet subbands more precisely during joint CS recovery, which consequently, helps in improving the signal reconstruction quality, especially at low number measurements.

## 5.2 MMV CS-based Joint Compression/Reconstruction Method

The proposed method in this chapter employs the same encoder as used in the previous chapter. The $L$ channels of $N$-dimensional MECG signals in $\boldsymbol{X} = [\boldsymbol{x}_1,\ \boldsymbol{x}_2,\ \boldsymbol{x}_3,\ \ldots,\ \boldsymbol{x}_L] \in \mathbb{R}^{N\times L}$ are compressed using MMV formulation (2.15) and compressed measurement vectors are obtained in $\boldsymbol{Y}$.

In **Chapter 4**, a weighted MNM (WMNM)-based joint CS recovery algorithm (4.7) was proposed to solve the MMV problem (4.1), which is revisited here:

$$\widehat{\boldsymbol{A}}_{MAP} = \underbrace{\arg\min}_{\boldsymbol{A}} \frac{1}{2}\left\|\boldsymbol{Y} - \boldsymbol{\Theta}\widehat{\boldsymbol{A}}\right\|_F^2 + \lambda \sum_j w_j \boldsymbol{A}_j^{\ell_2}$$

where $w_j$'s are the weighting parameters.

The weights $w_j,\ j = 1, 2, ..., N$ in the above joint sparse solution can be considered as free parameters and can be set in many ways depending on the understanding of the underlying problem. In the previous chapter, weights were designed on the coefficient-level using $\ell_2$-norm of each row of row-sparse matrix $\boldsymbol{A}$ and were different for each wavelet coefficient. In this chapter we explored a clinically more relevant weighting scheme defined at subband-levels, where all coefficients at each wavelet subband have equal weights, chosen according to the clinical significance of the subband (discussed in next subsection). This approach is expected to emphasize the diagnostically important wavelet subbands more effectively during joint CS recovery and improve the reconstruction performance further at low measurements.

### 5.2.1 Proposed subband weighting-based WMNM algorithm

The judicious weight selection in (4.7) would help enforce row-sparsity at the right locations in $\boldsymbol{A}$ while preserving diagnostic ECG features from all the channels. Weights, if chosen properly, can enhance the recovery performance of standard MNM up to a significant level. In the proposed WMNM approach in this chapter, weights $w_j,\ j = 1, 2, \ldots, N$ are designed to incorporate clinically important information about MECG signals in the joint optimization problem formulation (4.7). We utilized the distribution of diagnostically relevant information about MECG signals in different wavelet subbands and incorporated it as the additional information in (4.7) through the weighting parameters. Using wavelet transform, the ECG spectra is grossly segmented into various subbands [44]. The $n$ level wavelet decomposition of each lead of MECG gives $n+1$ number of subbands: $cD_1, cD_2, ..., cD_{n-1}, cD_n, cA_n$. Here, the subband $cA_n$ consists of the approximation coefficients and carries most of the low frequency information of the ECG signal. The finer details (or high frequency ECG information) are associated with $n$ number of detail subbands $cD_i,\ i = 1, 2, ..., n$. Based on the clinical importance of these subbands two specific classes of WMNM algorithms are proposed. One is iterative in nature and referred to as subband weighted MNM (SWMNM), and the second is a non-iterative algorithm called prior weighted MNM (PWMNM).

#### 5.2.1.1 Subband weighted MNM

This technique is an iterative version of standard MNM, which alternates between the estimation of $\boldsymbol{A}$ and updation of weight vector $\boldsymbol{w}$. Steps involved are similar to AWMNM Algorithm 1 defined

in previous chapter, but with a different weight selection criterion. The weights are initialized with unity as we give equal weightage to all the subbands. In each step, a standard MNM problem is solved and the corresponding weights are calculated according to the defined weighting rule. The weights emphasize clinically important subbands and they are used for a more accurate estimation of $\boldsymbol{A}$ in the next iteration. The weights get updated in each iteration using the dynamic entries of the coefficient matrix $\boldsymbol{A}$ estimated in the previous iteration. This adaptive weighting strategy produces more focal estimates of the signal as the optimization progresses and the reconstruction quality of MECG signals improves iteratively. The important task is now to define weighting rules for weight calculation. Motivated from the fact that important diagnostic ECG information lies in local subbands, we proposed to design the weights $w_j,\ j = 1, 2, \ldots, N$ on the basis of various subband level information. We investigated energy, amplitude and entropy at different wavelet scales under this category of weighting. In all the subband-based weighting approaches, equal weights are taken for the coefficients at same wavelet scale.

**Subband energy-based weighting**

This weighting strategy is motivated from reweighting $\ell_1$- and $\ell_2$-based algorithms [132,134,142], where the weights are chosen according to inverse of coefficients' amplitudes. The proposed technique differs from the above approaches in terms of a new weight selection criterion. Instead of designing weights at the coefficient level, we propose to choose weights on the wavelet subband level. Observing the gross segmentation of clinical ECG features in different wavelet scales, the subband-based weighting seems more intuitive. Here, the entries $w_j$ of the weighting vector are designed based on the energy associated with each subband. The subband energy corresponds to the clinical importance of each wavelet subband [81] and so this weighting strategy is expected to emphasize and preserve diagnostically important wavelet coefficients during joint reconstruction. Let $d_i(k),\ i = 1, 2, ..., n+1$ be the $k$-th dense coefficient of estimated vector $\widehat{A}^{\ell_2}$ (at $t$-th iteration) from the $i$-th wavelet subband. The weights for $i$-th subband at $(t+1)$-th iteration are defined as follows:

$$w_{sub_i}^{t+1} = \left( \frac{\sum_{k=1}^{N_{sub_i}} [d_i(k)^t]^2}{\sum_{k=1}^{N} [(\widehat{\boldsymbol{A}}_k^{\ell_2})^t]^2} + \varepsilon \right)^{p/2-1}, \quad p \in [0, 2],\ i = 1, 2, ..., n+1 \tag{5.1}$$

where $N_{sub_i}$ is the number of coefficients in the $i$-th wavelet subband. The parameters $\varepsilon$ and $p$ are same as introduced in (4.8) in previous chapter. They are used here for the similar purpose. So, the higher energy (i.e., low frequency) subbands are assigned with smaller weights while lower energy (i.e., high frequency) subbands are assigned with larger weights. Such type of weight selection can be justified by noting that, in (4.7), small weights emphasize nonzero rows (associated mainly to clinically important high energy wavelet subbands), while large weights deemphasize such rows. So, rows from lower energy subbands (clinically less important) will be pushed towards zero and their corresponding indices are more likely to be excluded from the row-support of final solution. This helps in inducing row-sparsity at favorable locations.

In place of taking the normalized energy of each subband for weight selection, the normalized sum of amplitudes of the subband coefficients are also explored and weighted recovery performance is analyzed.

**Subband entropy-based weighting**

The normalized relative wavelet subband energy (NRWSE) associated with each subband in the estimated dense coefficient vector $\widehat{\boldsymbol{A}}^{\ell_2}$ can be given as:

$$NRWSE_i = \frac{1}{N_i}\left(\frac{\sum_{k=1}^{N_{sub_i}}[d_i(k))]^2}{\sum_{k=1}^{N}[(\widehat{\boldsymbol{A}}_k^{\ell_2})]^2}\right),\ i = 1, 2, ..., n+1 \tag{5.2}$$

Since $\sum_{i=1}^{n+1} NRWSE_i = 1$, $NRWSE_i$ can be considered as energy probability density which captures local subband information according to their diagnostic importance [81]. Based on these probability densities, subband entropies $H_i,\ i = 1\ to\ n+1$ can be defined as follows:

$$H_i = -NRWSE_i \log(NRWSE_i),\ i = 1, 2, ..., n+1 \tag{5.3}$$

So weights $w_{sub_i}$ for different local subbands at $(t+1)$-th iteration are defined as $w_{sub_i}^{t+1} = (H_i^t + \varepsilon)^{p/2-1},\ p \in [0, 2],\ i = 1, 2, ..., n+1$.

After getting weights $w_{sub_i},\ i = 1, 2, ..., n+1$ for each of the $n+1$ subbands, these weighting factors are replicated within each subband. Equal weights are assigned to the coefficients within same subband to get the complete weighting vector, $w_j,\ j = 1, 2, ..., N$ in (4.7).

#### 5.2.1.2 Prior weighted MNM

It is a non-iterative WMNM algorithm, where weights are designed based on the prior structural knowledge about MECG wavelet representation. Unlike SWMNM, here weights are set before the start of the algorithm as weighting rule does not depend on the coefficient matrix $\boldsymbol{A}$. Final reconstruction can be achieved in a single step solving a weighted MNM problem. This weighting strategy is motivated from the fact that decay of wavelet coefficients across the scales can be modeled exponentially, i.e., *a priori* information is available about the decay characteristics of subband coefficients [143]. As illustrated in Figure 5.1, approximation subband carries significant ECG information. So, most of the coefficients in the approximation subband $cA_n$ are always nonzero. Due to strong spatial correlation across the channels, similar variation can be observed in approximation subbands of each channel (as shown in three leads in Figure 5.1). So, indices corresponding to these entries are highly likely to fall within the row support of jointly sparse MECG signals. Therefore, in a joint sparse approximation, there is no need to put row-sparsity constraint in sub-matrix of $\boldsymbol{A} \in \mathbb{R}^{N_{sub_{n+1}} \times L}$, where $N_{sub_{n+1}}$ is the number of rows of $\boldsymbol{A}$ carrying approximation subband coefficients from all the channels. So, the weights for the dense coefficients in approximation subband of $\boldsymbol{A}^{\ell_2}$ are taken to be zero, i.e.,

$$w_{sub_i} = 0, \ i = n+1 \tag{5.4}$$

The weighting factors for detail coefficients should be judicially chosen by studying the decay characteristics of the coefficients at different wavelet scales. The amplitude of detail coefficients decays exponentially with increasing resolution level and can be given as $2^{-is}$, where $i$ is the resolution level and $s$ is the local smoothness of the underlying signal [46, 135]. For ECG signals, $s = 1$ can be chosen due to its piece-wise polynomial characteristics [46]. A similar type of weighting strategy is employed in [46] for SMV CS recovery of single channel ECG signal using weighted $\ell_1$ approach. However, the effectiveness of this type of weighting is enhanced significantly when used in MMV paradigm for simultaneous channel reconstruction. The detail subband weights are given as follows:

$$w_{sub_i} = 2^{-(i-1)s}, \ i = 1, 2, ..., n \tag{5.5}$$

After getting approximation and detail subband weights from (5.4) and (5.5), these weighting factors are replicated by assigning equal weights to the coefficients within same subband to get the com-

plete weighting vector, $w_j,\ j = 1, 2, ..., N$ for each row of coefficient matrix $\boldsymbol{A}$. It is demonstrated in the results section that the prior weighting strategy performs superior in case of simultaneous reconstruction of all channels using PWMNM compared to channel-by-channel recovery using weighted $\ell_1$-minimization as done in [46].

## 5.3 Performance Measures

The performance evaluation of the proposed method is carried out using publicly available Physikalisch-Technische Bundesanstalt (PTB) [2,3] and Massachusetts Institute of Technology-Boston's Beth Israel Hospital (MIT-BIH) database [2, 3], and commercially available Common Standards for Electrocardiography (CSE) database [4]. Widely used performance metrics, namely the percentage-root mean square difference ($PRD$), $PRD1$, joint $PRD$, reconstruction signal to noise ratio ($R\text{-}SNR$), compression ratio ($CR$) and quality score ($QS$) [34, 45, 144] are used for the performance evaluation. $PRD1$ is a variant of $PRD$ and joint $PRD$ is an extension of traditional $PRD$ to calculate the joint error in the case of multiple signals, i.e., MECG. They are defined as follows:

$$PRD1\ (\%) = (\|\boldsymbol{x} - \widehat{\boldsymbol{x}}\|_2 / \|\boldsymbol{x} - \overline{\boldsymbol{x}}\|_2) \times 100, \tag{5.6}$$

$$Joint\ PRD\ (\%) = \frac{\left\|\boldsymbol{X} - \widehat{\boldsymbol{X}}\right\|_F}{\left\|\widehat{\boldsymbol{X}}\right\|_F} \times 100, \tag{5.7}$$

where $\boldsymbol{x}$ and $\widehat{\boldsymbol{x}}$ are the $N$-dimensional original and recovered signals, respectively, and their capital versions are the corresponding matrices containing all the channels. The term $\|.\|_2$ and $\|.\|_F$ denotes the $\ell_2$-norm and frobenius norm of $\boldsymbol{x}$, and $\boldsymbol{X}$, respectively. The term $\overline{\boldsymbol{x}}$ in the definition of $PRD1$ is the signal mean/baseline. We used $PRD1$ for distortion calculation in ECG signals from the MIT-BIH database, where a baseline of $\overline{\boldsymbol{x}} = 1024$ is present. In addition to the above quality measures, we also calculated the wavelet energy-based diagnostic distortion ($WEDD$) [81] as a diagnostic distortion measure.

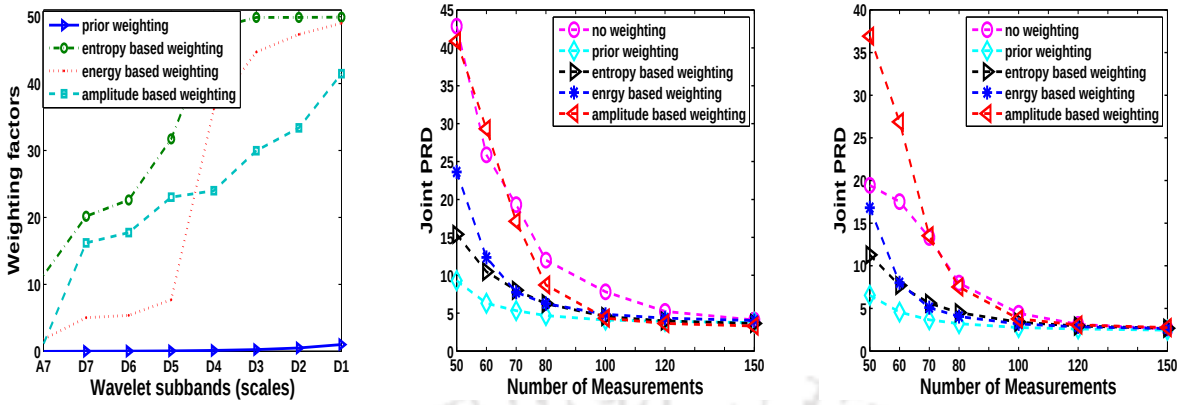


(a) Weight variation across subbands (b) Healthy control (HC) (c) Hypertrophy

**Figure 5.2:** (a) Variation of weighting factors in different weighting strategies for eight wavelet subbands (scales) resulted from $n = 7$ level wavelet decomposition. Performance comparison of different weighting schemes in (b) HC and (c) Hypertrophy cases. For SWMNM, $p = 0.2$ and $t_{max} = 3$ is taken. The performance analysis is done for 25 cases of health control and 7 cases of hypertrophy.

## 5.4 Joint Recovery Analysis Under Different Weighting Rules

This section analyses the effect of incorporating additional information in the joint optimization formulation through the proposed weighting strategies. The variation of weighting factors in different weighting rules of SWMNM (at $p = 0$) and PWMNM are shown in Figure 5.2(a). For effective weighting in sparse recovery problems, weighting strategy should be in such a way that it sets large weights for insignificant (almost zero) coefficients/rows whose indices are not desirable in the final support set [132]. However, small weights must be set for significant nonzero coefficients/rows as it emphasizes them in the final recovery. If MECG wavelet structure is seen, the wavelet coefficients decay exponentially with the increase in resolution level [46, 135]. So, the weights should increase towards the lower wavelet scales. All types of proposed weighting schemes follow this trend starting with minimum weights for the highest scale wavelet subband $A_7$ and ending with maximum weights for the lowest scale subband $D_1$ (Figure 5.2(a)). The effect of weighting schemes on the joint MECG reconstruction is accessed in terms of joint $PRD$ values which reflects the joint reconstruction error in all the channels. The study is done on 25 healthy control (HC) and 7 hypertrophy datasets from the PTB data base. Figures 5.2(b) and 5.2(c) show the variation of the joint $PRD$ value under different weighting rules at a varying number of measurements ($M$) for healthy (HC) and pathological (hyper-

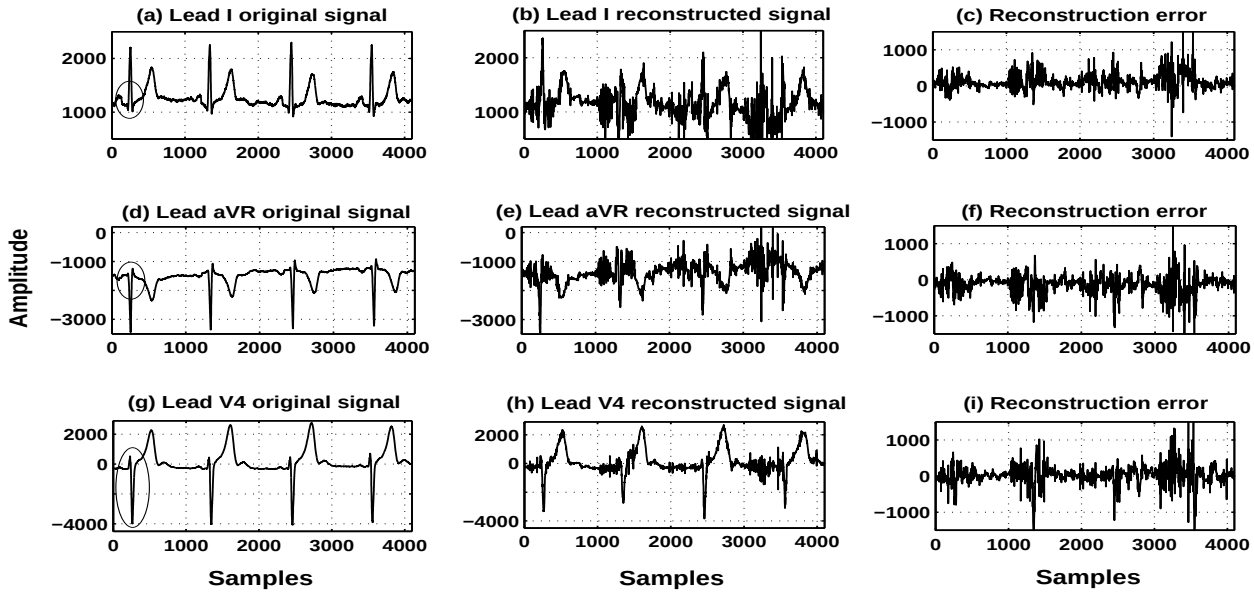


(a) Recovered results by regular MNM

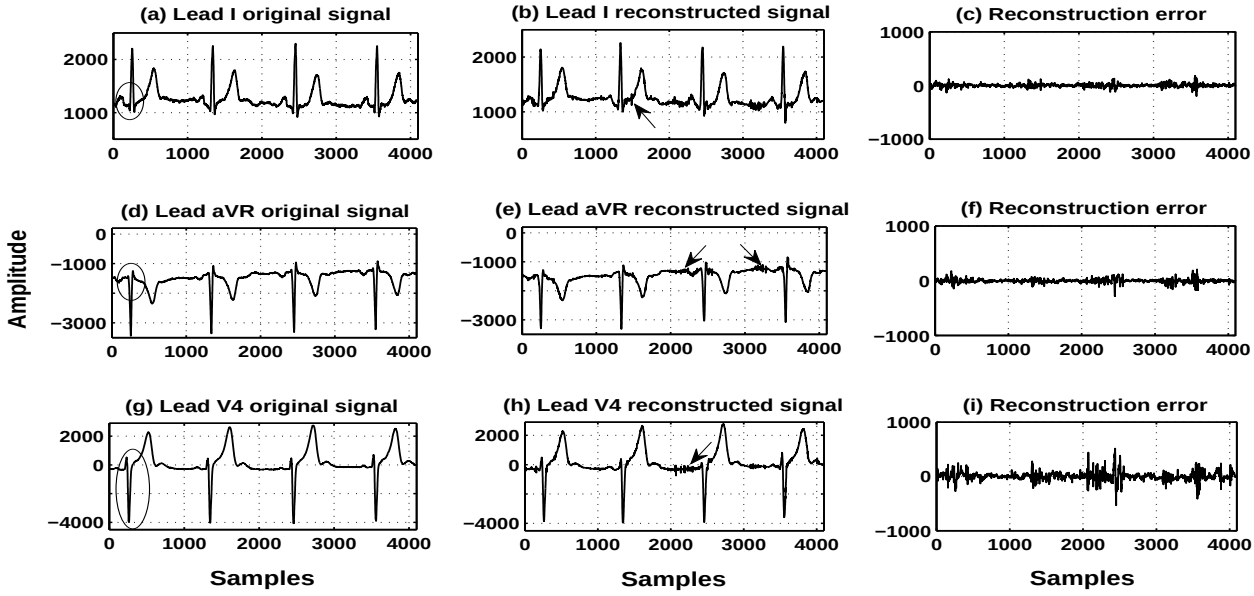


(b) Recovered results by proposed SWMNM

**Figure 5.3:** Original and recovered signals (first 4096 samples, around 4-sec data) (a) using regular non-weighted MNM technique, (b) using proposed SWMNM technique when the number of measurements, $M = 70$. Data-set s0424_rem exhibiting bundle branch block is used from the PTB database. Characteristic pathological features are encircled in the original signal waveforms. Arrows in the reconstruction plots indicate the distortion points.

trophy) cases, respectively. For, SWMNM, $t_{max} = 3$ is taken. It can be observed that prior weighting performs better at low values of $M$ followed by entropy and energy-based weightings. After $M = 100$, all the weighting approaches perform equally well, but still better than the non-weighted case. The poor performance of subband amplitude-based weighting is mainly due to its almost linear variation across the subbands (Figure 5.2(a)), which was expected to follow the exponential decay characteristics of wavelet coefficients. Prior weighting best captures this exponential decay characteristics followed by entropy and energy-based weightings. In the rest of the paper, the presented SWMNM recovery results are produced under the entropy weighting scheme.

## 5.5 Results and Discussions

The performance of the proposed approach is evaluated in terms of visual quality of the reconstructed MECG signals and compression efficiency of the method. Reconstruction performance is also analyzed in the presence of measurement noise.

### 5.5.1 Evaluation of the reconstruction results

The main objective of this subsection is to demonstrate the effectiveness of the weighting strategy proposed in this work for better reconstruction at the low measurement rates (higher compression ratios). Visual evaluation test [45] is done to verify the preservation of important diagnostic ECG features in the reconstructed MECG signals. It involves visual analysis of different pathological ECG features in the reconstructed waveforms. To make visualization more clear, the original and the reconstructed ECG signals corresponding to the first 4096 time points (approx. 4-sec data) of the PTB database from different channels are plotted together. Figure 5.3 depicts a bundle branch block (BBB) pathology reconstruction (data-record s0424) and Figure 5.4 shows a cardiomyopathy data recovery (data-record s0423) using the proposed SWMNM and PWMNM techniques, respectively, at a low number of measurements, $M = 70$. In both of the above recovery, the reconstruction error is also plotted along with the reconstructed signals. By observing the reconstruction error plot in both the figures, it is clear that both the proposed techniques significantly reduce the reconstruction error compared to the regular (non-weighted) MNM at the same value of $M$. The SWMNM technique preserves the important diagnostic features of BBB pathology (encircled in the original signal waveforms) such

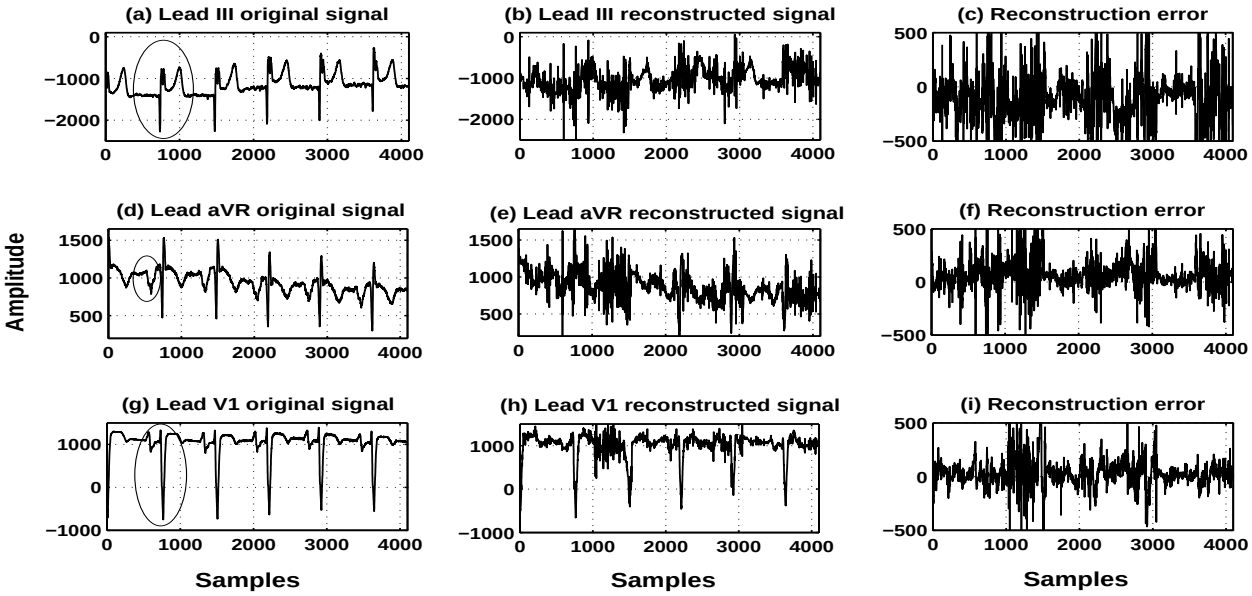


(a) Recovered results by regular MNM

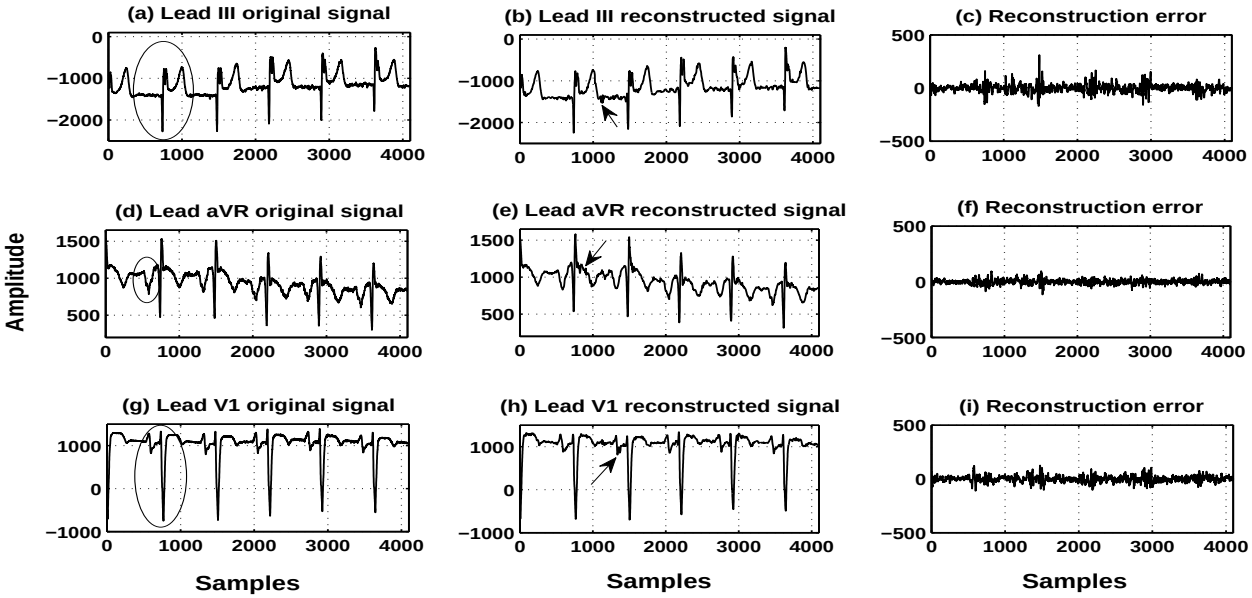


(b) Recovered results by proposed PWMNM

**Figure 5.4:** Original and recovered signals (first 4096 samples, around 4-sec data) (a) using regular non-weighted MNM technique, (b) using proposed PWMNM technique when the number of measurements, $M = 70$. Data-set s0423_rem exhibiting cardiomyopathy is used from the PTB database. Characteristic pathological features are encircled in the original signal waveforms. Arrows in the reconstruction plots indicate the distortion points.

as $QRS$ complex duration, secondary $R$-wave ($RSr'$ complex) and slurred $S$-wave (Figure 5.3(b)). On the other hand, severe distortions can be noted in the above diagnostic features in the reconstructed MECG signals using regular MNM (Figure 5.3(a)). Similar observations are also made in Figure 5.4, where the MECG signals belong to cardiomyopathy arrhythmia. The regular MNM fails to recover the clinically important features like pathological $Q$-wave, $R$-wave amplitude, and $T$-wave (Figure 5.4(a)), while PWMNM technique preserves the same (Figure 5.4(b)). The proposed WMNM techniques exploit the joint correlation of MECG wavelet coefficients to incorporate multi-source priors about wavelet subbands having high clinical relevance in the joint optimization problem formulation. This helps WMNM to emphasize the diagnostically important wavelet coefficients and improve the joint MECG recovery.

Signal reconstruction is not the ultimate goal in WBAN-enabled telemonitoring applications. The acquired and transmitted signals through WBAN have to be examined by the cardiologist at healthcare centers for disease detection and classification purposes [1, 41]. Also, the popular distortion measure $PRD$ is not a diagnostic distortion measure and hence a low $PRD$ may not necessarily correspond to clinically good reconstruction [1]. So, clinical evaluation or diagnosability of the reconstructed ECG signals from the disease classification point of view also becomes important [36]. We followed the steps suggested in [145] for extracting the multi-scale wavelet energies and eigenvalues of multi-scale covariance matrices, which are further used as diagnostic features for classification purpose. Support vector machine (SVM) with RBF kernel is used as the classifier. Classification results for MI and HC classes are given in Table 5.1. Classification is performed at different number of measurements, $M$. Ground truth accuracy of the classifier was 91.5%. It can be seen that the proposed WMNM delivers better classification results compared to its non-weighted counterpart. WMNM gives 73.2% accuracy even when data packet of length $N = 512$ was recovered using only around 10% measurements ($M = 50$). This verifies the good clinical quality even at higher data reduction. On the other hand, MNM performs inferior at this value of $M$ with 62.4% accuracy. It can be noted that the classification accuracy increases when more number of measurements are used for reconstruction. The comparison between the performance of the proposed method and wavelet-based SPIHT method is also carried out. The SPIHT method is implemented using open-source SPIHT software [146, 147]. Evaluation results in the form of classification accuracy for the PTB database at three different $CR$ values (or $M$ values)

**Table 5.1:** Classification accuracy (diagnosibility) of the system when joint MECG recovery is done by different methods at different number of measurements. Datasets are taken from the PTB database.

| Class | $M$ | Ground Truth (%) | Classification accuracy (%) | | |
|---|---|---|---|---|---|
| | | | MNM | PWMNM | SPIHT |
| HC/MI | | 91.5 (Original signal is used) | | | |
| | 50 | | 62.4 | **73.2** | 65 |
| | 60 | | 66.4 | **75.2** | |
| | 70 | | 67.2 | **77.2** | 70.3 |
| | 80 | | 70.8 | **78.0** | |
| | 100 | | 73.6 | **80.4** | 75.6 |

are given in Table 5.1. It is noted that, despite having better performance in case of single channel ECG compression, as established in earlier studies [1, 45], SPIHT algorithm does not yield encouraging performance in case of MECG signal compression. This is clear by observing the classification accuracy of SPIHT, which is also an indirect assessment of reconstruction accuracy (Table 5.1). The SPIHT method performs marginally better than the traditional MNM technique, but underperforms the proposed method. It ignores the spatial correlation as it is designed to process each channel individually, whereas the proposed method exploits it during simultaneous compression/reconstruction. This might be the reason behind the lower performance by SPIHT in the case of MECG signals.

Average distortion values in terms of average $PRD$ for HC and four major pathological classes present in the PTB database are given in Table 5.2 at $M = 100$. Class specific average results are calculated over 52 healthy control, 148 myocardial infarction, 7 hypertrophy, 15 bundle branch block, and 18 cardiomyopathy datasets available in the PTB database in order to analyze the inter-class performance variation of the proposed method. The output $PRD$ value in each class falls in *good* category reconstruction. It is also evident from the table that each class is having variable reconstruction performances at the same number of measurements in each channel. Each class is having its own diagnostic ECG features, which results in different morphological changes in the signals from different channels. This may change the joint sparse representation of MECG resulting in different recovery performance of the proposed algorithm for each class. The average $PRD$ calculated across different classes also ensures the *good* quality reconstruction. To highlight the variability among the set of ECG data-records, average output $PRD$ of all the pathological data records of PTB database

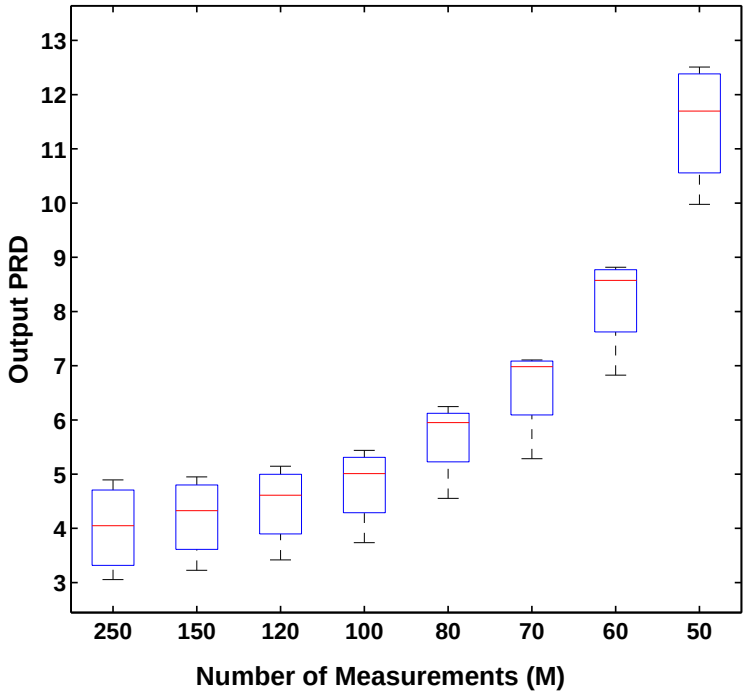


**Figure 5.5:** Box plot showing variation of output $PRD$ across the data records of PTB database when recovered using PWMNM at different number of measurements.

for Lead $aVR$ is shown in the form of box plots in Figure 5.5. The extreme values in the individual box plot depict the minimum and maximum $PRD$ values obtained at a particular value of $M$ using different datasets. With more compression of the data by reduction in the size of sensing matrix (with low $M$ values), output $PRD$ increases and vice-versa.

**Table 5.2:** Channel-wise reconstruction error in terms of average output $PRD$ value for different types of normal and pathological cases using the proposed technique when the number of measurements, $M = 100$. Results are averaged over all the data-sets available in that particular class in the PTB database.

| Pathological classes | No. of Datasets | Different ECG channels | | | | | | | | | | | |
|---|---|---|---|---|---|---|---|---|---|---|---|---|---|
| | | Lead I | Lead II | Lead III | aVR | aVL | aVF | V1 | V2 | V3 | V4 | V5 | V6 |
| Healthy control | 52 | 8.35 | 3.75 | 5.87 | 5.03 | 4.30 | 3.47 | 4.00 | 4.21 | 4.36 | 5.44 | 5.09 | 5.18 |
| Myocardial Infarction | 148 | 10.17 | 6.96 | 7.78 | 5.39 | 10.96 | 6.57 | 5.64 | 4.60 | 4.11 | 4.84 | 6.77 | 7.07 |
| Hypertrophy | 7 | 6.42 | 4.30 | 4.70 | 4.77 | 5.23 | 4.77 | 2.77 | 2.56 | 3.18 | 3.74 | 3.90 | 3.46 |
| Bundle branch block | 15 | 4.19 | 4.26 | 5.53 | 4.41 | 3.62 | 3.52 | 7.05 | 4.77 | 4.33 | 5.18 | 4.36 | 4.27 |
| Cardiomyopathy | 18 | 5.71 | 4.11 | 3.69 | 3.51 | 4.19 | 3.11 | 2.98 | 3.03 | 3.23 | 3.53 | 2.88 | 2.60 |
| **Average** | **240** | **6.96** | **4.67** | **5.51** | **4.62** | **5.66** | **4.28** | **4.48** | **3.83** | **3.84** | **4.54** | **4.60** | **4.51** |

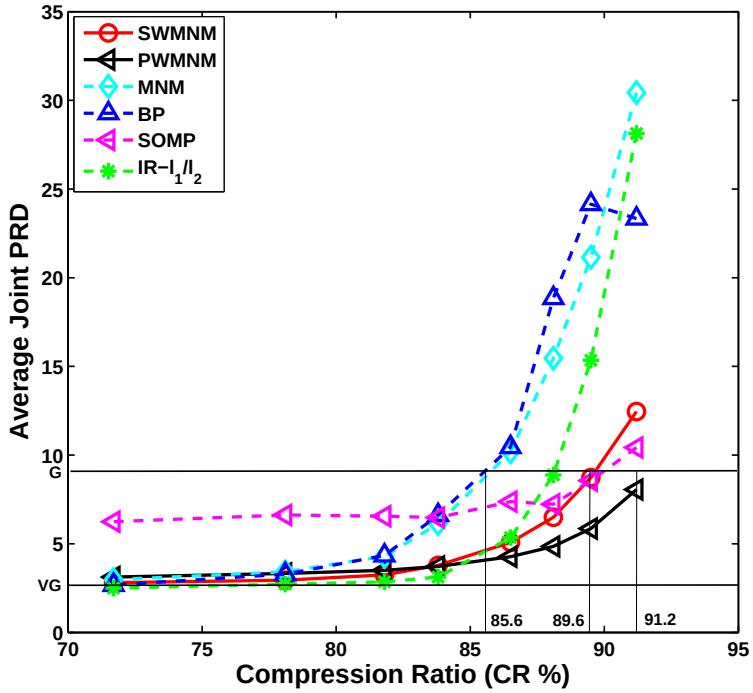


**Figure 5.6:** Comparison plot between proposed techniques (SWMNM, PWMNM) and existing techniques at different compression ratios ($CR$) in terms of average joint $PRD$. Results are averaged over all data-sets taken from the PTB database.

### 5.5.2 Evaluation of the compression performance

The size of sensing matrix $\mathbf{\Phi} \in \mathbb{R}^{M \times 512}$ directly corresponds to the compression efficiency of the proposed method. Compression is performed at different $M$ values and the resulting $CR$ at 8-bit quantization is plotted against average joint $PRD$ over all the PTB records in Figure 5.6. Recovery is also done using the existing CS-based techniques for the performance comparison purpose. Benchmark techniques included for comparison are standard MNM [34], Basis pursuit (BP) [1, 44], modified simultaneous orthogonal matching pursuit (SOMP) [97], and iterative reweighted $\ell_1/\ell_2$ (IR-$\ell_1/\ell_2$) [134]. Above techniques are implemented using publicly available toolboxes. Convex optimization toolbox $CVX$ [148] is used to implement MNM and IR-$\ell_1/\ell_2$, $SPGL1$ [139] is used for BP and a modified-SOMP tool-box [97] is used for SOMP implementation.

First, we compare the performance of the proposed WMNM techniques (i.e., SWMNM, and PWMNM) with their non-weighted counterpart, i.e., standard MNM which is a special case of WMNM

when no weighting is done, i.e., $\boldsymbol{w} = I_{1\times N}$. The MNM as a joint sparse recovery algorithm, is earlier used by Mamaghanian et al. [34] for joint CS reconstruction of MECG signals. However, the trend of $PRD$ in Figure 5.6 indicates that WMNM performs much better than MNM for joint CS MECG recovery. Incorporation of additional information through the proposed subband weighting schemes in the joint recovery algorithm helps identify the supports of subband coefficients having high clinical relevance. So, these clinically important coefficients are emphasized during the recovery process in all the channels even when data recovery is done at smaller $M$ value. This helps proposed WMNM techniques to preserve the overall diagnostic quality in the reconstructed MECG signals at higher $CR$. However, MNM lacks this type of feature as it only leverages group sparsity leading to performance degradation, especially, at higher $CR$ values.

IR-$\ell_1/\ell_2$ algorithm [134, 149] is a reweighted version of standard MNM and is an MMV extension of reweighted $\ell_1$ [132]. The proposed SWMNM approach differs with this technique in terms of weight selection criterion. It can be noted in Figure 5.6 that performance of IR-$\ell_1/\ell_2$ can be substantially improved in low measurement scenarios by using a wavelet subband-based weighting scheme (i.e., SWMNM). Prior knowledge-based PWMNM, which uses decaying characteristics of subband coefficients, can give further performance improvement. Marginal improvement in the recovery performance of IR-$\ell_1/\ell_2$ is observed in low data compression conditions (low $CR$). However, in the intended resource-constrained ambulatory applications, low $CR$ is undesirable as it increases the bandwidth requirement and energy consumption resulting in higher system cost [1,34]. Basis pursuit (BP) is a classic CS recovery algorithm for SMV models and has been used in earlier CS ECG works [1,41]. When the group BP is used for joint MECG recovery, it is outperformed by both SWMNM and PWMNM. A greedy algorithm, SOMP was modified in [97] by utilizing prior signal knowledge with it. Authors have used it for jointly recovering consecutive ECG beats of single channel ECG. We used the same modified SOMP for the joint recovery of all the channels and found that it performs poorly compared to WMNM techniques. It gets saturated early and the performance gains marginally even at lower $CR$ values.

Channel-wise performance comparison with some other works is given in Table 5.3 in terms of $PRD$, $SNR$, $WEDD$, and $QS$. The average quantitative values calculated over all the datasets of PTB database are listed. A higher level of distortion can be noted in the case of regular MNM recovery

compared to the proposed PWMNM technique at $M = 70$. The proposed method shows substantial reduction in the distortion levels in all distortion metrics in each channel. In order to demonstrate the database robustness of the proposed methods, the performance is also calculated using the CSE multilead library database. The existing works that use CSE database [34, 44], are also compared in Table 5.3. Significant reduction in the reported average $PRD$ is noted for most of the leads. For the CSE database, level of distortions are relatively high compared to the PTB database at the same value of $M$. This may be due to the higher noise contents and a relatively lower sampling frequency ($f_s$) of the MECG signals in the CSE database. The low value of $f_s$ may reduce the level of redundancies and hence sparsity, resulting in low compressible ECG signals. Most of the existing CS-based data compression works [45,46] deal with single channel ECG recovery. So, it is interesting to compare these works with the proposed work, where all channels are recovered simultaneously. Table 5.3 includes the results when each channel of the MIT-BIH database is recovered individually in earlier reported works [45, 46] and when both channels are jointly recovered by the proposed method. Results suggest that the proposed technique performs better than the above works in terms of reduced $PRD$ value at same reported $M = 192$ and $CR = 6.4$ ($M = 125$). The proposed method exploits the inter-channel correlation information while jointly recovering both channels resulting in reduced $PRD$ at same $M$ or $CR$ values, whereas [45, 46] ignores this information. This also validates the importance of correlation information in CS-based MECG telemonitoring systems and makes the proposed WMNM techniques a preferable choice for joint data recovery.

**Table 5.3:** Performance comparison between proposed technique and other existing techniques. Results are averaged over all the PTB data records and 40 data records of the CSE Multilead Library database (M01_001-M01_040).

| Techniques | $M$ | Metrics | ECG channels | | | | | | | | | | | | Database |
|---|---|---|---|---|---|---|---|---|---|---|---|---|---|---|---|
| | | | Lead I | Lead II | Lead III | aVR | aVL | aVF | V1 | V2 | V3 | V4 | V5 | V6 | **Average** | |
| MNM [34] | 70 | PRD | 19.51 | 14.92 | 16.02 | 16.85 | 14.51 | 13.83 | 20.51 | 19.49 | 19.01 | 22.43 | 19.80 | 20.58 | 18.12 | **PTB** ($f_s = 1000\ Hz$) |
| | | SNR | 14.19 | 16.52 | 15.90 | 15.46 | 16.76 | 17.18 | 13.76 | 14.20 | 14.42 | 12.98 | 14.07 | 13.73 | 14.93 | |
| | | WEDD | 19.19 | 14.43 | 13.71 | 17.67 | 12.01 | 12.55 | 21.44 | 20.31 | 18.67 | 23.03 | 20.07 | 22.01 | 17.92 | |
| **Proposed** | 70 | PRD | 8.73 | 6.02 | 7.78 | 5.93 | 7.52 | 5.96 | 6.35 | 5.58 | 5.54 | 6.59 | 6.74 | 6.54 | **6.60** | |
| | | SNR | 21.18 | 24.41 | 22.18 | 24.54 | 22.47 | 24.49 | 23.95 | 25.07 | 25.13 | 23.62 | 23.43 | 23.68 | **23.67** | |
| | | WEDD | 8.13 | 6.65 | 6.69 | 5.65 | 6.39 | 5.44 | 5.70 | 4.73 | 4.89 | 6.14 | 6.27 | 6.20 | **6.07** | |
| MNM [34] | 70 | PRD | 33.68 | 34.22 | 32.74 | 33.58 | 34.34 | 33.18 | 32.69 | 36.24 | 37.68 | 39.10 | 38.50 | 36.33 | 35.19 | **CSE** ($f_s = 500\ Hz$) |
| | | WEDD | 28.98 | 29.97 | 29.04 | 28.68 | 30.13 | 28.98 | 29.98 | 33.11 | 33.80 | 35.65 | 34.01 | 31.25 | 31.13 | |
| MCS [44] | 70 | PRD | 20.26 | 19.51 | 21.97 | 17.91 | 23.84 | 23.75 | 14.66 | 13.97 | 17.73 | 18.91 | 19.35 | 15.88 | 18.97 | |
| **Proposed** | 70 | PRD | 16.56 | 16.76 | 16.52 | 15.28 | 18.84 | 16.76 | 13.24 | 15.36 | 17.19 | 19.20 | 19.00 | 16.27 | **16.74** | |
| | | WEDD | 12.92 | 13.60 | 13.50 | 11.87 | 15.02 | 13.67 | 11.57 | 13.47 | 15.05 | 17.15 | 16.22 | 13.54 | **13.96** | |
| WLM [46] | 192 | PRD1 | - | - | - | - | - | - | - | - | - | - | - | - | 3.64 | |
| **Proposed** | 192 | PRD1 | - | - | - | - | - | - | - | - | - | - | - | - | **1.13** | |
| MMB-IHT [45] | 125 | PRD1 | - | - | - | - | - | - | - | - | - | - | - | - | 3.74 | **MIT-BIH** ($f_s = 360\ Hz$) |
| | | QS | - | - | - | - | - | - | - | - | - | - | - | - | 1.71 | |
| **Proposed** | 125 | PRD1 | - | - | - | - | - | - | - | - | - | - | - | - | **1.31** | |
| | | QS | - | - | - | - | - | - | - | - | - | - | - | - | **4.88** | |

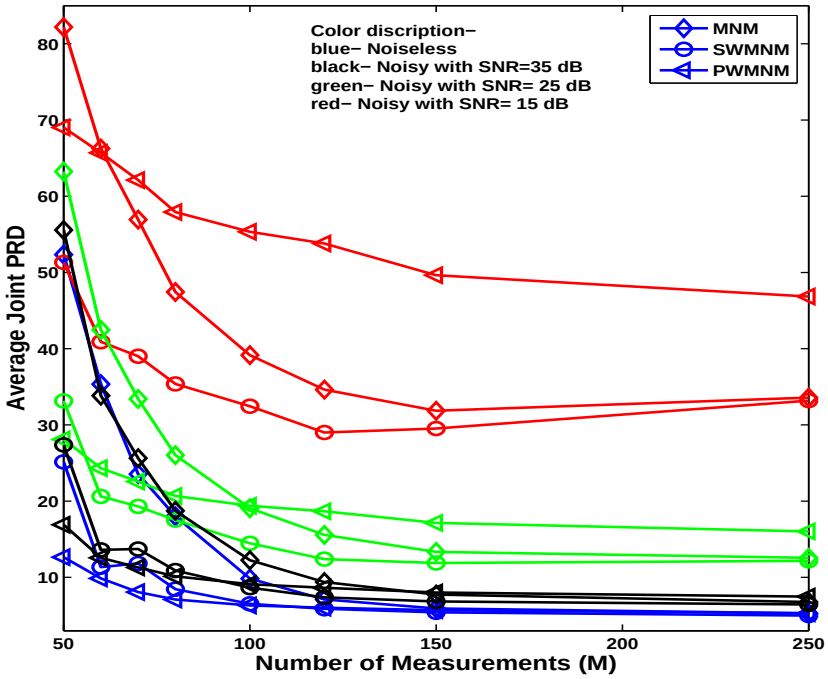


**Figure 5.7:** Recovery performances of the proposed methods (SWMNM, PWMNM) at different measurement noise levels

### 5.5.3 Recovery performance in noisy scenarios

In this section, we studied the performance of the proposed techniques in the presence of measurement noise. We contaminated the measurement vectors in $\boldsymbol{Y}$ by adding Gaussian noise of different powers and analyzed the recovery performance. Average joint $PRD$ obtained in the case of standard MNM, SWMNM and PWMNM is plotted in Figure 5.7 at different number of measurements ($M$) for four cases, i.e., noiseless, noisy with $SNR = 35\ dB$, noisy with $SNR = 25\ dB$ and noisy with $SNR = 15\ dB$. The study reveals that in noiseless scenarios, the PWMNM technique performs better than the standard MNM and SWMNM at low value of $M$ (<100). At higher values of $M$, all three methods perform equally well. However, as the level of noise increases, SWMNM outperforms both the other techniques. This can be observed by looking at the trend of the joint $PRD$ in different color graphs in Figure 5.7 (different color depicts different noise levels). This may be due to subband-based adaptive weighting strategy, which gives better noise handling capabilities to SWMNM compared to non-adaptive PWMNM technique. Therefore, SWMNM is preferable over PWMNM in noisy scenarios.

### 5.5.4 Application Considerations

ECG telemonitoring is a resource-constrained application which requires a low complexity encoder with the least energy consumption. The use of binary sensing matrices results in least computation requirements, low data storage, and easy hardware implementation [1,46]. We have taken only $d = 12$ number of $1s$ in each column of $bm\Phi$ that saves 65.7% energy in the encoding process compared to MNM-based work [34], which uses $d = 35$. From the perspective of energy consumption in wireless data transmission, the experimental results shown in Figure 5.6 indicate that the proposed method can achieve *good* quality reconstruction even when data is compressed up to 90%. The net $CR$ gain is 5.6% (from 85.6% to 91.2%) in PWMNM and 4% (from 85.6% to 89.6%) in SWMNM as pointed out in Figure 5.6 for a *good* quality reconstruction (denoted by $G$). The higher data compression ability of the proposed method results in lowering the power consumption in CS-based WBAN systems. A rough estimate of the transmission power in CS-based systems can be calculated using a method suggested in [58] using the following formula:

$$P_{trans} = L * CR^{'} * J * f_s * R \tag{5.8}$$

where $L$ is the total number of channels, $J$ is the transmission power per bit, $f_s$ is the sampling frequency (samples per second) of the ADC and $R$ is the number of bits per sample (resolution) and $CR^{'} = (1 - CR/100)$. Transmission power is calculated using the above formula with $L = 8$ (fundamental channels), $J = 5\ nJ$ per bit for the DSP chip of TI MSP430 family, $f_s = 500$ samples per second and $R = 12$ bits per sample for a particular ADC. It is found that PWMNM (21.12 $\mu W$) and SWMNM (24.96 $\mu W$) lead to 38.89% and 27.77% power savings, respectively compared to their non-weighted counterpart MNM (34.56 $\mu W$). Also, other works such as SOMP (24.96 $\mu W$) [97], BP (34.56 $\mu W$) [44] and IR-$\ell_1/\ell_2$ (28.56 $\mu W$) have low $CR$ values and hence require more power in order to meet the same reconstruction quality. It must be noted that the authors in [58] have used the power calculation formula (5.8) for theoretical power calculation only. The value of $J$ is taken from some other study for a particular processor family. Its value may change for other processors. We have also used (5.8) just to demonstrate approximate power saving using the proposed technique.

The decoding complexity and memory requirements of subband weighting-based WMNM techniques (i.e., SWMNM and PWMNM) remains same as that of coefficient weighting-based WMNM

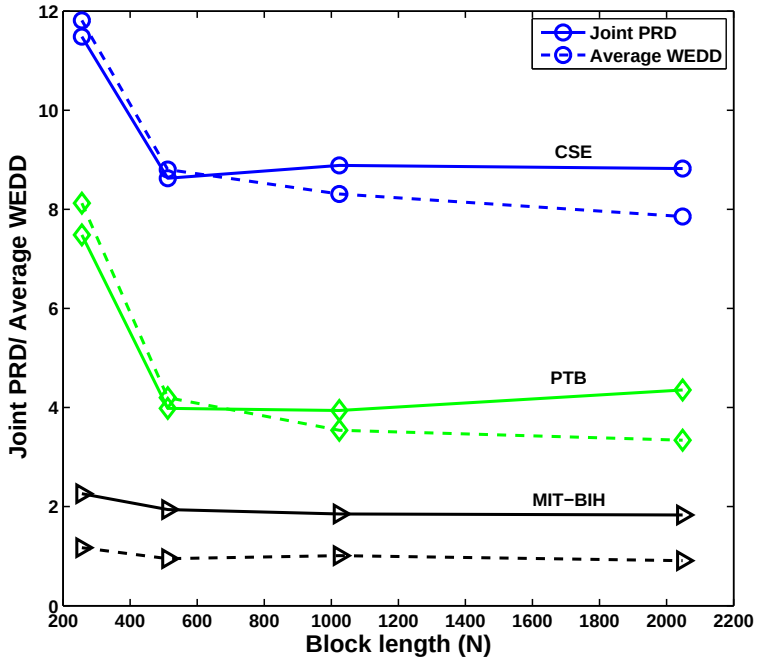


**Figure 5.8:** Recovery performances of the proposed method when different block length ($N$) of the signal is used

(i.e., AWMNM and BWMNM) presented in previous chapter.

Computational requirements also depend on the size of the data packet being processed at a time. Aforementioned analysis is for a data packet of size $[512 \times 8]$. However, if we vary the window, or block length of the signal, the corresponding encoding and decoding time will change along with the changes in the recovery performance. Figure 5.8 shows the performance study of the proposed method with varying window lengths for three databases. Four different window lengths, i.e., $N = 256, 512, 1024, 2048$ are considered in this study. The reconstruction errors in terms of joint $PRD$ and $WEDD$ averaged over ten data-sets from each database are plotted against $N$. It can be noted that error drops significantly when $N$ is increased from 256 to 512 and varies slowly for further increase in $N$. This trend is followed in all the three databases. Higher window length would increase the computational burden and can lead to delay in signal encoding/decoding, which is undesirable in practical applications. Therefore, there should be a trade-off between speed and reconstruction accuracy for the selection of $N$. As there is not much change in the performance after $N = 512$ (Figure 5.8), we chose this window length for all three databases. The same window length (i.e.,

$N = 512$) is also taken in earlier studies [34, 46] with the PTB and MIT-BIH databases for similar remote healthcare applications.

## 5.6 Exploiting Block-sparse Structure of MECG Signals

So far we have exploited the inter-channel correlation in both of the two joint CS recovery algorithms proposed in Chapter 4 and present chapter. The resulting row-sparse structure due to spatial correlation among channels was utilized in the WMNM algorithms (AWMNM/BWMNM in Chapter 4 and SWMNM/PWMNM in this chapter) for simultaneous reconstruction of all the ECG channels. However, one important aspect that was not considered in these works is that MECG signals also have intra-channel or temporal correlation within the channel itself. This spatio-temporal correlated structure of MECG signals is shown in Figure 2.5 in Chapter 1. Exploitation of both types of correlations during joint CS recovery is expected to deliver better performance. The existing CS-based works [1, 34, 45, 46] also consider either of the correlations but not both, which results in a suboptimal performance. Therefore, as an exploratory work, in this section we attempt to exploit both correlations simultaneously, assuming a block-sparse structure of MECG signals in wavelet domain. The block-sparse assumption in joint CS recovery is expected to capture the spatio-temporal correlated structure of MECG signals more efficiently compared to simple row-sparse structure and consequently, improves the reconstruction performance further.

### 5.6.1 Block-sparse-based joint MECG recovery

To exploit the block-sparse structure of MECG signals, we employed a spatio-temporal sparse Bayesian learning (STSBL)-based algorithm [39] for joint CS reconstruction. It is proposed recently for joint sparse recovery in a multi-channel scenario, when signals share spatio-temporal information. The STSBL model assumes that signals in ensemble posses inter-signal as well as intra-signal correlations. It processes signals ensemble in the form of groups/blocks containing spatially and temporally correlated signal samples. For MECG signals in $\boldsymbol{X}$, following block structure is assumed in wavelet

domain:

$$\boldsymbol{A} = \begin{bmatrix} \boldsymbol{A}_{[1]} \\ \boldsymbol{A}_{[2]} \\ . \\ . \\ . \\ \boldsymbol{A}_{[g]} \end{bmatrix}$$

where $\boldsymbol{A}_{[i]} \in \mathbb{R}^{d_i \times L}$ is the $i$-th block of $\boldsymbol{A}$ containing $d_i$ samples from each $L$ ECG channel and $\sum_{i=1}^{g} d_i = N$. So, each block $\boldsymbol{A}_{[i]}$ now contains correlated MECG signal samples from across the channels (in rows) and from within the channels (in columns). Each block is either a non-zero block or almost a zero block. An example of such block structure in real MECG signals can be seen in Figure 2.3 discussed in Chapter 2.

The STSBL model assumes each block $\boldsymbol{A}_{[i]}$ having parameterized Gaussian distribution:

$$p(vec(\boldsymbol{A}_{[i]}^T); \gamma_i, B, C_i) = \mathcal{N}(0, (\gamma_i C_i) \otimes B), \quad i = 1, 2, ..., g \tag{5.9}$$

where $\boldsymbol{B} \in \mathbb{R}^{\mathbb{L} \times \mathbb{L}}$ and $\boldsymbol{C} \in \mathbb{R}^{d_i \times d_i}$ are the unknown positive definite matrices capturing the inter-channel (spatial) and intra-channel (temporal) correlations in $\boldsymbol{A}_{[i]}$, respectively, and $\otimes$ is the Kronecker product. The $\gamma$ is a hyperparameter controlling the block sparsity of $\boldsymbol{A}$ i.e., a block is zero or not. The $vec(A_{[i]}^T)$ is a column vector formed by the vectorization of 2-D block $A_{[i]}$ (by stacking its columns in a vector). Assuming blocks $A_{[i]}, i = 1, 2, ..., g$ to be mutually independent, the distribution of matrix $A$ is given by $p(vect(A^T); B, \{\gamma_i, A_i\}_i) = \mathcal{N}(0, \prod \otimes B)$, where $\prod$ is block diagonal matrix with $i$-th element $\gamma_i \boldsymbol{C}_i (\forall_i)$. Similarly, noise matrix $\boldsymbol{V}$ is assumed to have similar distribution with mutually independent rows: $p(vect(V^T), \lambda, B) = \mathcal{N}(0, \lambda I \otimes B)$, where $\lambda$ is a scalar. Using these priors, maximum a posterior (MAP) estimation of wavelet coefficient matrix $\boldsymbol{A}$ is estimated as the mean of the posterior. An expectation maximization based approach is adopted to estimate the parameters $\gamma$, $\boldsymbol{C}$, $\boldsymbol{B}$ and $\lambda$. More details about the parameter estimation and learning can be found in [39].

### 5.6.2 Comparative performance analysis

The performance comparison of the spatio-temporal correlation-based STSBL recovery approach is done with two types of CS-based works reported in the literature: one that targets temporal correla-

**Table 5.4:** Performance comparison table

| Techniques | Distortion metrics | | CR/M | Correlation type |
|---|---|---|---|---|
| **STSBL** | PRD | **2.15** | 6.58 | **Spatio-temporal** |
| | QS | **3.09** | | |
| | WEDD | **1.13** | | |
| MMB-IHT [45] | PRD | 3.74 | 6.4 | **Temporal** |
| | QS | 1.71 | | |
| **STSBL** | PRD | **1.67** | 192 | **Spatio-temporal** |
| WLM [46] | PRD | 3.64 | 192 | **Temporal** |
| **STSBL** | PRD | **4.68** | 73.3% | **Spatio-temporal** |
| | WEDD | **3.61** | | |
| JCS [34] | PRD | 9.00 | 72.7% | **Spatial** |
| AWMNM | PRD | 5.5 | 73.4% | |
| BWMNM | PRD | 6.9 | 73.4% | |
| PWMNM | PRD | 3.3 | 73.9% | |
| SWMNM | PRD | 2.9 | 73.9% | |

tions and deals with single channel ECG signals only [45,46], and second type includes those algorithms, which exploit spatial correlations and deal multiple ECG channels simultaneously [34]. Results are also compared with our row-sparsity-based joint CS recovery algorithms proposed in previous chapter (AWMNM and BWMNM) and this chapter (PWMNM and SWMNM), which too exploit spatial correlation. The comparison results in terms of reconstruction distortion at almost same $CR$ values or $M$ values (as reported in the respective works) are given in Table 5.4. In [45,46], weighted $l_1$ (WLM) and iterative hard thresholding (MMB-IHT) algorithms were used to individually compress and reconstruct each ECG channel of MIT-BIH database. However, the spatially correlated information that exists between different channels was ignored in above works. The STSBL approach processes multiple channels simultaneously and recovers ECG signals jointly exploiting their block-sparse structure. Therefore, it exploits spatial correlation in addition to temporal correlation during joint CS recovery, which results in lower $PRD$ and higher $QS$ values at reported $CR = 6.4$ and $M = 192$. Joint CS (JCS) [34], AWMNM, BWMNM, PWMNM, and SWMNM are all row-sparsity-based works, which exploit spatial correlation from different ECG channels to recover them jointly. However, these approaches ignore the rich temporally correlated structure that is present within channel itself. The STSBL approach exploits this correlation and models it with spatial correlation by assuming a block-sparse structure in wavelet domain. Exploitation of both type of correlations might help STSBL to perform better

than the JCS, AWMNM, and BWMNM techniques in form of reduced $PRD$ levels at almost same $CR$ values. However, it is noticeable that $PRD$ value for STSBL is relatively high than subband weighting-based PWMNM and SWMNM algorithms. Though PWMNM and SWMNM are also based on spatial correlation only, they exploit diagnostically important multi-scale information additionally, through the subband-based weighting approaches. On the other hand, STSBL only leverages block-sparsity and do not utilize any other additional prior information. In this way, PWMNM/SWMNM becomes more signal-adaptive than STSBL, which might help them to emphasize clinically relevant ECG features more precisely compared to STSBL during joint CS recovery. This might be the reason subband weighting-based CS recovery outperforms STSBL. Though AWMNM/BWMNM also uses a weighting approach, their weighting schemes are not as effective as subband-based PWMNM/SWMNM, as explained in subsection 5.2.1. Because of this reason, PWMNM/SWMNM delivers better recovery performance with low $PRD$ value compared to AWMNM/BWMNM as shown in Table 5.4. It is also worth noting that, STSBL performs well than coefficient-level weighting-based AWMNM/BWMNM and is little inferior than subband weighting-based PWMNM/SWMNM. This opens scope for further improvement in block-sparsity-based joint CS recovery of MECG signals. If we could incorporate some additional diagnostically relevant information in STSBL also, through some weighting strategy, recovery performance of STSBL could be improved further.

## 5.7 Summary

In this chapter, new subband weighting-based joint sparse recovery algorithms are introduced for joint CS of MECG signals in telemonitoring applications. The proposed recovery algorithms exploit multi-scale signal information through a subband weighting strategy. This weighting approach incorporates additional information about diagnostically relevant wavelet subbands in the optimization problem formulation and emphasizes them in the final reconstruction. The proposed methods are found capable of reducing the number of CS measurements required for accurate recovery, or equivalently, they improved the joint reconstruction results at a given number of measurements. The experimental results are evaluated on a variety of databases encompassing a wide range of noisy and pathological ECG signals. Superior reconstruction quality is achieved compared to the existing CS-based works. The results are also verified by a diagnostic distortion measure and post-reconstruction classification task.

The reduction in the number of measurements directly translates into lower on-chip computations and reduced volume of data to be transmitted over the wireless links. This results in lowering the energy consumption in resource-constrained long term MECG telemonitoring applications. Additionally, a block-sparsity-based joint CS recovery is also explored in this chapter to exploit spatio-temporal correlated MECG structure.

भारतीय प्रौद्योगिकी संस्थान गुवाहाटी
Indian Institute of Technology Guwahati

# 6

# Conclusions

Contents

Present dissertation investigates the compressed sensing (CS) framework for multichannel electrocardiogram (MECG) signals. In the proposed framework, we have explored the simple and energy-efficient data reduction procedure of CS for resource-constrained MECG telemonitoring applications. We have proposed few approaches for efficient data encoding and joint recovery of all ECG channels using minimum number of CS measurements.

**Chapter 1** discusses the short introduction and the clinical relevance of single channel and multi-channel ECG signals. Their use in telemonitoring systems for healthcare applications is also discussed. The role of wireless body area network (WBAN)-enabled telemonitoring systems to cater next generation healthcare demands is discussed along with challenges faced in this area. **Chapter 2** presents the basics on CS and a detailed review of existing literature on the applications of CS for energy-efficient ECG data compression in WBAN-enabled telemonitoring. Few existing methods have been evaluated and their limitations are discussed. Few salient points that are noted from these two chapters are: 1) MECG signals are having spatio-temporal correlated structure, 2) CS framework is a single step data reduction process and hence involves least computations and low power consumption, 3) State-of-the-art CS-based ECG data compression methods exploit temporal ECG structure but ignore spatial or inter-channel correlated structure.

In **Chapter 3**, a joint PCA-CS approach is investigated for MECG signals. PCA over MECG signals facilitates the application of CS framework in eigenspace. PCA is used to decorrelate the mutually-correlated 12-channel ECG signals and capture their clinical features in reduced-dimension sparse eigenspace signals. The retained eigenspace MECG signals are further compressed using CS to get their compressed measurements. The compressed measurements are quantized using a uniform quantizer and encoded by a lossless Huffman encoder to get the compressed bit-streams. Using orthogonal matching pursuit (OMP) and inverse PCA, original MECG data is successfully recovered while preserving the important clinical features. Performance evaluations are carried out on different databases with a variety of ECG morphologies including pathological, noisy and normal MECG datasets. Denoising ability of the algorithm is also analyzed, and it is found that the proposed method can significantly reduce the noise levels from the ECG signals during the compressed signal reconstruction. This chapter also investigates some practical issues in implementing the joint PCA-CS for MECG signals. This includes study of required feature length for learning optimal PCA transformation matrix

and the corresponding reconstruction error variation. A study regarding how frequently the eigenspace transformation matrix needs to be updated in signal specific applications is also presented. In addition to the eigenspace CS recovery, we also investigated the CS recovery of eigenspace MECG signals in other sparsifying domains, such as DWT, DCT, and DFT. It is found that DWT can sparsify eigenspace MECG signals and can improve the CS recovery performance further. The proposed joint PCA-CS approach is found to be helpful in exploiting all possible correlations present in MECG signals. This helps it to achieve higher compression efficiency compared to the state-of-the-art CS-based ECG compression methods, which are mainly based on temporal correlations. The average value of *PRD* across the PTB database is found to be 5.24% at a compression ratio of 17.76 in Lead V3. The visual quality of the reconstructed MECG signals is validated through mean opinion score (MOS) and it is found to be 6.66%, which implies a very good signal reconstruction quality. Despite having high compression efficiency, the proposed joint PCS-CS approach is found to be computationally intensive compared to pure CS-based methods.

In **Chapter 4**, a low-complex joint CS approach is explored, which can simultaneously compress/reconstruct all the ECG channels. A WMNM-based joint sparse recovery algorithm is introduced, which exploits inter-channel correlation at the decoder and enables simultaneous reconstruction of all the channels. A simple matrix multiplication of the MECG data matrix with a random sparse binary sensing matrix having binary entries (with very fews ones), is done to directly compress the data from all ECG channels and WMNM is employed to jointly retrieve them back exploiting their wavelet domain joint sparsity. Thus, joint CS approach minimizes the computational resources required in data encoding and transfers most of the load to the resourceful decoder. The proposed WMNM recovery technique is based on a coefficient-level weighting strategy, which emphasizes the high amplitude wavelet coefficients and deemphasizes insignificant low amplitude coefficients simultaneously during joint CS recovery. Thus, it helps in inducing row-sparsity at diagnostically favorable locations. The high amplitude wavelet coefficients directly correspond to the clinically important ECG features. So, their preservation helps maintain the diagnostic quality of reconstructed MECG signals at higher compression ratios. Joint recovery through the proposed method reduces the number of CS measurements needed for an accurate recovery, or equivalently, improves the joint reconstruction at a given number of measurements. Performance evaluations on various databases show that the proposed

method can jointly recover MECG signals with a wide range of morphologies. Moreover, it is also observed that in the presence of the inter-channel correlated information, joint CS-based approach is more advantageous than the traditional CS-based approaches in terms of improved reconstruction quality at a lower number of measurements. The reduction in the number of measurements directly translates into the reduced volume of data to be transmitted. Substantial improvement in the signal recovery performance (up to 77% drop in $PRD$ value) and measurements requirements (41.18% saving) is obtained for the proposed method compared to non-weighted CS approaches. Higher data compression efficiency and low complexity of the proposed method makes it suitable for energy-efficient continuous wireless telemonitoring of MECG signals. It can also be concluded that weighting-based CS recovery approach gives flexibility to incorporate additional constraints into the recovery problem formulation. This helps make the traditional sparse recovery algorithms more signal-adaptive, which may result in better CS recovery performance at low measurements.

In **Chapter 5**, multi-scale wavelet structure of MECG signals is studied and exploited in the joint CS recovery problem through clinically more relevant subband-based weighting schemes. The subband weighting approach helps emphasize the clinically important MECG features present in some particular subbands more precisely during WMNM-based joint CS recovery. Motivated from the gross segmentation of clinical ECG features in various wavelet subbands, new subband-based weighting schemes are investigated in this chapter. The subband-level weighting-based WMNM exploits multi-scale signal information through the proposed weighting strategy. Clinically relevant information is captured in the form of subband energy, entropy, and amplitude decay, and based on this, weighting rules are defined at each wavelet scale. Through these weighting rules, additional information about diagnostically relevant wavelet subbands is incorporated in the optimization problem formulation. Such a weighting approach emphasizes ECG features present in wavelet subbands having high diagnostic importance. Coefficients in clinically less relevant high frequency subbands are deemphasized simultaneously, resulting in a sparser (and hence, more accurate) solution. The proposed approach is found capable of significantly reducing the number of CS measurements required for accurate recovery, or equivalently, improves the joint reconstruction results at a given number of measurements. The experimental results evaluated on a variety of databases show that the proposed method performs equally well for a wide range of ECG morphologies including noisy and pathological signals. Superior recon-

struction quality is achieved compared to the existing CS-based works. Out of all the subband-based weighting schemes explored in this work, it is found that the exponential type weighting criterion captures the amplitude decay characteristic of detail wavelet subband coefficients more closely followed by multi-scale entropy-based weighting. This is the reason, recovery performance of PWMNM is found to be better than SWMNM. Accuracy of reconstruction is validated through a post-reconstruction classification task, which gives classification accuracy of 73.2% even when MECG signals are jointly reconstructed using only about 10% of the compressed measurements. The reduction in the number of measurements directly translates into lower on-chip computations and reduced volume of data to be transmitted over the power-hungry wireless links. This may result in lowering further the energy consumption in resource-constrained long-term MECG telemonitoring applications. Additionally, a block-sparsity-based joint CS recovery is also explored in this chapter, which suggests a new approach to exploit the spatio-temporal correlated MECG structure during simultaneous recovery .

Major contributions of the work reported in this thesis include:

(i) Exploitation of spatio-temporal redundancies in MECG signals using a joint PCA-CS approach.

(ii) MECG data compression using eigenspace CS approach.

(iii) Exploitation of wavelet domain joint sparsity of MECG signals for joint CS recovery using a weighted mixed-norm minimization-based recovery approach.

(iv) Use of a coefficient-level weighting strategy to emphasize high amplitude wavelet coefficients during joint CS recovery.

(v) Study of multi-scale wavelet structure and its exploitation in the joint CS recovery problem through different subband-based weighting schemes.

## 6.1 Scope for the Future Work

- With a proper selection of sparsifying basis, the proposed joint PCA-CS approach can be employed for other signals, which share spatio-temporal information.

- Proposed WMNM-based joint sparse recovery algorithms can be generalized for any joint-sparse

multi-channel signals (e.g., multi-channel EEG) by following a signal-adaptive weighting criterion.

- Compressed measurements/random projections of the ECG signal can be explored for compressed domain classification task as they have discriminative features. Random projections preserve the underlying structure of the original signal even in low dimensional measurement space.

- Block-sparsity based joint CS recovery approaches can be further explored using new diagnostically relevant weighting schemes to effectively exploit the spatio-temporal correlated structure of MECG channels.

- Sparse representation of ECG signals can be investigated over signal-adaptive dictionaries for more effective sparse approximation.

# Bibliography


[1] H. Mamaghanian, N. Khaled, D. Atienza, and P. Vandergheynst, "Compressed sensing for real-time energy-efficient ECG compression on wireless body sensor nodes," *IEEE Transactions on Biomedical Engineering*, vol. 58, no. 9, pp. 2456–2466, 2011.

[2] *www.physionet.org*.

[3] A. Goldberger, L. Amaral, L. Glass, J. Hausdorff, P. Ivanov, R. Mark, J. Mietus, G. Moody, C.-K. Peng, and H. Stanley, "Physiobank, physiotoolkit, and physionet: Components of a new research resource for complex physiologic signals," *Circulation*, vol. 101 (23), pp. e215–e220, 2000.

[4] J. L. Willems, "CSE multilead atlas, measurement results - data set 3," in *Common standards for quantitative electrocardiography, commission of the European communities, medical and public health research, Ref. Nr. CSE 88-04-15, Leuven*, 15th. April 1988.

[5] B. Surawich and T. Knilans, *Chou's electrocardiography in clinical practice*, 6th ed. Elsevier, 2008.

[6] A. Milenkovi, C. Otto, and E. Jovanov, "Wireless sensor networks for personal health monitoring: Issues and an implementation," *Computer Communications*, vol. 29, no. 13-14, pp. 2521 – 2533, 2006, wirelsess Senson Networks and Wired/Wireless Internet Communications.

[7] E. Jovanov, A. Milenkovic, C. Otto, and P. C. de Groen, "A wireless body area network of intelligent motion sensors for computer assisted physical rehabilitation," *Journal of NeuroEngineering and Rehabilitation*, vol. 2, no. 1, pp. 1–10, 2005.

[8] C. C. Y. Poon, B. P. L. Lo, M. R. Yuce, A. Alomainy, and Y. Hao, "Body sensor networks: In the era of big data and beyond," *IEEE Reviews in Biomedical Engineering*, vol. 8, pp. 4–16, 2015.

[9] B. Malik and V. R. Singh, "A survey of research in WBAN for biomedical and scientific applications," *Health and Technology*, vol. 3, no. 3, pp. 227–235, 2013.

[10] R. S. H. Istepanian, E. Jovanov, and Y. T. Zhang, "Guest editorial introduction to the special section on M-health: Beyond seamless mobility and global wireless health-care connectivity," *IEEE Transactions on Information Technology in Biomedicine*, vol. 8, no. 4, pp. 405–414, Dec 2004.

[11] Y. L. Zheng, X. R. Ding, C. C. Y. Poon, B. P. L. Lo, H. Zhang, X. L. Zhou, G. Z. Yang, N. Zhao, and Y. T. Zhang, "Unobtrusive sensing and wearable devices for health informatics," *IEEE Transactions on Biomedical Engineering*, vol. 61, no. 5, pp. 1538–1554, May 2014.

[12] Y. L. Zheng, B. P. Yan, Y. T. Zhang, and C. C. Y. Poon, "An armband wearable device for overnight and cuff-less blood pressure measurement," *IEEE Transactions on Biomedical Engineering*, vol. 61, no. 7, pp. 2179–2186, July 2014.

[13] S. Patel, K. Lorincz, R. Hughes, N. Huggins, J. Growdon, D. Standaert, M. Akay, J. Dy, M. Welsh, and P. Bonato, "Monitoring motor fluctuations in patients with parkinson's disease using wearable sensors," *IEEE Transactions on Information Technology in Biomedicine*, vol. 13, no. 6, pp. 864–873, Nov 2009.

[14] J. A. Ward, P. Lukowicz, G. Troster, and T. E. Starner, "Activity recognition of assembly tasks using body-worn microphones and accelerometers," *IEEE Transactions on Pattern Analysis and Machine Intelligence*, vol. 28, no. 10, pp. 1553–1567, Oct 2006.

[15] B. Perriot, J. Argod, J. L. Pepin, and N. Noury, "Characterization of physical activity in COPD patients: Validation of a robust algorithm for actigraphic measurements in living situations," *IEEE Journal of Biomedical and Health Informatics*, vol. 18, no. 4, pp. 1225–1231, July 2014.

[16] *Seiko Pulse Graph Wrist Watch, Available at: http://www.seikopgt.or.jp// (Japanese), Accessed: July 2016.*

[17] *Polar, Available at: http://www.polarusa.com//, Accessed: July 2016..*

[18] Z. Zhang, T.-P. Jung, S. Makeig, and B. Rao, "Compressed sensing of EEG for wireless telemonitoring with low energy consumption and inexpensive hardware," *IEEE Transactions on Biomedical Engineering*, vol. 60, no. 1, pp. 221–224, Jan 2013.

[19] S. J. M. Bamberg, A. Y. Benbasat, D. M. Scarborough, D. E. Krebs, and J. A. Paradiso, "Gait analysis using a shoe-integrated wireless sensor system," *IEEE Transactions on Information Technology in Biomedicine*, vol. 12, no. 4, pp. 413–423, July 2008.

[20] D. Jarchi, C. Wong, R. M. Kwasnicki, B. Heller, G. A. Tew, and G. Z. Yang, "Gait parameter estimation from a miniaturized ear-worn sensor using singular spectrum analysis and longest common subsequence," *IEEE Transactions on Biomedical Engineering*, vol. 61, no. 4, pp. 1261–1273, April 2014.

[21] H. Ghasemzadeh, R. Jafari, and B. Prabhakaran, "A body sensor network with electromyogram and inertial sensors: Multimodal interpretation of muscular activities," *IEEE Transactions on Information Technology in Biomedicine*, vol. 14, no. 2, pp. 198–206, March 2010.

[22] C. F. Lai, M. Chen, J. S. Pan, C. H. Youn, and H. C. Chao, "A collaborative computing framework of cloud network and WBSN applied to fall detection and 3-d motion reconstruction," *IEEE Journal of Biomedical and Health Informatics*, vol. 18, no. 2, pp. 457–466, March 2014.

[23] Z. Zhang, H. Wang, A. V. Vasilakos, and H. Fang, "Ecg-cryptography and authentication in body area networks," *IEEE Transactions on Information Technology in Biomedicine*, vol. 16, no. 6, pp. 1070–1078, Nov 2012.

[24] *Shimmer Research. (2008). [Online]. Available: http://shimmer-research.com.*

[25] *Toumaz Technology. (2009). [Online]. Available: http://www.toumaz.com/public/news.php?id=92.*

[26] R. F. Yazicioglu, T. Torfs, J. Penders, I. Romero, H. Kim, P. Merken, B. Gyselinckx, H. J. Yoo, and C. V. Hoof, "Ultra-low-power wearable biopotential sensor nodes," in *2009 Annual International Conference of the IEEE Engineering in Medicine and Biology Society*, Sept 2009, pp. 3205–3208.

[27] . Alesanco and J. Garca, "Clinical assessment of wireless ECG transmission in real-time cardiac telemonitoring," *IEEE Transactions on Information Technology in Biomedicine*, vol. 14, no. 5, pp. 1144–1152, Sept 2010.

[28] R. H. Matsunaga, E. Almeida, D. Pereira, A. Valente, and . dos Santos, "A multipoint videoconference-based telemedicine system for electrocardiogram monitoring," in *2010 Annual International Conference of the IEEE Engineering in Medicine and Biology*, Aug 2010, pp. 2180–2183.

[29] R. Agarwal and S. Sonkusale, "Input-feature correlated asynchronous analog to information converter for ecg monitoring," *IEEE Transactions on Biomedical Circuits and Systems*, vol. 5, no. 5, pp. 459–467, Oct 2011.

[30] C. J. Deepu and Y. Lian, "A joint QRS detection and data compression scheme for wearable sensors," *IEEE Transactions on Biomedical Engineering*, vol. 62, no. 1, pp. 165–175, Jan 2015.

[31] S. D. Joshi, "A low cost multichannel central ECG monitoring system," in *Engineering in Medicine and Biology Society, 1995 and 14th Conference of the Biomedical Engineering Society of India. An International Meeting, Proceedings of the First IEEE Regional Conference*, Feb 1995, pp. SPC11–SPC12.

[32] J. S. Besnoff, T. Deyle, R. R. Harrison, and M. S. Reynolds, "Battery-free multichannel digital ECG biotelemetry using UHF RFID techniques," in *IEEE International Conference on RFID*, April 2013, pp. 16–22.

[33] D.-S. Kim and J.-S. Kwon, "A lossless multichannel bio-signal compression based on low-complexity joint coding scheme for portable medical devices," *Sensors (Basel, Switzerland)*, vol. 14, no. 9, pp. 17 516–17 529, 2014.

[34] H. Mamaghanian, G. Ansaloni, D. Atienza, and P. Vandergheynst, "Power-efficient joint compressed sensing of multi-lead ECG signals," in *IEEE International Conference on Acoustics, Speech and Signal Processing (ICASSP)*, May 2014, pp. 4409–4412.

[35] L. H. Wang, T. Y. Chen, K. H. Lin, Q. Fang, and S. Y. Lee, "Implementation of a wireless ECG acquisition soc for IEEE 802.15.4 (zigbee) applications," *IEEE Journal of Biomedical and Health Informatics*, vol. 19, no. 1, pp. 247–255, Jan 2015.

[36] A. Majumdar and R. K. Ward, "Non-convex row-sparse multiple measurement vector analysis prior formulation for EEG signal reconstruction," *Biomedical Signal Processing and Control*, vol. 13, pp. 142–147, 2014.

[37] A. Shukla and A. Majumdar, "Exploiting inter-channel correlation in EEG signal reconstruction," *Biomedical Signal Processing and Control*, vol. 18, pp. 49–55, 2015.

[38] Z. Zhang and B. D. Rao, "Exploiting correlation in sparse signal recovery problems: Multiple measurement vectors, block sparsity, and time-varying sparsity," ICML 2011 Workshop on Structured Sparsity, 2011.

[39] Z. Zhang, T.-P. Jung, S. Makeig, Z. Pi, and B. Rao, "Spatiotemporal sparse bayesian learning with applications to compressed sensing of multichannel physiological signals," *IEEE Transactions on Neural Systems and Rehabilitation Engineering*, vol. 22, no. 6, pp. 1186–1197, Nov 2014.

[40] E. Candes and M. Wakin, "An introduction to compressive sampling," *IEEE Signal Processing Magazine*, vol. 25, no. 2, pp. 21–30, 2008.

[41] A. Dixon, E. Allstot, D. Gangopadhyay, and D. Allstot, "Compressed sensing system considerations for ECG and EMG wireless biosensors," *IEEE Transactions on Biomedical Circuits and Systems*, vol. 6, no. 2, pp. 156–166, 2012.

[42] Z. Zhang, T.-P. Jung, S. Makeig, and B. Rao, "Compressed sensing for energy-efficient wireless telemonitoring of noninvasive fetal ECG via block sparse bayesian learning," *IEEE Transactions on Biomedical Engineering*, vol. 60, no. 2, pp. 300–309, Feb 2013.

[43] M. Balouchestani, K. Raahemifar, and S. Krishnan, "Low sampling rate algorithm for wireless ECG systems based on compressed sensing theory," *Signal, Image and Video Processing*, pp. 1–7, 2013.

[44] L. Sharma, "Coding ECG beats using multiscale compressed sensing based processing," *Computers & Electrical Engineering*, vol. 45, pp. 211–221, 2015.

[45] L. Polania, R. Carrillo, M. Blanco-Velasco, and K. Barner, "Exploiting prior knowledge in compressed sensing wireless ECG systems," *IEEE Journal of Biomedical and Health Informatics*, vol. 19, no. 2, pp. 508–519, March 2015.

[46] J. Zhang, Z. Gu, Z. L. Yu, and Y. Li, "Energy-efficient ECG compression on wireless biosensors via minimal coherence sensing and weighted $\ell_1$ minimization reconstruction," *IEEE Journal of Biomedical and Health Informatics*, vol. 19, no. 2, pp. 520–528, March 2015.

[47] F. Chen, A. Chandrakasan, and V. Stojanovic, "Design and analysis of a hardware-efficient compressed sensing architecture for data compression in wireless sensors," *IEEE Journal of Solid-State Circuits*, vol. 47, no. 3, pp. 744–756, March 2012.

[48] E. Candes, N. Braun, and M. Wakin, "Signal and image recovery from compressive samples," in *4th IEEE International Symposium on Biomedical Imaging: From Nano to Macro, 2007. ISBI 2007*, 2007, pp. 976–979.

[49] U. Gamper, P. Boesiger, and S. Kozerke, "Compressed sensing in dynamic MRI," *Magnetic Resonance in Medicine*, vol. 59, no. 2, pp. 365–373, 2008.

[50] W. Wang, B. Zhang, and J. Mu, "Compressive SAR raw data with principal component analysis," *EURASIP Journal on Wireless Communications and Networking*, vol. 2012, no. 1, pp. 1–7, 2012.

[51] S. A. Nandhini, R. Sankararajan, and K. Rajendiran, "Video compressed sensing framework for wireless multimedia sensor networks using a combination of multiple matrices," *Computers & Electrical Engineering*, vol. 44, pp. 51–66, 2015.

[52] R. Hemalatha, S. Radha, and S. Sudharsan, "Energy-efficient image transmission in wireless multimedia sensor networks using block-based compressive sensing," *Computers & Electrical Engineering*, vol. 44, pp. 67–79, 2015.

[53] S. Aviyente, "Compressed sensing framework for EEG compression," in *Proc. IEEE/SP 14th Workshop Stat. Signal Process*, 2007, pp. 181–184.

[54] M. H. Kamal, M. Shoaran, Y. Leblebici, A. Schmid, and P. Vandergheynst, "Compressive multichannel cortical signal recording," in *2013 IEEE International Conference on Acoustics, Speech and Signal Processing*. IEEE, 2013, pp. 4305–4309.

[55] A. M. Abdulghani, A. J. Casson, and E. Rodriguez-Villegas, "Compressive sensing scalp EEG signals: implementations and practical performance," *Medical & Biological Engineering & Computing*, vol. 50, no. 11, pp. 1137–1145, 2012.

[56] M. Balouchestani, K. Raahemifar, and S. Krishnan, "Compressed sensing in wireless sensor networks: Survey," *Canadian Journal on Multimedia and Wireless Networks*, vol. 2, no. 1, pp. 1–4, 2011.

[57] M. Mohsina and A. Majumdar, "Gabor based analysis prior formulation for EEG signal reconstruction," *Biomedical Signal Processing and Control*, vol. 8, no. 6, pp. 951 – 955, 2013.

[58] A. Shukla and A. Majumdar, "Row-sparse blind compressed sensing for reconstructing multi-channel EEG signals," *Biomedical Signal Processing and Control*, vol. 18, pp. 174–178, 2015.

[59] A. Majumdar and R. K. Ward, "Energy efficient EEG sensing and transmission for wireless body area networks: A blind compressed sensing approach," *Biomedical Signal Processing and Control*, vol. 20, pp. 1 – 9, 2015.

[60] Y. Liu, M. D. Vos, and S. V. Huffel, "Compressed sensing of multichannel EEG signals: The simultaneous cosparsity and low-rank optimization," *IEEE Transactions on Biomedical Engineering*, vol. 62, no. 8, pp. 2055–2061, Aug 2015.

[61] B. Liu, Z. Zhang, G. Xu, H. Fan, and Q. Fu, "Energy efficient telemonitoring of physiological signals via compressed sensing: A fast algorithm and power consumption evaluation," *Biomedical Signal Processing and Control*, vol. 11, no. 0, pp. 80–88, 2014.

[62] Z.-L. Zhang and Z. Yi, "Extraction of temporally correlated sources with its application to non-invasive fetal electrocardiogram extraction," *Neurocomputing*, vol. 69, no. 7-9, pp. 894–899, 2006.

[63] Z. Zhang, "Photoplethysmography-based heart rate monitoring in physical activities via joint sparse spectrum reconstruction," *IEEE Transactions on Biomedical Engineering*, vol. 62, no. 8, pp. 1902–1910, 2015.

[64] Z. Zhang, Z. Pi, and B. Liu, "Troika: A general framework for heart rate monitoring using wrist-type photoplethysmographic signals during intensive physical exercise," *IEEE Transactions on Biomedical Engineering*, vol. 62, no. 2, pp. 522–531, 2015.

[65] Y. Zhang, B. Liu, and Z. Zhang, "Combining ensemble empirical mode decomposition with spectrum subtraction technique for heart rate monitoring using wrist-type photoplethysmography," *Biomedical Signal Processing and Control*, vol. 21, pp. 119–125, 2015.

[66] B. Sun and Z. Zhang, "Photoplethysmography-based heart rate monitoring using asymmetric least squares spectrum subtraction and bayesian decision theory," *IEEE Sensors Journal*, vol. 15, no. 12, pp. 7161–7168, 2015.

[67] B. Liu and Z. Zhang, "Quantized compressive sensing for low-power data compression and wireless telemonitoring," *IEEE Sensors Journal*, 2016.

[68] J. Wan, Z. Zhang, B. D. Rao, S. Fang, J. Yan, A. Saykin, and L. Shen, "Identifying the neuroanatomical basis of cognitive impairment in alzheimer's disease by correlation- and nonlinearity-aware sparse bayesian learning," *IEEE Transactions on Medical Imaging*, vol. 33, no. 7, pp. 1475–1487, 2014.

[69] M. Balouchestani and S. Krishnan, "Effective low-power wearable wireless surface EMG sensor design based on analog-compressed sensing," *Sensor Journal, Special Issue on Wireless Sensor Network for Pervasive Medical Care*, vol. 14, no. 12, pp. 24 306–24 328, 2014.

[70] ——, "Long-term surface EMG monitoring using K-means clustering and compressive sensing," in *Proc. SPIE*, vol. 9484, 2015, pp. 94 840Q–94 840Q–10.

[71] ——, "Robust compressive sensing algorithm for wireless surface electromyography applications," *Biomedical Signal Processing and Control*, vol. 20, no. May, 2015, pp. Pages–100, 2015.

[72] ——, "Biomedical sensor design using analog compressed sensing," in *Proc. SPIE*, vol. 9484, 2015, pp. 94 840O–94 840O–12.

[73] M. Balouchestani, K. Raahemifar, and S. Krishnan, "New channel model for wireless body area network with compressed sensing theory," *IET Wireless Sensor Systems*, vol. 3, no. 2, pp. 85–92, 2013.

[74] M. Balouchestani and S. Krishnan, "Advanced k-means clustering algorithm for large ECG data sets based on a collaboration of compressed sensing theory and k-svd approach," *Signal, Image and Video Processing*, vol. 10, no. 1, pp. 113–120, 2016.

[75] G. M. Friesen, T. C. Jannett, M. A. Jadallah, S. L. Yates, S. R. Quint, and H. T. Nagle, "A comparision of the noise sensitivity of nine QRS detection algorithms," *IEEE Transaction on Biomedical Engineering*, vol. 37(1), pp. 85–98, Jan. 1990.

[76] B.-U. Kohler, C. Hennig, and R. Orglmeister, "The principles of software QRS detection," *IEEE Engineering in Medicine and Biology*, pp. 42–57, Jan.-Feb. 2002.

[77] J. Pan and W. J. Tompkins, "A real-time QRS detection algorithm," *IEEE Transaction on Biomedical Engineering*, vol. 32(3), p. 230236, 1985.

[78] P. S. Hamilton and W. J. Tompkins, "Quantitative investigation of QRS detection rules using the MIT/BIH arrhythmia database," *IEEE Transaction on Biomedical Engineering*, vol. 33(12), pp. 1157–1165, Dec. 1986.

[79] Y. Zigel, A. Cohen, and A. Katz, "The weighted diagnostic distortion (WDD) measure for ECG signal compression," *IEEE Transactions on Biomedical Engineering*, vol. 47, no. 11, pp. 1422–1430, Nov 2000.

[80] A. Al-Fahoum, "Quality assessment of ECG compression techniques using a wavelet-based diagnostic measure," *IEEE Transactions on Information Technology in Biomedicine*, vol. 10, no. 1, pp. 182–191, Jan 2006.

[81] M. S. Manikandan and S. Dandapat, "Wavelet energy based diagnostic distortion measure for ECG," *Biomedical Signal Processing and Control*, vol. 2, no. 2, pp. 80–96, 2007.

[82] S. Fauvel and R. K. Ward, "An energy efficient compressed sensing framework for the compression of electroencephalogram signals," *Sensors*, vol. 14, no. 1, pp. 1474–1496, 2014.

[83] R. Baraniuk, "Compressive sensing [lecture notes]," *IEEE Signal Processing Magazine*, vol. 24, no. 4, pp. 118–121, 2007.

[84] H. Mamaghanian, N. Khaled, D. Atienza, and P. Vandergheynst, "Design and exploration of low-power analog to information conversion based on compressed sensing," *IEEE Journal on Emerging and Selected Topics in Circuits and Systems*, vol. 2, no. 3, pp. 493–501, 2012.

[85] Z. Lu, D. Y. Kim, and W. Pearlman, "Wavelet compression of ECG signals by the set partitioning in hierarchical trees algorithm," *IEEE Transactions on Biomedical Engineering*, vol. 47, no. 7, pp. 849–856, July 2000.

[86] B. Rajoub, "An efficient coding algorithm for the compression of ECG signals using the wavelet transform," *IEEE Transactions on Biomedical Engineering*, vol. 49, no. 4, pp. 355–362, 2002.

[87] R. Kumar, A. Kumar, and G. Singh, "Electrocardiogram signal compression based on singular value decomposition (SVD) and adaptive scanning wavelet difference reduction (ASWDR) technique," *AEU - International Journal of Electronics and Communications*, pp. –, 2015.

[88] L. N. Sharma, S. Dandapat, and A. Mahanta, "Multichannel ECG data compression based on multiscale principal component analysis," *IEEE Journal of Information Technology in Biomedicine*, vol. 16, no. 4, pp. 730–736, 2012.

[89] L. J. Hadjileontiadis and S. M. Panas, "Separation of discontinuous adventitious sound from vesicular sounds using a wavelet based filter," *IEEE Transaction on Biomedical Engineering*, vol. 44, no. 12, Dec 1997.

[90] A. Cohen and J. Kovacevic, "Wavelets: the mathematical background," *Proceedings of the IEEE*, vol. 84, no. 4, pp. 514 –522, apr 1996.

[91] M. M. Shaker, "EEG waves classifier using wavelet transform and fourier transform," *International Journal of Biomedical and Medical Sciences*, vol. 1,2, pp. 85 – 90, 2006.

[92] A. Graps, "Intrduction to wavelets," *IEEE Computer Siciety ( Original paper published by IEEE Computer Siciety, 1995)*, vol. 2 (2), 2003.

[93] A. G. Ramakrishnan and S. Saha, "ECG coding by wavelet-based linear prediction," *IEEE Transaction on Biomedical Engineering*, vol. vol. 44, no. 12, Dec. 1997.

[94] S. S. Chen, D. L. Donoho, Michael, and A. Saunders, "Atomic decomposition by basis pursuit," *SIAM Journal on Scientific Computing*, vol. 20, pp. 33–61, 1998.

[95] J. Tropp and A. Gilbert, "Signal recovery from random measurements via orthogonal matching pursuit," *IEEE Transactions on Information Theory*, vol. 53, no. 12, pp. 4655–4666, 2007.

[96] D. Needell and J. Tropp, "CoSaMP: Iterative signal recovery from incomplete and inaccurate samples," *Applied and Computational Harmonic Analysis*, vol. 26, no. 3, pp. 301 – 321, 2009.

[97] L. Polania, R. Carrillo, M. Blanco-Velasco, and K. Barner, "Compressed sensing based method for ECG compression," in *IEEE International Conference on Acoustics, Speech and Signal Processing (ICASSP)*, 2011, pp. 761–764.

[98] H. Mamaghanian, N. Khaled, D. Atienza, and P. Vandergheynst, "Structured sparsity models for compressively sensed electrocardiogram signals: A comparative study," in *IEEE Biomedical Circuits and Systems Conference (BioCAS), 2011*, Nov 2011, pp. 125–128.

[99] L. F. Polania, R. E. Carrillo, M. Blanco-Velasco, and K. E. Barner, "On exploiting interbeat correlation in compressive sensing-based ECG compression," *Proc. SPIE*, vol. 8365, pp. 83 650D–83 650D–7, 2012.

[100] L. Polania and K. Barner, "A weighted $\ell_1$ minimization algorithm for compressed sensing ECG," in *IEEE International Conference on Acoustics, Speech and Signal Processing (ICASSP)*, May 2014, pp. 4413–4417.

[101] Z. Zhang and B. Rao, "Sparse signal recovery with temporally correlated source vectors using sparse bayesian learning," *IEEE Journal of Selected Topics in Signal Processing*, vol. 5, no. 5, pp. 912–926, Sept 2011.

[102] N. Vaswani and W. Lu, "Modified-cs: Modifying compressive sensing for problems with partially known support," in *IEEE International Symposium on Information Theory, 2009. ISIT 2009*, June 2009, pp. 488–492.

[103] R. E. Carrillo, L. F. Polania, and K. E. Barner, "Iterative algorithms for compressed sensing with partially known support," in *2010 IEEE International Conference on Acoustics, Speech and Signal Processing*. IEEE, 2010, pp. 3654–3657.

[104] L. F. Polania, R. E. Carrillo, M. Blanco-Velasco, and K. E. Barner, "Compressive sensing exploiting wavelet-domain dependencies for ECG compression," pp. 83 650E–83 650E–9, 2012.

[105] S. Cotter, B. Rao, K. Engan, and K. Kreutz-Delgado, "Sparse solutions to linear inverse problems with multiple measurement vectors," *IEEE Transactions on Signal Processing*, vol. 53, no. 7, pp. 2477–2488, July 2005.

[106] E. van den Berg and M. Friedlander, "Theoretical and empirical results for recovery from multiple measurements," *IEEE Transactions on Information Theory*, vol. 56, no. 5, pp. 2516–2527, May 2010.

[107] M. Kowalski and B. Torrsani, "Sparsity and persistence: mixed norms provide simple signal models with dependent coefficients," *Signal, Image and Video Processing*, vol. 3, no. 3, pp. 251–264, 2009.

[108] J. Tropp, A. Gilbert, and M. Strauss, "Simultaneous sparse approximation via greedy pursuit," in *IEEE International Conference on Acoustics, Speech, and Signal Processing (ICASSP)*, vol. 5, 2005, pp. v/721–v/724 Vol. 5.

[109] M. Manikandan and S. Dandapat, "Wavelet threshold based TDL and TDR algorithms for real-time ECG signal compression," *Biomedical Signal Processing and Control*, vol. 3, no. 1, pp. 44–66, 2008.

[110] S. Miaou, H. L. Yen, and C. L. Lin, "Wavelet-based ECG compression using dynamic vector quantization with tree code vectors in single codebook," *IEEE Transaction on Biomedical Engineering*, vol. 49 (7), pp. 671 – 680, July 2002.

[111] Y. Zigel, A. Cohen, and A. Katz, "ECG signal compression using analysis by synthesis coding," *IEEE Transaction on Biomedical Engineering*, vol. 47, no.10, pp. 308 – 316, Oct. 2000.

[112] A. S. Al-Fahoum, "Quality assessment of ECG compression techniques using a wavelet-based diagonstic measure," *IEEE Transaction on Information Technology in Biomedicine*, vol. 10, no.1, pp. 182 –191, Jan.2006.

[113] M. Kotas, "Application of projection pursuit based robust principal component analysis to ECG enhancement," *Biomedical Signal Processing and Control, Elsevier*, vol. 1 (4), pp. 289–298, 2006.

[114] F. Castells, P. Laguna, L. Sornmo, A. Bollmann, and J. Roig, "Principal component analysis in ECG signal processing," *EURASIP Journal on Advances in Signal Processing, Hindawi Publishing Corporation*, vol. doi:10.1155/2007/74580, p. 21, 2007.

[115] M. P. S. Chawla, "A comparative analysis of principal component and independent component techniques for electrocardiograms," *Neural Comput and Applic, Springer-Verlag London Limited*, vol. 18, pp. 539 – 556, 2009.

[116] S. Maheshwari, A. Acharyya, P. Rajalakshmi, P. Puddu, and M. Schiariti, "Accurate and reliable 3-lead to 12-lead ECG reconstruction methodology for remote health monitoring applications," in *15th IEEE International Conference one-Health Networking, Applications Services (Healthcom)*, Oct 2013, pp. 233–237.

[117] S. Maheshwari, A. Acharyya, P. E. Puddu, and M. Schiariti, "Reduced lead system selection methodology for reliable standard 12-lead reconstruction targeting personalised remote health monitoring applications," *Computer Methods in Biomechanics and Biomedical Engineering: Imaging & Visualization*, vol. 2, no. 2, pp. 107–120, 2014.

[118] S. Maheshwari, A. Acharyya, P. Rajalakshmi, M. Schiariti, and P. Puddu, "Personalized reduced 3-lead system formation methodology for remote health monitoring applications and reconstruction of standard 12-lead system," *International Archives of Medicine*, vol. 8, no. 62, pp. 1–15, 2015.

[119] R. Masiero, G. Quer, D. Munaretto, M. Rossi, J. Widmer, and M. Zorzi, "Data acquisition through joint compressive sensing and principal component analysis," in *IEEE Global Telecommunications Conference, 2009. GLOBECOM 2009*, 2009, pp. 1–6.

[120] L. Sharma, S. Dandapat, and A. Mahanta, "Multiscale principal component analysis to denoise multichannel ECG signals," in *5th Cairo International Biomedical Engineering Conference (CIBEC), 2010*, Dec 2010, pp. 17–20.

[121] A. Cetin, H. Koymen, and M. Aydin, "Multichannel ECG data compression by multirate signal processing and transform domain coding techniques," *IEEE Transactions on Biomedical Engineering*, vol. 40, no. 5, pp. 495–499, 1993.

[122] R. Sameni, "OSET: The open-source electrophysiological toolbox," Jan 2012, available: http://www.oset.ir/.

[123] G. Golub and C. van Loan, *Matrix Computations*, third ed., Ed. John Hopkins University Press, 1996.

[124] T. Park, J. Kim, and J. Rho, "Low-power, low-complexity bit-serial VLSI architecture for 1D discrete wavelet transform," *Circuits, Systems & Signal Processing*, vol. 26, no. 5, pp. 619–634, 2007.

[125] A. Abdulghani, A. Casson, and E. Rodriguez-Villegas, "Foundations of augmented cognition neuroergonomics and operational neuroscience," in *Lecture Notes in Computer Science, Springer 5638*, 2009, pp. 319–328.

[126] M. Zare and M. Maymandi-Nejad, "A fully digital front-end architecture for ECG acquisition system with 0.5 v supply," *IEEE Transactions on Very Large Scale Integration (VLSI) Systems*, vol. 24, no. 1, pp. 256–265, Jan 2016.

[127] N. Verma and A. Chandrakasan, "An ultra low energy 12-bit rate-resolution scalable SAR ADC for wireless sensor nodes," *IEEE Journal of Solid-State Circuits*, vol. 42, no. 6, pp. 1196–1205, June 2007.

[128] T.-C. Chen, W. Liu, and L.-G. Chen, "VLSI architecture of leading eigenvector generation for on-chip principal component analysis spike sorting system," in *30th IEEE Annual International Conference of the Engineering in Medicine and Biology Society (EMBS)*, Aug 2008, pp. 3192–3195.

[129] J. Holleman, B. Otis, S. Bridges, A. Mitros, and C. Diorio, "A 2.92 $\mu W$ hardware random number generator," in *Proceedings of the 32nd European Solid-State Circuits Conference (ESSCIRC)*, Sept 2006, pp. 134–137.

[130] R. Chartrand, "Nonconvex splitting for regularized low-rank + sparse decomposition," *IEEE Transactions on Signal Processing*, vol. 60, no. 11, pp. 5810–5819, Nov 2012.

[131] B. Joseph, A. Acharyya, and P. Rajalakshmi, "A low complexity on-chip ECG data compression methodology targeting remote health-care applications," in *36th IEEE Annual International Conference of the Engineering in Medicine and Biology Society (EMBC)*, Aug 2014, pp. 5944–5947.

[132] E. Candes, M. B. Wakin, and S. P. Boyd, "Enhancing sparsity by reweighted $\ell_0$-minimization," *Journal of Fourier Analysis and Applications*, vol. 14, no. 5-6, pp. 877–905, 2008.

[133] C. Zheng, G. Li, Y. Liu, and X. Wang, "Subspace weighted $\ell_{2,1}$ minimization for sparse signal recovery," *EURASIP Journal on Advances in Signal Processing*, vol. 2012, no. 1, 2012.

[134] D. Wipf and S. Nagarajan, "Iterative reweighted $\ell_1$ and $\ell_2$ methods for finding sparse solutions," *IEEE Journal of Selected Topics in Signal Processing*, vol. 4, no. 2, pp. 317–329, April 2010.

[135] J. Zhang, Z. L. Yu, Y. Li, G. Liu, and Z. Gu, "Weighted regularized sparse recovery method for optical power monitoring," *IEEE Photonics Technology Letters*, vol. 24, no. 1, pp. 55–57, Jan 2012.

[136] Y. Avonds, Y. Liu, and S. Van Huffel, "Simultaneous greedy analysis pursuit for compressive sensing of multi-channel ECG signals," in *36th Annual International Conference of the IEEE Engineering in Medicine and Biology Society (EMBC)*, Aug 2014, pp. 6385–6388.

[137] B. Liu, Z. Zhang, H. Fan, and Q. Fu, "Compression via compressive sensing: A low-power framework for the telemonitoring of multi-channel physiological signals," in *IEEE International Conference on Bioinformatics and Biomedicine (BIBM)*, Dec 2013, pp. 9–12.

[138] M. M. Hyder and K. Mahata, "An improved smoothed $\ell_0$ approximation algorithm for sparse representation," *IEEE Transactions on Signal Processing*, vol. 58, no. 4, pp. 2194–2205, Apr. 2010.

[139] E. van den Berg and M. P. Friedlander, "SPGL1: A solver for large-scale sparse reconstruction," June 2007, http://www.cs.ubc.ca/labs/scl/spgl1.

[140] M. S. Manikandan and S. Dandapat, "Wavelet threshold based ECG compression using USZZQ and huffman coding of DSM," *Biomedical Signal Processing and Control*, vol. 1, no. 4, pp. 261–270, 2006.

[141] ——, "Multiscale entropy-based weighted distortion measure for ECG coding," *IEEE Signal Processing Letters*, vol. 15, pp. 829–832, 2008.

[142] R. Chartrand and W. Yin, "Iteratively reweighted algorithms for compressive sensing," in *IEEE International Conference on Acoustics, Speech and Signal Processing (ICASSP)*, March 2008, pp. 3869–3872.

[143] J. Romberg, H. Choi, and R. Baraniuk, "Bayesian tree-structured image modeling using wavelet-domain hidden markov models," *IEEE Image Processing*, vol. 10, no. 7, pp. 1056–1068, Jul 2001.

[144] M. Blanco-Velasco, F. Cruz-Roldn, J. Godino-Llorente, J. Blanco-Velasco, C. Armiens-Aparicio, and F. Lpez-Ferreras, "On the use of PRD and CR parameters for ECG compression," *Medical Engineering & Physics*, vol. 27, no. 9, pp. 798–802, 2005, this issue contains a special section on Effects of Mechanical Forces Engineering Reactions at the Cellular Level.

[145] L. Sharma, R. Tripathy, and S. Dandapat, "Multiscale energy and eigenspace approach to detection and localization of myocardial infarction," *IEEE Transactions on Biomedical Engineering*, vol. 62, no. 7, pp. 1827–1837, July 2015.

[146] *http://www.cipr.rpi.edu/research/SPIHT/spiht0.html*.

[147] Z. Lu, D. Y. Kim, and W. Pearlman, "Wavelet compression of ECG signals by the set partitioning in hierarchical trees algorithm," *IEEE Transactions on Biomedical Engineering*, vol. 47, no. 7, pp. 849–856, 2000.

[148] M. Grant and S. Boyd, "CVX: Matlab software for disciplined convex programming, version 2.1," http://cvxr.com/cvx, Mar. 2014.

[149] Z. Zeinalkhani and A. Banihashemi, "Iterative reweighted $\ell_2/\ell_1$ recovery algorithms for compressed sensing of block sparse signals," *IEEE Transactions on Signal Processing*, vol. 63, no. 17, pp. 4516–4531, Sept 2015.

भारतीय प्रौद्योगिकी संस्थान गुवाहाटी
Indian Institute of Technology Guwahati

# LIST OF PUBLICATIONS

**Journals:**

1. **Anurag Singh**, S. Dandapat, Block sparsity-based joint compressed sensing recovery of multi-channel ECG signals", IET Healthcare Technology Letters, 2017, DOI: 10.1049/htl.2016.0049.

2. **Anurag Singh**, L.N. Sharma, S. Dandapat, Multi-channel ECG data compression using compressed sensing in eigenspace, Computers in Biology and Medicine (Elsevier), vol 73, 1 June 2016, pp. 24-37, ISSN 0010-4825.

3. **Anurag Singh**, S. Dandapat, Exploiting multi-scale signal information in joint compressed sensing recovery of multi-channel ECG signals, Biomedical Signal Processing and Control (Elsevier), vol 29, August 2016, pp. 53-66, ISSN 1746-8094.

4. **Anurag Singh**, S. Dandapat, Weighted mixed-norm minimization based joint compressed sensing recovery of multi-channel electrocardiogram signals, Computers & Electrical Engineering (Elsevier), vol 53, July 2016, pp. 203-218, ISSN 0045-7906.

**Conferences:**

1. **Anurag Singh**, S. Dandapat, "Exploiting inter-channel correlation in multichannel compressed sensing ECG systems", *IEEE UPCON 2015*, pp.1-7, 4-6 Dec. 2015.

2. **Anurag Singh**, J. J. Nallikuzhy, S. Dandapat, "Compressed sensing framework of data reduction at multiscale level for eigenspace multichannel ECG signals", *IEEE NCC 2015*, pp.1-6, Feb. 27 -March 1 2015.

3. **Anurag Singh**, S. Dandapat, "Distributed compressive sensing for multichannel ECG signals over learned dictionaries", *IEEE INDICON 2014*, pp.1-6, 11-13 Dec. 2014.

4. **Anurag Singh**, L.N. Sharma, and S. Dandapat, "Compressive sensing in eigenspace for multichannel electrocardiogram signals", *IEEE International Conference on Advanced Electronic Systems (ICAES 2013)*, pp.166-170, Sept 2013.

**Book Chapter:**

1. **Anurag Singh**, S. Dandapat, "Two-dimensional processing of multichannel ECG signals for efficient exploitation of inter and intra-channel correlation", *Lecture Notes in Electrical Engineering, Springer*, vol 347, pp 201-209, 2015.